ESA PECS STUDY ARRANGEMENT REPORT

No ESA PECS Study Arrangement Report will be accepted unless this sheet is inserted at the beginning of each volume of the Report.

ESA Contract (Arrangement) No:	SUBJECT:	INSTITUTE:
4000103741/11/NL/KML	Relativistic GNSS: Relativistic Global Navigation System	UL FMF, University of Ljubljana, Faculty of Mathematics and Physics

* ESA CR( )No:	No. of Volumes: 3 This is Volume No: 1	INSTITUTE'S REFERENCE: ESA-Gomboc-2014-Final Report

ABSTRACT:

Current GNSS systems rely on global reference frames which are fixed to the Earth (via the ground stations) so their precision and stability in time are limited by our knowledge of the Earth dynamics. These drawbacks could be avoided by giving to the constellation of satellites the possibility of constituting by itself a primary and autonomous positioning system, without any a priori realization of a terrestrial reference frame. Our work continues the two Ariadna studies, which showed that it is possible to construct such a system, an Autonomous Basis of Coordinates, via emission coordinates, and modelled it in the idealized case of Schwarzschild metric. Here we implement the idea of the Autonomous Basis of Coordinates in the perturbed space-time of Earth, where the motion of satellites, light propagation, and gravitational perturbations (due to Earth's multipoles, solid and ocean tides, rotation and celestial bodies) are treated in the formalism of general relativity. We also study a possibility to use such a system of satellites as probes of gravitational field and refine current knowledge of gravitational parameters.

The work described in this report was done under ESA PECS Arrangement. Responsibility for the contents resides in the author or organisation that prepared it.

Names of authors: Andreja Gomboc, Martin Horvat, Uroš Kostić

** NAME OF ESA PECS PROGRAMME MANAGER: DIV: DIRECTORATE:	** ESA BUDGET HEADING:

* Sections to be completed by ESA

** Information to be provided by ESA PECS Programme Manager

Univerza *v Ljubljani*
Fakulteta za *matematiko in fiziko*

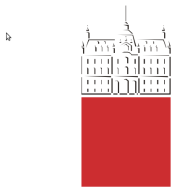

The PECS project
Relativistic GNSS

– Final Report –

Andreja Gomboc
Martin Horvat
Uroš Kostić

UL-FMF, University of Ljubljana
Faculty of Mathematics and Physics

PECS Contract No. 4000103741/11/NL/KML

UL-FMF Reference No. ESA-Gomboc-2014-Final Report

June 29, 2014

Abstract

Current GNSS systems rely on global reference frames which are fixed to the Earth (via the ground stations) so their precision and stability in time are limited by our knowledge of the Earth dynamics. These drawbacks could be avoided by giving to the constellation of satellites the possibility of constituting by itself a primary and autonomous positioning system, without any a priori realization of a terrestrial reference frame. Our work continues the two Ariadna studies, which showed that it is possible to construct such a system, an Autonomous Basis of Coordinates, via emission coordinates, and modelled it in the idealized case of Schwarzschild metric. Here we implement the idea of the Autonomous Basis of Coordinates in the perturbed space-time of Earth, where the motion of satellites, light propagation, and gravitational perturbations (due to Earth's multipoles, solid and ocean tides, rotation and celestial bodies) are treated in the formalism of general relativity. We also study a possibility to use such a system of satellites as probes of gravitational field and refine current knowledge of gravitational parameters.

Contents

Chapter 1

Introduction

1.1 Newtonian concept of a Positioning System

Current Global Navigation Satellites Systems (GNSS), such as the Global Positioning System and the European Galileo system, are based on Newtonian concept of absolute space and time. The signals from four satellites are needed for a receiver to determine its position and time via the time difference between the emission and the reception of the signal:

- First, let us assume that we have three clocks onboard three satellites $S_i (i = 1, 2, 3)$ and that a user-receiver has his own clock. Each satellite sends an electromagnetic signal, in which the time of emission t_i is encoded. The user-receiver, receives the signal from the satellite, and having his own clock, knows the time of reception t_R of the signal. From this he can deduce his distance with respect to the three satellites: $c(t_R - t_i)$, where c is the speed of light/electromagnetic waves in vacuum. Therefore he knows that he lies on a sphere of radius $c(t_R - t_i)$ centered on the satellite S_i. The three spheres centered on the three satellites intersect usually in two points, and using the method of trilateration, the position of the receiver can be determined - it is usually taken that the receiver's position is the point being the closest to the surface of the Earth. In mathematical language this means solving the system of three equations:

$$(x - x_i)^2 + (y - y_i)^2 + (z - z_i)^2 = c^2(t_R - t_i)^2;\ i = 1, 2, 3, \tag{1.1}$$

  where the three unknowns x, y, z are the Cartesian coordinates of the receiver in the Euclidean space, and (x_i, y_i, z_i) are the coordinates of the satellite S_i at the time of emission t_i. In general, such system of equations has 0, 1 or 2 solutions.

- However, the receiver's clock is usually not very accurate and would limit the precision of the positioning. Therefore, the poorly known time of reception of the signal is treated as an unknown, and we need to add one more satellite to obtain a fourth equation. Thus, our problem consists of a system of four equations:

$$(x - x_i)^2 + (y - y_i)^2 + (z - z_i)^2 = c^2(t - t_i)^2;\ i = 1, 2, 3, 4, \tag{1.2}$$

for four unknowns: the position of the receiver and the time of reception of the signal, i.e. the receiver's position in the space-time (t, x, y, z).

This concept of absolute space and time would work ideally if all satellites and the receiver were at rest in an inertial reference frame. It is also a good approximation for a slowly moving receiver with velocity $v \ll c$, and in a very weak gravitational field $|\phi/c^2| \ll 1$, where $\phi = -GM/r$ is the gravitational potential of a central mass M (G is the gravitational constant and r the radial distance to the central mass).

1.2 The concept of a Relativistic Positioning System

However, at the level of precision needed by a GNSS, space and time around Earth can not be considered as absolute and we have to take into account the effects of inertial reference frames and curvature of the space-time in the vicinity of Earth. In fact, general relativistic effects are far from being negligible Ashby (2003), Pascual-Sánchez (2007). The most important ones are the gravitational frequency shift between clocks and the Doppler shift of the second order. As it was estimated in Čadež et al. (2010), they amount for Galileo GNSS to around 12 km error after one day of integration. Since this is much more than the required precision, it is clear that relativistic effects have to be included in the description of the GNSS.

There are two ways of including relativity in the description of GNSS: one way is to keep the Newtonian concept of absolute time and space, and add a number of relativistic corrections to the level of the accuracy desired. An alternative, and more consistent, approach is to abandon the concept of absolute space and time and describe a GNSS directly in general relativity, i.e. to define a **Relativistic Positioning System (RPS)** with the so-called **emission coordinates** Coll and Morales (1991); Rovelli (2002); Blagojević et al. (2002); Coll (2003); Tarantola et al. (2009). Let us have four particles $a = 1, 2, 3, 4$. Their worldlines $\mathcal{C}_a$ are parametrized by their proper time τ_a. Let P be an arbitrary event. The *past* null cone of P crosses each of the four worldlines $\mathcal{C}_a$ in τ_a^P (see Fig.1.1). Having four particles with four wordlines $\mathcal{C}_1$, $\mathcal{C}_2$, $\mathcal{C}_3$, $\mathcal{C}_4$, the past cone of P crosses them at $\tau_1^P, \tau_2^P, \tau_3^P, \tau_4^P$. Then $(\tau_1^P, \tau_2^P, \tau_3^P, \tau_4^P)$ are the emission coordinates of the event P.

These coordinates define the event P. We can see this by looking at it in a different way. The worldline $\mathcal{C}_a$ of the particle a defines a one-parameter family of *future* null cones, which can be parametrized by proper time τ_a^A (see Fig.1.2). The intersection of four future null cones from four worldlines $\mathcal{C}_a$ at τ_a defines an event with coordinates $\tau_1, \tau_2, \tau_3, \tau_4$. Position of event P is therefore defined in this particular coordinate system.

Four particles can be chosen as four satellites broadcasting their proper time. A user of an RPS (event P) receives, at a given moment, four signals from four different satellites and is able to determine the proper time τ_i of each satellite at the moment of emission of these signals. These four proper times $(\tau_1, \tau_2, \tau_3, \tau_4)$ therefore constitute its emission coordinates. By receiving them at subsequent times, the receiver knows its trajectory in the emission coordinates.

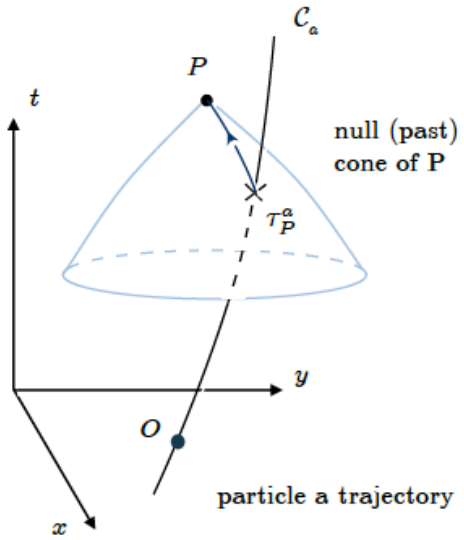

Figure 1.1: $\mathcal{C}_a$ is the worldline of a particle a parametrized by its proper time τ_a; its origin O is in $\tau_a = 0$. Past null cone of the event P crosses the worldline $\mathcal{C}_a$ of the particle a at its proper time τ_a^P. Figure from Čadež et al. (2010).

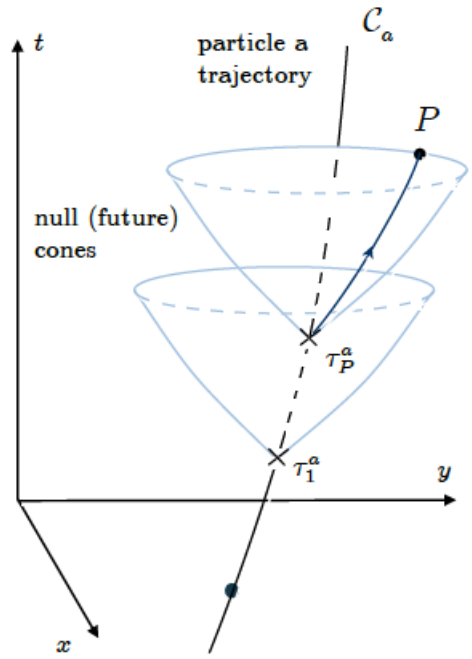

Figure 1.2: The worldine $\mathcal{C}_a$ defines a one-parameter family of future null cones. These null cones are hypersurfaces of τ_a =const. Figure from Čadež et al. (2010).

Emission coordinates are not "usual" coordinates with three space and one time coordinates. This is a complete change of paradigm and leads to amelioration and simplification of GNSS. There are several advantages of an RPS. Firstly, no relativistic corrections are necessary, as relativity is already included in the definition of the positioning system. Secondly, the emission coordinates are covariant quantities; they are independent of the observer (although dependent on the set of satellites chosen and their trajectories).

1.3 Previous work in the Ariadna studies

To demonstrate feasibility, stability and accuracy of an RPS, ESA Advanced Concepts Team started a collaboration with the University of Ljubljana. Two ESA Ariadna projects were carried out in 2010 and 2011 Čadež et al. (2010, 2011); Delva et al. (2011), in which the authors modelled an RPS in the idealized case of Schwarzschild geometry.

- In the first study *Mapping the Spacetime Metric with a Global Navigation Satellite System* Čadež et al. (2010) modeled the satellites' orbits, emission and reception of their signal by a receiver. They showed that it is possible to highly accurately determine the receiver's position in emission coordinates and transform them to Schwarzshild coordinates.

- In the second study,*Mapping the Spacetime Metric with a Global Navigation Satellite System - extension of study*, Čadež et al. (2011) and Delva et al. (2011) studied the concept of **Autonomous Basis of Coordinates (ABC)**. Namely, in addition to emitting its proper time, each satellite can also receive other satellites' signals with their proper times encoded. Thus, the satellite can use its emission coordinates to determine its own position with respect to other satellites. By using inter-satellite communication, satellites can therefore determine their orbits and, as it was shown in this study, their orbital parameters and constants of motion. Such a system of satellites would be independent from terrestrial reference frames and would constitute an ABC. Results of this study show that the concept of emission coordinates and ABC, i.e. relativistic description of a satellite constellation with inter-satellite links in Schwarzschild geometry, provides numerically accurate, stable and autonomous system. They found that by communicating their proper times solely, two satellites can determine their orbits (i.e., their constants of motion) to a high accuracy. Any additional satellites could serve to increase the system's accuracy.

Further advantage of an RPS is thus, that if each satellite broadcasts its own and also receives proper times of other satellites, the system of satellites is autonomous and constitutes a primary reference system, with no need to define a terrestrial reference frame. Therefore tracking of satellites with ground stations is necessary only to link an RPS to a terrestrial frame, although this link can also be obtained by placing several receivers at the known terrestrial positions. There is no need to synchronize satellite clocks to a time-scale realized on the ground.

The work in the Ariadna studies was performed in Schwarzschild geometry, i.e. taking into account only the gravitational influence of Earth and describing it as spherically symmetric. The aim of this PECS project is to model the Galileo GNSS as an RPS with inter-satellite links defining an ABC, including in the description all relevant gravitational perturbations due to Solar System bodies and Earth's multipoles and tides, and to test and discuss the level of accuracy and stability of the system's reference frame.

Chapter 2

Activities

Abstract In this ESA PECS project *Relativistic Global Navigation System* we continue the work done in the Ariadna studies. We aim to demonstrate that an RPS and the ABC concept are highly accurate and stable also if the space-time is not purely spherically symmetric, but contains small gravitational perturbations due to the Earth's multipoles, tides and rotation and gravitational influences of the Moon, the Sun, Jupiter and Venus. We use a framework, which is similar to the one used in Ariadna projects (i.e. emission coordinates, inter-satellite communication, description of satellites' orbit in the ABC, and recovery of their orbits) and add to a Hamiltonian/space-time metric also gravitational perturbations.

In order to deliver a high accuracy GNSS, several gravitational perturbations need to be taken into account. Before starting detailed calculations it is useful to get an estimation of the order of magnitude of various perturbations on a satellite orbit. From Fig. 2.1, we can see that at Galileo GNSS altitude of about 20.000 km above Earth, the most important gravitational perturbations are due to Earth's multipoles, followed by the gravitational field of the Moon and the Sun. Several orders of magnitude smaller are perturbations due to Solar radiation pressure and the Earth's albedo (not considered in our project) and due to Earth's tides. About one order of magnitude smaller are relativistic effects and the gravitational influence of Jupiter and Venus. Relativistic effects due to Earth's rotation are about an order of magnitude smaller again. We therefore consider an RPS of satellites, such as the Galileo system, in a space-time described by a background Schwarzschild metric and small gravitational perturbations due to the Earth's rotation, multipoles and tides, and the gravity of the Moon, the Sun, Jupiter, and Venus.

We would like to note, that Earth tides were originally not part of this project as it was proposed and accepted by ESA. But because we subsequently discovered that their effects are comparable or even larger than effects of some other gravitational perturbations included in the project, we decided that it is necessary to include also perturbations due to Earth tides in our study.

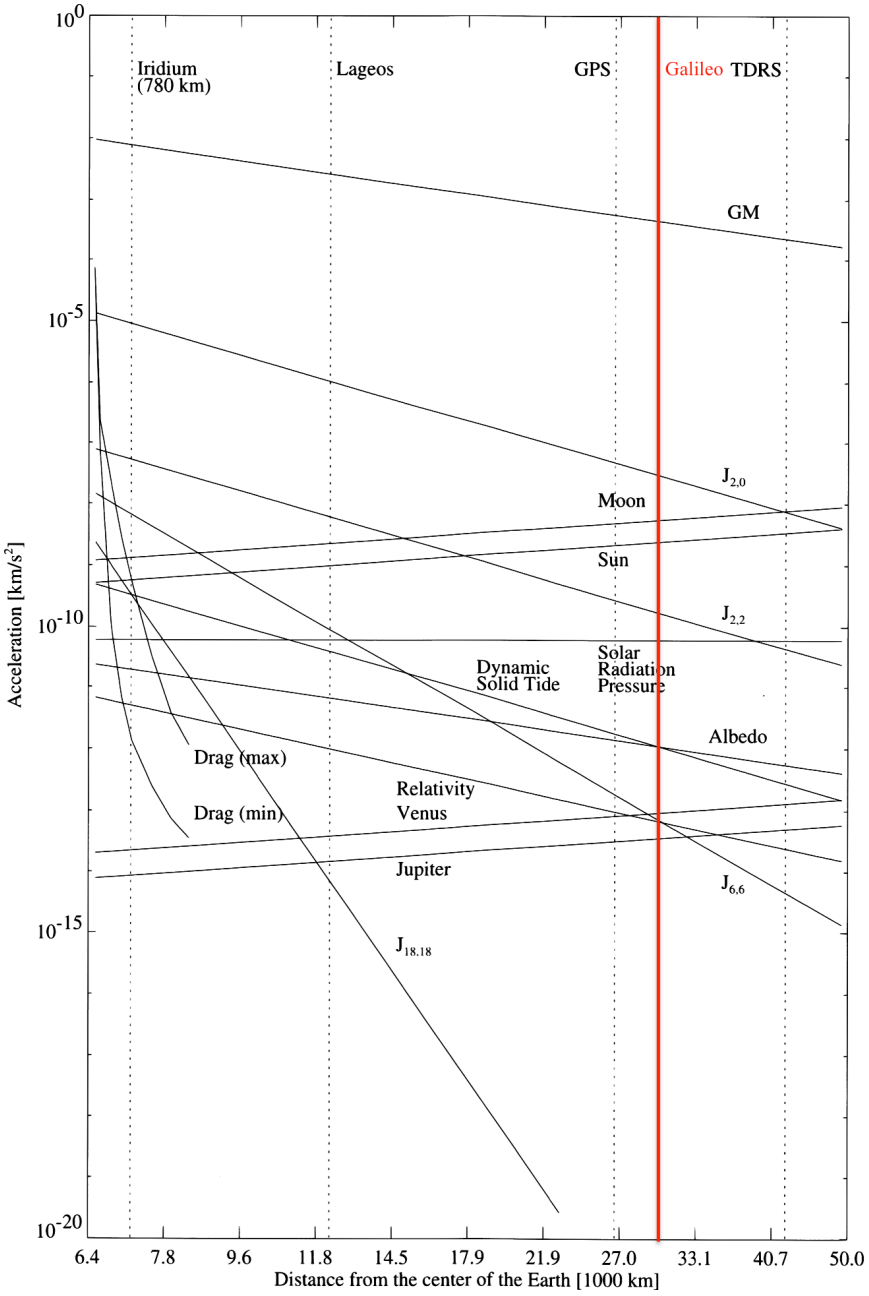

Figure 2.1: Order of magnitude of various perturbations of a satellite orbit (Montenbruck and Gill 2005). Red line indicates position of Galileo satellites.

Outline of the PECS Relativistic GNSS project and its goals

The main goal of this project is to model a relativistic GNSS in a space-time, which includes all relevant gravitational perturbations and investigate GNSS's accuracy and stability. In brief, we start by modelling an RPS by writing the perturbed space-time metric and Hamiltonian, corresponding equations of motion, calculating orbits of satellites and time-of-flight of signals between a user-receiver and satellites. Then we model the ABC, by simulating inter-satellite communication and use the emission/reception of their proper times to highly accurately determine satellites' orbital parameters. In the last stage, we investigate if and to which accuracy such a system of satellites could be used as a probe of gravitational perturbations and for refinement of gravitational parameters.

Our work is divided in four Work Packages (WP):

1 **Work Package 1: Metric around Earth**
We include all relevant gravitational perturbations to the background of the Schwarzschild metric in the weak-field limit with the linear perturbation theory. We use the Regge-Wheeler-Zerilli formalism, i.e., expand perturbations in terms of tensor spherical harmonics. We find perturbation coefficients and connection between them and Newtonian multipole coefficients. Resulting explicit expressions for the perturbed Schwarzschild metric incorporate effects due to Earth's multipoles, tides, and rotation; and weak gravitational influences of celestial bodies: the Sun, the Moon, Jupiter, Venus (could be expanded to other celestial bodies as well).

2 **Work Package 2: Dynamics of satellites**
We use Hamiltonian formalism and perturbation theory to solve the perturbed geodesic equations for satellite orbits. We derive expressions for time evolution of 0^{th} order constants of motion (i.e. quantities which are constants of motion in unperturbed Schwarzschild metric). We simulate satellite orbits by using analytic geodesic solutions for the unperturbed Schwarzschild metric, however with slowly evolving 0^{th} order constants of motion. We investigate the influence of different gravitational perturbations on the orbital parameters evolution, satellite's position and time, and on the user-satellite and inter-satellite light signal propagation.

3 **Work Package 3: Determination of orbital parameters**
We use perturbed satellite orbits from Work Package 2 and test the accuracy of positioning by such an RPS in gravitationally perturbed space-time. We simulate a constellation of GNSS satellites as an RPS with inter-satellite links. Satellite orbits can be described by their initial values of 0^{th} order constants of motion. In the following, we assume that their values are known with only limited accuracy and by using solely inter-satellite links and information on emission coordinates over several orbital periods we refine them. In this way satellites can themselves highly accurately determine the initial values of their 0^{th} order constants of motion and therefore their own orbital parameters, i.e. they constitute an ABC system. We study possible degeneracies among orbital parameters.

4 **Work Package 4: Determination of gravitational parameters**
In a similar way as in Work Package 3, we simulate a constellation of GNSS satellites with inter-satellite links and assume that in addition to initial values of 0^{th} order constants of motion also gravitational perturbation coefficients are known only with limited accuracy. We investigate if and to which level of accuracy we can refine their values by using residual errors between orbit prediction and orbit determination through inter-satellite communication. We discuss prospects and limitations of using GNSS constellation of satellites to probe the space-time around Earth.

2.1 Work Package 1 - Metric around Earth

Abstract of WP1: In WP1 we include gravitational perturbations to the background of the Schwarzschild metric in the weak-field limit with the linear perturbation theory. We use the Regge-Wheeler-Zerilli formalism, i.e., expand perturbations in terms of tensor spherical harmonics, and find connection between our solutions and Newtonian multipole coefficients. Resulting explicit expressions for the perturbed Schwarzschild metric incorporate effects due to Earth's multipoles, tides, and rotation, and weak gravitational influences of celestial bodies: the Sun, the Moon, Jupiter, Venus (could be expanded to other celestial bodies as well).

2.1.1 Introduction

Perturbations of the Schwarzschild metric have been studied by several authors, most of them focused on radiative solutions which are useful for studies of gravitational waves (Nollert 1999; Nagar and Rezzolla 2005; Berti et al. 2009). However, gravitational perturbations of the Schwarzschild metric can also be relevant in the weak-field limit. An example of this is the space-time around Earth, which is populated by artificial satellites, for which we need to know their orbits with ever increasing accuracy, namely the RPS system. We will describe the space-time around Earth as a Schwarzschild background metric with addition of smaller perturbative parts. We fully and explicitly determine the leading order approximation of the metric perturbations using multipole expansion in the Regge-Wheeler and Zerilli (RWZ) formalism (Regge and Wheeler 1957; Zerilli 1970), where we use the Newtonian multipoles to approximate the metric elements by comparing the first order perturbations in this formalism to the solution of the linear theory and by taking appropriate Newtonian limits (see e.g. Geroch (1970); Hansen (1974)).

2.1.2 Regge-Wheeler-Zerilli formalism

We describe the spherically symmetric and time independent background with the Schwarzschild metric $g^{(0)}_{\mu\nu}$: we take coordinate variables $(ct, r, \theta, \varphi) \in \mathbb{R} \times \mathbb{R}_+ \times [0, \pi] \times [0, 2\pi]$ and write the Schwarzschild metric tensor:

$$[g^{(0)}_{\mu\nu}] = \mathrm{diag}(-X, X^{-1}, r^2, r^2 \sin^2\theta) \tag{2.1}$$

with $X = 1 - r_\mathrm{s}/r$, where r_s is the Schwarzschild radius: $r_\mathrm{s} = 2GM_\mathrm{E}/c^2$ (M_E is the Earth's mass, G gravitational constant and c speed of light in vacuum).

We denote metric perturbations with $h_{\mu\nu}$. Because gravitational perturbations are several orders of magnitude smaller than Earth's gravitational GM_E term ($h_{\mu\nu} \ll g^{(0)}_{\mu\nu}$), we use linear perturbation theory and write the perturbed metric as

$$g_{\mu\nu} = g^{(0)}_{\mu\nu} + h_{\mu\nu} + O(h^2)\,. \tag{2.2}$$

Because we are interested in the space-time outside Earth, the perturbed metric must satisfy the Einstein equation for vacuum:

$$R_{\mu\nu} - \frac{1}{2} g_{\mu\nu} R = 0 \tag{2.3}$$

where

$$R_{\mu\nu} = R^{(0)}_{\mu\nu} + \delta R_{\mu\nu} \tag{2.4}$$

is the Ricci tensor (symbol $^{(0)}$ denotes unperturbed quantities and δ perturbations). The Einstein equation becomes:

$$\begin{aligned} & h_{\alpha}{}^{\alpha}{}_{;\mu\nu} - h_{\mu}{}^{\alpha}{}_{;\nu\alpha} - h_{\nu}{}^{\alpha}{}_{;\mu\alpha} + h_{\mu\nu;}{}^{\alpha}{}_{\alpha} \\ & + g^{(0)}_{\mu\nu}(h_{\alpha}{}^{\lambda\,\alpha}{}_{;\,\lambda} - h_{\lambda}{}^{\lambda}{}_{;\alpha}{}^{\alpha}) - h_{\mu\nu} R^{(0)} \\ & + g^{(0)}_{\mu\nu} h_{\lambda\sigma} R^{(0)\lambda\sigma} = 0 \end{aligned} \tag{2.5}$$

where a semi-colon (;) denotes covariant derivative, calculated with respect to the unperturbed metric $g^{(0)}_{\mu\nu}$.

To find solutions of these equations for vacuum we use the RWZ formalism (Regge and Wheeler 1957; Zerilli 1970). In the RWZ formalism, the metric perturbation $h_{\mu\nu}$ is expanded into a series of independent tensor harmonics, a tensor analog to spherical harmonic functions, labeled by indices n (degree) and m (order). The tensor harmonics contributions with similar properties, i.e. same parity and indices (n, m), are joined together to form independent metric functions, called in Vishveshwara (1970) the normal modes. The full set of these functions represents a complete functional basis for decomposition of metric perturbations, and as such, it is appropriate for solving the linearized Einstein equation.

In general, the metric perturbation $h_{\mu\nu}$ can be expanded in a functionally independent set of tensor harmonics. By adopting the notation from Nagar and Rezzolla (2005), the general expansion of the metric perturbation $h_{\mu\nu}$ can be written as

$$h_{\mu\nu} = \sum_{n=2}^{\infty} \sum_{m=-n}^{n} \left((h^{nm}_{\mu\nu})^{(\mathrm{e})} + (h^{nm}_{\mu\nu})^{(\mathrm{o})} \right) , \tag{2.6}$$

where the expansion terms $(h^{nm}_{\mu\nu})^{(\mathrm{e})}$ and $(h^{nm}_{\mu\nu})^{(\mathrm{o})}$ are the even-parity and the odd-parity metric functions (or modes), respectively. The parity inversion operator $\hat{P} : \vec{r} \mapsto -\vec{r}$, written in spherical coordinates as $(\theta, \varphi) \mapsto (\pi - \theta, \varphi + \pi)$, applied to the metric functions yields:

$$\begin{aligned} \hat{P}(h^{nm}_{\mu\nu})^{(\mathrm{e})} &= (-1)^n (h^{nm}_{\mu\nu})^{(\mathrm{e})} , \\ \hat{P}(h^{nm}_{\mu\nu})^{(\mathrm{o})} &= (-1)^{n+1} (h^{nm}_{\mu\nu})^{(\mathrm{o})} . \end{aligned} \tag{2.7}$$

The gauge transformations in Regge-Wheeler-Zerrilli solutions

We find it most convenient to work in the gauge from Regge and Wheeler (1957), where a coordinate transformation $x'^{\nu} = x^{\nu} + \xi^{\nu}$ is proposed, which conserves the background metric and transforms the metric perturbation in such a way that the resulting metric functions are reduced in complexity. The transformation Regge and Wheeler (1957) also preserves the degree, the order, and the parity, if defined by the metric perturbation.

General additivity of coordinate transformations Under infinitesimal linear coordinate transformation

$$x^{\mu} \rightarrow x'^{\mu} = x^{\mu} + \xi^{\mu} \tag{2.8}$$

the metric tensor changes to

$$g'_{\mu\nu} = g^{(0)}_{\mu\nu} + h'_{\mu\nu} \tag{2.9}$$

Under the condition that the line element is invariant to coordinate transformations

$$g_{\mu\nu}\mathrm{d}x^{\mu}\mathrm{d}x^{\nu} = g'_{\mu\nu}\mathrm{d}x'^{\mu}\mathrm{d}x'^{\nu} \ , \tag{2.10}$$

the new metric perturbation $h'_{\mu\nu}$ is written as

$$h'_{\mu\nu} = h_{\mu\nu} - S_{\mu\nu}[\xi] \ , \tag{2.11}$$

where $S_{\mu\nu}$ is the symmetrized covariant derivative

$$S_{\mu\nu}[\xi] := \xi_{\mu;\nu} + \xi_{\nu;\mu} \ . \tag{2.12}$$

The relation (2.11) holds up to the first order in the metric perturbation.

Next, we write the metric perturbation as a sum

$$h_{\mu\nu} = \sum_{\alpha} (h_{\mu\nu})^{(\alpha)} \ . \tag{2.13}$$

where α can be, for example, odd and even parity.

We also write the coordinate shift (ξ^{μ}) as the sum:

$$\xi^{\mu} = \sum_{\alpha} (\xi^{\mu})^{(\alpha)} \tag{2.14}$$

Taking into account linearity of $S_{\mu\nu}$ ($S_{\mu\nu}[\sum_i f_i] = \sum_i S_{\mu\nu}[f_i]$), we can write:

$$S_{\mu\nu}[\xi] = \sum_{\alpha} S_{\mu\nu}[\xi^{(\alpha)}] \tag{2.15}$$

Inserting (2.13) and (2.15) in (2.11) we see that we can write also $h'_{\mu\nu}$ as the sum:

$$h'_{\mu\nu} = \sum_{\alpha} (h'_{\mu\nu})^{(\alpha)} \tag{2.16}$$

where

$$(h'_{\mu\nu})^{(\alpha)} = (h_{\mu\nu})^{(\alpha)} - S_{\mu\nu}[\xi^{(\alpha)}] \ . \tag{2.17}$$

We can therefore choose different gauges, $(\xi^{\mu})^{\alpha}$, for different α (as it most suits us) and still co-add $(h'_{\mu\nu})^{(\alpha)}$ in $h'_{\mu\nu}$.

Regge-Wheeler-Zerilli gauge If we expand metric prturbations as in (2.6) into odd and even parity metric functions $h^{nm)(\mathrm{o})}_{\mu\nu}$, $h^{nm)(\mathrm{e})}_{\mu\nu}$, these are totally decoupled from each other (Cruciani, 2005). From Regge and Wheeler (1957) or Vishveshwara (1970) or Zerilli (1970), the even-parity or electric contributions are written as

$$(h_{\mu\nu})^{(nm,\mathrm{e})} = \begin{bmatrix} XH_0Y^m_n & H_1Y^m_n & h_0\partial_\theta Y^m_n & h_0\partial_\varphi Y^m_n \\ H_1Y^m_n & X^{-1}H_0Y^m_n & h_1\partial_\theta Y^m_n & h_1\partial_\varphi Y^m_n \\ \star & \star & r(K+G\partial^2_\theta)Y^m_n & \star \\ \star & \star & r^2G\hat{U}Y^m_n & r^2[K\sin^2\theta + G\hat{V}]Y^m_n \end{bmatrix}, \tag{2.18}$$

where $\star$ indicates symmetric part of the tensor, Y^m_n are spherical harmonics (Abramowitz and Stegun 1964), and $\hat{U} = \partial_{\theta\varphi} - \cot\theta\partial_\phi$ and $\hat{V} = \partial^2_\varphi + \sin\theta\cos\theta\partial_\theta$. The odd-parity or magnetic contributions are:

$$(h_{\mu\nu})^{(nm,\mathrm{o})} = \begin{bmatrix} 0 & 0 & -h_0\csc\theta\partial_\varphi Y^m_n & -h_0\sin\theta\partial_\theta Y^m_n \\ 0 & 0 & -h_1\csc\theta\partial_\varphi Y^m_n & -h_1\sin\theta\partial_\theta Y^m_n \\ \star & \star & h_2\csc\theta\hat{U}Y^m_n & \star \\ \star & \star & \frac{1}{2}h_2\hat{W}Y^m_n & -h_2\sin\theta\hat{U}Y^m_n \end{bmatrix}, \tag{2.19}$$

with $\hat{W} = \csc\theta\partial^2_\varphi + \cos\theta\partial_\theta - \sin\theta\partial^2_\theta$. In Eqs. (2.18) and (2.19) indices (nm) on the r.h.s. are omitted for clarity from H_i, h_i, K and G, which are functions of (t,r), while Y^m_n are functions of (θ,φ). Although h_i appear in both harmonics they are not the same functions.

Next, we can introduce shifts of coordinates $(\xi^\mu)^{(nm,\mathrm{e})}$, $(\xi^\mu)^{(nm,\mathrm{o})}$ such that $S_{\mu\nu}[\xi^{(nm,\mathrm{e})}]$, $S_{\mu\nu}[\xi^{(nm,\mathrm{o})}]$ are tensor harmonics with indices (nm). Coordinate shifts corresponding to even-parity tensor harmonics are

$$\begin{aligned} \xi^0 &= M^0(T,r)Y^m_n(\theta,\varphi)\,, \qquad \xi^1 = M^1(T,r)Y^m_n(\theta,\varphi)\,, \\ \xi^2 &= M^2(T,r)\partial_\theta Y^m_n(\theta,\varphi)\,, \qquad \xi^3 = M^2(T,r)\csc^2\theta\partial_\phi Y^m_n(\theta,\varphi)\,, \end{aligned} \tag{2.20}$$

and the ones corresponding to odd-parity tensors harmonics are

$$\begin{aligned} \xi^0 &= \xi^1 = 0\,, \\ \xi^d &= \Lambda(T,r)\epsilon^{cd}Y^m_{n\,,d} \quad \text{for} \quad d = 2,3\,, \end{aligned} \tag{2.21}$$

where we omit indices (nm) in ξ^μ, M^μ, and Λ for clarity.

If the coordinate shift ξ^μ is given as a sum of shifts associated to different types of tensor harmonics:

$$\xi^\mu = \sum_{n=0}^{\infty}\sum_{m=-n}^{n}\left((\xi^\mu)^{(nm,\mathrm{o})} + (\xi^\mu)^{(nm,\mathrm{o})}\right), \tag{2.22}$$

then the metric perturbation $h'_{\mu\nu}$ in (2.11) is in new coordinates written as:

$$h'_{\mu\nu} = \sum_{n=0}^{\infty}\sum_{m=-n}^{n}\left((h'_{\mu\nu})^{(nm,\mathrm{e})} + (h'_{\mu\nu})^{(nm,\mathrm{o})}\right) \tag{2.23}$$

where

$$(h'_{\mu\nu})^{(nm,\mathrm{e})} = (h_{\mu\nu})^{(nm,\mathrm{e})} - S_{\mu\nu}[\xi^{(nm,\mathrm{e})}] \tag{2.24}$$

$$(h'_{\mu\nu})^{(nm,\mathrm{o})} = (h_{\mu\nu})^{(nm,\mathrm{o})} - S_{\mu\nu}[\xi^{(nm,\mathrm{o})}] \tag{2.25}$$

where $(h'_{\mu\nu})^{(nm,\mathrm{e})}$, $(h'_{\mu\nu})^{(nm,\mathrm{o})}$ are again harmonic tensors with the same indices.

It was shown by Regge and Wheeler (1957) that for each (nm,e), (nm,o) we can choose functions M_i (in $\xi^{(nm,\mathrm{e})}$ in 2.20) in such a way, that in $(h'_{\mu\nu})^{(nm,\mathrm{e})}$ we have:

$$h_0 = h_1 = G = 0\,. \tag{2.26}$$

and choose the function Λ (in $\xi^{(nm,\mathrm{o})}$ in 2.21) so that in $(h'_{\mu\nu})^{(nm,\mathrm{o})}$ is

$$h_2 = 0\,. \tag{2.27}$$

This is called the *Regge&Wheeler choice of gauge* and with using it, we get a simplified decomposition of metric perturbation $h'_{\mu\nu}$ into functionally independent parts. In this gauge the even parity metric functions are:

$$(h^{nm}_{\mu\nu})^{(\mathrm{e})} = \left[\begin{array}{cc|cc} H_0X & H_1 & 0 & 0 \\ \star & H_2X^{-1} & 0 & 0 \\ \hline 0 & 0 & r^2K & 0 \\ 0 & 0 & 0 & r^2K\sin^2\theta \end{array}\right] Y^m_n\ , \tag{2.28}$$

and for odd parity, the metric functions are

$$(h^{nm}_{\mu\nu})^{(\mathrm{o})} = \left[\begin{array}{cc|cc} 0 & 0 & -h_0\csc\theta\partial_\varphi & h_0\sin\theta\partial_\theta \\ 0 & 0 & -h_1\csc\theta\partial_\varphi & h_1\sin\theta\partial_\theta \\ \hline \star & \star & 0 & 0 \\ \star & \star & 0 & 0 \end{array}\right] Y^m_n\ . \tag{2.29}$$

It is shown in Regge and Wheeler (1957) and Zerilli (1970) that in vacuum $H_0 = H_2$, therefore, both functions are marked with H in the following text.

Einstein equations The linearized Einstein equations for perturbations in the Schwarzschild background preserve pairs of indices (n,m) as well as the parity, and are homogeneous in the case of vacuum. Inserting $h_{\mu\nu}$ from (2.6) into (2.5), leads to a set of homogeneous field equations for functions describing each normal mode independently. From Zerilli (1970), we rewrite the field equations for the even parity metric functions:

$$\begin{aligned} &XK_{,rr} + (5X-2)\frac{1}{r}K_{,r} - X\frac{1}{r}H_{,r} \\ &-\frac{1}{r^2}(H-K) - \frac{1}{2r^2}n(n+1)(H+K) = 0 \end{aligned} \tag{2.30}$$

$$K_{,rT} + \frac{1}{r}(K-H)_{,T} + \frac{r_\mathrm{s}}{2r^2X}K - \frac{n(n+1)}{2r^2}H_1 = 0 \tag{2.31}$$

$$\frac{1}{X}K_{,TT} - \frac{1+X}{2r}K_{,r} - \frac{2}{r}H_{1,T} + X\frac{1}{r}H_{,r} + \frac{1}{r^2}(H-K) + \frac{1}{2r^2}n(n+1)(K-H) = 0 \tag{2.32}$$

$$(XH_1)_{,r} - (H+K)_{,T} = 0 \tag{2.33}$$

$$H_{1,T} + X(H-K)_{,r} + \frac{r_\mathrm{s}}{r^2}H = 0 \tag{2.34}$$

$$-\frac{1}{X}K_{,TT} + XK_{,rr} + (1+X)\frac{1}{r}K_{,r} - \frac{1}{X}H_{,TT} + 2H_{1,rT} - XH_{,rr} + \frac{1+X}{rX}H_{1,T} - \frac{2}{r}H_{,r} = 0\ , \tag{2.35}$$

and for the odd parity metric functions:

$$h_{0,rr} - h_{1,rT} - \frac{2}{r}h_{1,T} + \left[\frac{2r_\mathrm{s}}{r^2} - \frac{n(n+1)}{r}\right]\frac{h_0}{rX} = 0 \tag{2.36}$$

$$h_{1,TT} - h_{0,rT} + \frac{2}{r}h_{0,T} + (n-1)(n+2)X\frac{h_1}{r^2} = 0 \tag{2.37}$$

$$Xh_{1,r} - \frac{1}{X}h_{0,T} + \frac{r_\mathrm{s}}{r^2}h_1 = 0 \tag{2.38}$$

where a comma (,) denotes derivative.

From various possible choices of coordinate transformations, we found the Regge-Wheeler gauge the most convenient for the following reasons: (i) the gauge is completely fixed, (ii) the angular and radial dependence are decoupled in the resulting field equations, and (iii) the solutions have a Newtonian limit, which is important when comparing metric tensor elements with their weak-field limits.

2.1.3 Time-independent metric perturbations

We first consider a stationary space-time case: Schwarzschild background with time-independent perturbations (e.g., non-rotating, slightly non-spherical Earth, presence of (hypothetical) non-moving celestial objects). We find solutions of the differential equations from the previous subsection. We treat even and odd parity modes separately.

Even parity contributions

In the case of time-independent perturbations of even parity $H_1 = 0$ (Regge and Wheeler 1957). It follows that the even metric mode (2.28) is diagonal:

$$(h^{nm}_{\mu\nu})^{(\mathrm{e})} = \mathrm{diag}(HX, HX^{-1}, r^2K, r^2K\sin^2\theta)Y^m_n\ . \tag{2.39}$$

Inserting it in (2.5) gives differential equations for functions H and K. With substitution

$$S(x) = x(x-1)H(x) \tag{2.40}$$

these two functions are determined up to a constant prefactor (Zerilli 1970):

$$x(1-x)S'' + (2x-1)S' + wS = 0\ , \tag{2.41}$$

$$x(x-1)(H-K)' + H = 0 \,, \tag{2.42}$$
$$2(x-1)H' - (2x-1)K' - w(H-K) = 0 \,, \tag{2.43}$$

where we use rescaled radius $x = r/r_\mathrm{s}$, constant $w = (n-1)(n+2)$, and derivative $()' = \mathrm{d}/\mathrm{d}x$. Because we are interested in solutions outside the Schwarzschild radius (i.e., $x > 1$), we can in (2.41) use a substitution $x = 1/u$ and rewrite it on the domain $u \in [0, 1]$:

$$(u-1)u^2\ddot{S} + u(3u-4)\dot{S} + wS = 0 \tag{2.44}$$

with $\dot{()} = \mathrm{d}/\mathrm{d}u$. Because $u = 0$ is a regular singular point, we can solve this equation with the Frobenius method (Arfken 1985) around $u = 0$ and obtain the solution as the superposition of two independent terms:

$$S(u) = A_{nm}u^{n-1}P_n^{(0)}(u) + B_{nm}u^{-n-2}R_n^{(0)}(u) \,, \tag{2.45}$$

where A_{nm} and B_{nm} are integration constants. The functions $P_n^{(0)}$ and $R_n^{(0)}$ are expressed by Gaussian hypergeometric functions ${}_2F_1$ (Abramowitz and Stegun 1964):

$$P_n^{(0)}(u) = {}_2F_1(-1+n, 1+n; 2(n+1); u) \tag{2.46}$$
$$R_n^{(0)}(u) = {}_2F_1(-2-n, -n; -2n; u). \tag{2.47}$$

The first few terms in the Taylor series of $P_n^{(0)}$ and $R_n^{(0)}$ around $u = 0$ are

$$\begin{aligned} P_n^{(0)}(u) &= 1 + \frac{1}{2}(n-1)u + \frac{(n+2)n(n-1)}{4(2n+3)}u^2 \\ &+ \frac{(n+3)(n^2-1)n}{24(2n+3)}u^3 + O(u^4) \,, \end{aligned} \tag{2.48}$$

and

$$\begin{aligned} R_n^{(0)}(u) &= 1 - \frac{2+n}{2}u + \frac{(n^2-1)(n+2)}{4(2n-1)}u^2 \\ &- \frac{(n^2-4)n(n+1)}{24(2n-1)}u^3 + O(u^4) \,. \end{aligned} \tag{2.49}$$

Using the relation (2.40) and the equation (2.45), we can write the solution for H as

$$H(r) = A_{nm}\frac{P_n^{(0)}\left(\frac{r_\mathrm{s}}{r}\right)}{r^n(r-r_\mathrm{s})} + B_{nm}\frac{r^{n+1}R_n^{(0)}\left(\frac{r_\mathrm{s}}{r}\right)}{r-r_\mathrm{s}} \,. \tag{2.50}$$

By combining equations (2.42) and (2.43) we can express function K with H:

$$K = H + \frac{H'}{w} + \frac{(2x-1)H}{wx(x-1)} \,. \tag{2.51}$$

and note that K is fully determined by H. Inserting in this expression the solution (2.50) for H, we obtain the solution for K:

$$K(r) = A_{nm} r^{-n-1} P_n^{(1)}\left(\frac{r_\mathrm{s}}{r}\right) + B_{nm} r^n R_n^{(1)}\left(\frac{r_\mathrm{s}}{r}\right) \ , \tag{2.52}$$

where the functions $P_n^{(1)}$ and $R_n^{(1)}$ are connected to $P_n^{(0)}$ and $R_n^{(0)}$. The first few terms of their Taylor expansion around $u = 0$ are

$$\begin{aligned} P_n^{(1)}(u) &= 1 - \frac{(n-2)(n+1)}{2(n-1)}u + \frac{(n-3)n(n+1)}{4(2n-1)}u^2 \\ &- \frac{(n-4)(n-2)n(n+1)}{24(2n-1)}u^3 + O(u^4) \ , \end{aligned} \tag{2.53}$$

and

$$\begin{aligned} R_n^{(1)}(u) &= 1 + \frac{n(n+3)}{2(n+2)}u + \frac{n(n+1)(n+4)}{4(2n+3)}u^2 \\ &+ \frac{n(n+1)(n+3)(n+5)}{24(2n+3)}u^3 + O(u^4) \ . \end{aligned} \tag{2.54}$$

Link to Newtonian coefficients To obtain the complete form of solutions for H and K, we need to determine the integration constants A_{nm} and B_{nm} in (2.50) and (2.52). Let us compare equation (2.50) with its Newtonian counterpart, i.e., the gravitational potential Φ of a non-rotating Earth expanded into a series of multipole contributions (Arfken 1985):

$$\Phi = \frac{GM}{r} + \sum_{nm} (M_{nm}^{\oplus} r^{-n-1} + M_{nm}^{\ominus} r^n) Y_n^m \ , \tag{2.55}$$

where $M_{nm}^{\oplus}$ and $M_{nm}^{\ominus}$ are time-independent spherical multipole momenta and notation $\sum_{nm} \equiv \sum_{n=2}^{\infty} \sum_{m=-n}^{n}$ is used (for more on multipoles see Appendix B.0.2). We choose the sign of (2.55) so that the force is $\mathbf{F} = \nabla\Phi$. The first term in the sum describes the gravitational potential of the perturbing sources positioned within the radius r, while the second term corresponds to those outside r. Comparing (2.50) with (2.55), we notice the same behaviour for $r \gg r_\mathrm{s}$ (i.e., the superposition of r^{-n-1} and r^n functional dependence) in the perturbative part of (2.55) and it is evident that the coefficients A_{nm} and B_{nm} are related to the multipole momenta. The relation between both is found from the weak field approximation

$$\frac{c^2}{2}(1 + g_{00}) \sim \Phi \ . \tag{2.56}$$

By inserting

$$g_{00} = g_{00}^{(0)} + \sum_{nm} (h_{00}^{nm})^{(\mathrm{e})} = X\left(-1 + \sum_{nm} H_{nm}\right) \tag{2.57}$$

into the above relation together with the Newtonian potential (2.55), we find that in the weak field limit A_{nm} and B_{nm} are asymptotically related to Newtonian spherical multipole momenta $M^{\oplus}_{nm}$ and $M^{\ominus}_{nm}$ as

$$A_{nm} \sim \frac{2}{c^2} M^{\oplus}_{nm} \quad \text{and} \quad B_{nm} \sim \frac{2}{c^2} M^{\ominus}_{nm} \,. \tag{2.58}$$

Note that for finite c, $M^{\oplus}_{nm}$ and $M^{\ominus}_{nm}$ only approximate A_{nm} and B_{nm}.[1]

Odd parity contributions

In case of time independent perturbations, the odd metric functions $(h^{nm}_{\mu\nu})^{(\mathrm{o})}$ in (2.29) have $h_1 = 0$ (Regge and Wheeler 1957) and can be written with a single function h_0 as

$$\begin{aligned} (h^{nm}_{\mu\nu})^{(\mathrm{o})} = &- h_0 \csc\theta \, Y^m_{n\,,\varphi} (\delta_{0,\mu}\delta_{2,\nu} + \delta_{2,\mu}\delta_{0,\nu}) \\ &+ h_0 \sin\theta \, Y^m_{n\,,\theta} (\delta_{0,\mu}\delta_{3,\nu} + \delta_{3,\mu}\delta_{0,\nu}) \,. \end{aligned} \tag{2.59}$$

The function h_0 is determined up to a pre-factor by equation

$$h_0'' + \frac{1}{X}\left[\frac{2}{x^3} - \frac{n(n+1)}{x^2}\right] h_0 = 0 \,, \tag{2.60}$$

We are interested in h_0 only at $x > 1$ and rewrite this equation using the variable $u = 1/x$ on the domain of interest $u \in [0, 1]$:

$$(1-u)u^2 \ddot{h}_0 + 2u(1-u)\dot{h}_0 + [2u - n(n+1)]h_0 = 0 \,, \tag{2.61}$$

The point $u = 0$ is a regular singular point, so it can be solved with Frobenius method in a similar way as equation (2.44). The solutions for h_0 is

$$h_0(r) = \alpha_{nm} r^{-n} P^{(2)}_n\left(\frac{r_\mathrm{s}}{r}\right) + \beta_{nm} r^{n+1} R^{(2)}_n\left(\frac{r_\mathrm{s}}{r}\right) \,, \tag{2.62}$$

where functions $P^{(2)}_n$ and $R^{(2)}_n$ are:

$$P^{(2)}_n(u) = {}_2F_1(-1+n, 2+n; 2(n+1); u) \tag{2.63}$$

$$R^{(2)}_n(u) = {}_2F_1(-2-n, 1-n; -2n; u) \,. \tag{2.64}$$

Their Taylor series around $u = 0$ are

$$\begin{aligned} P^{(2)}_n(u) = 1 &+ \frac{(n-1)(n+2)}{2(n+1)} u + \frac{(n-1)n(n+2)(n+3)}{4(n+1)(2n+3)} u^2 \\ &+ \frac{(n-1)n(n+3)(n+4)}{24(2n+3)} u^3 + O(u^4) \,, \end{aligned} \tag{2.65}$$

[1] For axial-symmetric case it was shown in Quevedo (1990); Backdahl and Herberthson (2005) that the leading order in the expansion of relativistic multipoles is identical to Newtonian multipoles.

and

$$R_n^{(2)}(u) = 1 - \frac{(n-1)(n+2)}{2n}u + \frac{(n^2-1)(n^2-4)}{4n(2n-1)}u^2 \\ - \frac{(n-3)(n^2-4)(n+1)}{24(2n-1)}u^3 + O(u^4)\,. \tag{2.66}$$

To determine the constants α_{nm} and β_{nm} in (2.62), we note that off-diagonal terms in the metric tensor are associated with frame-dragging effects. Since we are working in a weak field limit, we consider only the frame-dragging effect of Earth, and neglect frame-dragging effects arising from other celestial objects. Consequently, we set $\beta_{nm} = 0$, because the second term in (2.62) is due to objects outside r.

To determine α_{nm}, we notice that for $n = 1$ and $m = 0$ the corresponding h_0 matches the weak field and slow rotation approximation of the Kerr metric: if $r \gg r_\mathrm{s}$ and Earth's angular parameter is $a \ll 1$, then for $\alpha_{10} = a r_\mathrm{s}\sqrt{4\pi/3}$ it follows

$$h_0(r) = a\frac{r_\mathrm{s}}{r}\sqrt{\frac{4\pi}{3}}\,, \tag{2.67}$$

where we keep only the terms linear in a.

For higher multipoles ($n > 1$), it turns out that their dependence on a is not linear (Hartle and Sharp 1967). Therefore, the only multipole we include in the odd-parity metric function is the monopole, i.e., the one belonging to the linear (in a) part of the Kerr effect.

2.1.4 Time-dependent metric perturbations

Next we consider a slowly rotating Earth and weak gravitational influences of other nearby moving celestial objects. Therefore, we study time dependent perturbations of the Schwarzschild metric around the Earth, which is slowly rotating around z axis with angular velocity $\Omega_\oplus$. Due to Earth's rotation its multipoles vary periodically. Earth's tides can introduce additional time dependency in its multipoles (additional variability with different frequency, phase and varying amplitude, depending on the position of the Moon and the Sun). In addition, the gravitational influence of other celestial objects introduces time dependent perturbations to the space-time around the Earth, because their positions relative to Earth change with time. These perturbations can be expanded in a series of multipoles and treated with the same procedure as Earth's multipoles.[2] We consider time dependent metric perturbations for the case of perturbations oscillating slowly with angular velocities, which are smaller or of the same order of magnitude as $\Omega_\oplus$. Both angular velocities are defined with respect to the Schwarzschild time t.

[2]We considered also another approach, namely, to include perturbations due to the Moon, the Sun, Venus, and Jupiter with PPN Lagrangian as described in Einstein et al. (1938). We decided to use multipole expansion, because this approach is on our opinion more elegant and analogous to our treatment of Earth's multipoles.

Even-parity contributions

Even-parity modes $(h^{nm}_{\mu\nu})^{(\mathrm{e})}$ in (2.28) are connected to the Newtonian gravitational potential Φ, which in the case of time dependent multipoles can be written as:

$$\begin{aligned}\Phi = &\frac{GM}{r} \\ &+ \sum_{nm}(M^{\oplus}_{nm}(T)r^{-n-1} + M^{\ominus}_{nm}(T)r^{n})Y^{m}_{n} \,,\end{aligned} \tag{2.68}$$

where $T = ct$. Alternatively, it can be written in frequency domain as:

$$\begin{aligned}\Phi = &\frac{GM}{r} + \sum_{nm}\int_{-\infty}^{\infty}\mathrm{d}k\, e^{\mathrm{i}kT}\times \\ &\left[\widetilde{M}^{\oplus}_{nm}(k)r^{-n-1} + \widetilde{M}^{\ominus}_{nm}(k)r^{n}\right]Y^{m}_{n} \,,\end{aligned} \tag{2.69}$$

where k is the wavenumber and $\widetilde{M}^{\oplus}_{nm}$, $\widetilde{M}^{\ominus}_{nm}$ are the Fourier transforms of time dependent multipoles:

$$\widetilde{M}^{v}_{nm}(k) = \frac{1}{2\pi}\int_{-\infty}^{\infty}\mathrm{d}T\, e^{-\mathrm{i}kT}M^{v}_{nm}(T) \,, \tag{2.70}$$

where $v = \oplus, \ominus$.

Each time dependent multipole generates a time-dependent even metric perturbation $(h^{nm}_{\mu\nu})^{(\mathrm{e})}$. Functions H, H_1, and K determining the modes can be expressed with their Fourier transforms:

$$\begin{aligned}&(H(T,r), H_1(T,r), K(T,r)) = \\ &\int_{-\infty}^{\infty}\mathrm{d}k\, e^{\mathrm{i}kT}(\widetilde{H}(k,r), \widetilde{H}_1(k,r), \widetilde{K}(k,r)) \,.\end{aligned} \tag{2.71}$$

Using ansatz (2.71) in field equations (2.30) - (2.35) yields only three independent differential equations (with $()' = \mathrm{d}/\mathrm{d}r$) (Regge and Wheeler 1957):

$$\mathrm{i}k\left(\widetilde{K}' + \frac{\widetilde{K} - \widetilde{H}}{r} - \frac{r_{\mathrm{s}}}{2r^2X}\widetilde{K}\right) - \frac{q}{r^2}\widetilde{H}_1 = 0 \tag{2.72}$$

$$(X\widetilde{H}_1)' - \mathrm{i}k(\widetilde{K} + \widetilde{H}) = 0 \tag{2.73}$$

$$\mathrm{i}k\widetilde{H}_1 + X(\widetilde{K} - \widetilde{H})' - \frac{r_{\mathrm{s}}}{r}\widetilde{H} = 0 \,, \tag{2.74}$$

and an algebraic relation (Zerilli 1970):

$$\begin{aligned}&\left[\frac{3r_{\mathrm{s}}}{r} + w\right]\widetilde{H} + \mathrm{i}\left[2kr - q\frac{r_{\mathrm{s}}}{2kr^2}\right]\widetilde{H}_1 \\ &- \left[w + \frac{r_{\mathrm{s}}}{r} - \frac{2}{X}\left(\frac{r_{\mathrm{s}}^2}{(2r)^2} + (kr)^2\right)\right]\widetilde{K} = 0 \,,\end{aligned} \tag{2.75}$$

where $q = n(n+1)$. With variables $x = r/r_\mathrm{s}$ and $\kappa = kr_\mathrm{s}$, we can write this algebraic relation in a dimensionless form

$$\begin{aligned}&\left[\frac{3}{x} + w\right]\widetilde{H} + \mathrm{i}\left[2\kappa x - \frac{q}{2\kappa x^2}\right]\widetilde{H}_1 \\ &- \left[w + \frac{1}{x} - \frac{2x}{x-1}\left(\frac{1}{(2x)^2} + (\kappa x)^2\right)\right]\widetilde{K} = 0\,.\end{aligned} \tag{2.76}$$

Because in our studies $\kappa \ll 1$, we solve equations (2.72) - (2.75) perturbatively in κ. We assume that $\widetilde{H}$, $\widetilde{H}_1$, and $\widetilde{K}$ are smooth functions of κ, and write them as a power series of κ. We find that an appropriate expansion of these functions for $\kappa \to 0$ has the form

$$(\widetilde{H}, \widetilde{H}_1, \widetilde{K}) \sim \widetilde{N}(\kappa)\sum_{i=0}^{\infty}\kappa^{2i}(\widetilde{a}_i(r), \mathrm{i}\kappa\widetilde{b}_i(r), \widetilde{c}_i(r))\,. \tag{2.77}$$

Inserting this ansatz in the equations (2.72)-(2.74) and neglecting all higher than leading terms in the expansion (2.77), gives us two solutions for each function. The leading orders of $\widetilde{H}$ and $\widetilde{K}$ are given in (2.50) and (2.52), respectively, where instead of A_{nm}, B_{nm} from (2.58) we use another set of constants $\widetilde{A}_{nm}, \widetilde{B}_{nm}$ to describe a general case:

$$\widetilde{H}(k,r) \sim \widetilde{A}_{nm}(k)\frac{P_n^{(0)}\left(\frac{r_\mathrm{s}}{r}\right)}{r^n(r-r_\mathrm{s})} + \widetilde{B}_{nm}(k)\frac{r^{n+1}R_n^{(0)}\left(\frac{r_\mathrm{s}}{r}\right)}{r-r_\mathrm{s}} + O(\kappa^2)\,. \tag{2.78}$$

$$\widetilde{K}(k,r) \sim \widetilde{A}_{nm}(k)r^{-n-1}P_n^{(1)}\left(\frac{r_\mathrm{s}}{r}\right) + \widetilde{B}_{nm}(k)r^n R_n^{(1)}\left(\frac{r_\mathrm{s}}{r}\right) + O(\kappa^2)\,. \tag{2.79}$$

From the algebraic relation (2.75) we get the leading orders of $\widetilde{H}_1$:

$$\widetilde{H}_1(k,r) \sim -\frac{i\kappa}{q}\left(\frac{r}{r_\mathrm{s}}\right)^2\left[\frac{6r_\mathrm{s}}{r} + w(\widetilde{H}+\widetilde{K}) - \frac{4\widetilde{K}r_\mathrm{s}}{r-r_\mathrm{s}}\right] + O(\kappa^3)\,. \tag{2.80}$$

Using the above solutions for $\widetilde{H}$ and $\widetilde{K}$, (2.78) - (2.79), we can rewrite this in a more explicit form:

$$\widetilde{H}_1(k,r) \sim \widetilde{A}_{nm}(k)\frac{r^{-n+1}P_n^{(3)}\left(\frac{r_\mathrm{s}}{r}\right)}{r_\mathrm{s}(r-r_\mathrm{s})} + \widetilde{B}_{nm}(k)\frac{r^{n+2}R_n^{(3)}\left(\frac{r_\mathrm{s}}{r}\right)}{r_\mathrm{s}(r-r_\mathrm{s})}\,, \tag{2.81}$$

where functions $P_n^{(3)}$ and $R_n^{(3)}$ are given as a series in $u = r_\mathrm{s}/r$ for $u \to 0$:

$$\begin{aligned}P_n^{(3)}(u) &= \frac{2}{n} + \frac{n^2+3n+1}{(n+1)(n+2)}u + \frac{n^3+5n^2+6n+3}{2(n+2)(2n+3)}u^2 \\ &+ \frac{n^3+6n^2+8n+6}{12(2n+3)}u^3 + O(u^4)\,,\end{aligned} \tag{2.82}$$

and

$$R_n^{(3)}(u) = -\frac{2}{n+1} + \frac{n^2-n-1}{(n-1)n}u - \frac{n^3-2n^2-n-1}{2(n-1)(2n-1)}u^2 + \frac{n^3-3n^2-n-3}{12(2n-1)}u^3 + O(u^4)\,. \tag{2.83}$$

By considering the weak field limit (2.56) we find that

$$\widetilde{A}_{nm} \sim \frac{2}{c^2}\widetilde{M}^{\oplus}_{nm} \quad \text{and} \quad \widetilde{B}_{nm} \sim \frac{2}{c^2}\widetilde{M}^{\ominus}_{nm}\,. \tag{2.84}$$

The metric perturbation expressed with these functions is accurate up to the linear order in frequency. Since higher order perturbations naturally give rise to contributions with higher orders of frequencies, our approximation of the perturbation is consistently linear, i.e., it is linear in frequencies and in the order of perturbation.

Odd-parity contributions

For odd-parity contribution to the metric $(h^{nm}_{\mu\nu})^{(\mathrm{o})}$ (2.28) we use the same notation for solutions h_0, h_1 as in (2.71):

$$(h_0(T,r), h_1(T,r)) = \int_{-\infty}^{\infty} \mathrm{d}k\, e^{\mathrm{i}kT}(\tilde{h}_0(k,r), \tilde{h}_1(k,r))\,. \tag{2.85}$$

Because we are interested only in persistent phenomena, we limit ourselves to real wavenumbers, $k \in \mathbb{R}$. A more detailed discussion of all possible solutions is given in e.g. Vishveshwara (1970). Using ansatz (2.85) in field equations (2.36)-(2.38) for odd metric functions, we obtain only two independent equations

$$\mathrm{i}k\tilde{h}_0 - X(X\tilde{h}_1)' = 0\,, \tag{2.86}$$

$$k^2\tilde{h}_1 + \mathrm{i}k(\tilde{h}_0' - 2\frac{\tilde{h}_0}{r}) - wX\frac{\tilde{h}_1}{r^2} = 0\,, \tag{2.87}$$

with $()' = \mathrm{d}/\mathrm{d}r$. It was shown by Regge and Wheeler (1957) that we can use a substitution for h_1:

$$Q = X\frac{\tilde{h}_1}{r} \tag{2.88}$$

to eliminate h_0 from both equations. Thereby we obtain a wave equation for Q in the form

$$\frac{\mathrm{d}^2}{\mathrm{d}r_*^2}Q + k^2_{\mathrm{eff}}Q = 0\,, \tag{2.89}$$

where r_* is modified radius defined as

$$\mathrm{d}r_* = X^{-1}\mathrm{d}r \quad \text{or} \quad r^* = r + r_{\mathrm{s}}\log(r - r_{\mathrm{s}}) + \text{const.} \tag{2.90}$$

and an effective wave number

$$k_{\text{eff}}^2 = k^2 - \frac{n(n+1)X}{r^2} + 3\frac{r_{\text{s}}X}{r^3} \,. \tag{2.91}$$

By knowing Q, we can express $\tilde{h}_1$ from (2.88) and write $\tilde{h}_0$ using (2.86) as:

$$\tilde{h}_0 = -\frac{\mathrm{i}}{k} X (rQ)' \,. \tag{2.92}$$

From equation (2.89) we find that in the limit $r \to \infty$ its solution is $Q(r) \asymp \sin(kr+\phi)$. This determines asymptotic behavior of $\tilde{h}_0$ and $\tilde{h}_1$:

$$\tilde{h}_1(r) \asymp r \sin(kr+\phi) \quad \text{and} \quad \tilde{h}_0(r) \asymp r \cos(kr+\phi) \,. \tag{2.93}$$

We see that the asymptotic behaviour of solutions $\tilde{h}_0$ and $\tilde{h}_1$ is not flat, and therefore, these solutions are not relevant in our case. Because we neglect frame-dragging effects arising from other objects, as mentioned in 2.1.3, we neglect time dependent odd-parity contributions all together.

2.1.5 Metric around Earth

Finally, we can write the metric perturbation $h_{\mu\nu}$ around Earth, which in (2.6) was expressed as a series of normal modes $(h_{\mu\nu}^{nm})^{(\text{o})}$ and $(h_{\mu\nu}^{nm})^{(\text{e})}$. Based on the positions of the sources of perturbations, these modes can be grouped into two terms:

$$h_{\mu\nu} = h_{\mu\nu}^{\oplus} + h_{\mu\nu}^{\ominus} \,. \tag{2.94}$$

The term $h_{\mu\nu}^{\oplus}$ represents Earth's time dependent (exterior) multipoles (i.e., even-parity modes given in 2.1.4 with $\widetilde{B}_{nm} = 0$) and the Earth's frame-dragging effect via the Kerr contribution given in 2.1.3. This metric perturbation is asymptotically flat. In non-relativistic description we could say that the former arise from the shape of the Earth, which changes with time due to rotation and tidal forces. For the latter, Kerr effect, there is no non-relativistic counterpart.

The term $h_{\mu\nu}^{\ominus}$ represents the time dependent (interior) multipoles of other celestial bodies (i.e. even-parity modes given in 2.1.4 with $\widetilde{A}_{nm} = 0$). Their frame-dragging effect is neglected. The elements of this metric perturbation increase with radius, which means that this perturbation is not asymptotically flat. In non-relativistic description we could say that this term arises from the perturbative effects of other bodies, i.e. the Moon, The Sun, Venus, Jupiter etc., whose positions relative to Earth change with time.

To simplify expressions, we introduce the normalized complex multipoles ($v = \oplus, \ominus$) defined as:

$$\overline{M}_{nm}^{v} := \frac{2}{c^2} M_{nm}^{v} \,. \tag{2.95}$$

Taking into account the results of previous subsections, we can write the metric perturbations in a compact form. Metric perturbation due to Earth's multipoles and rotation can be written as:

$$
\begin{aligned}
&[h^{\oplus}_{\mu\nu}] = \sum_{nm} \overline{M}^{\oplus}_{nm} Y^m_n . \\
&\mathrm{diag}\left(\frac{P^{(0)}_n}{r^{n+1}}, \frac{P^{(0)}_n}{r^{n-1}(r-r_\mathrm{s})^2}, \frac{P^{(1)}_n}{r^{n-1}}, \frac{P^{(1)}_n \sin^2\theta}{r^{n-1}} \right) \\
&+ \sum_{nm} \overline{M}^{\oplus}_{nm,T} Y^m_n \frac{P^{(3)}_n}{r^{n-1}(r-r_\mathrm{s})} (\delta_{\mu,1}\delta_{\nu,0} + \delta_{\nu,1}\delta_{\mu,0}) \\
&- a\frac{r_\mathrm{s}}{r} \sin^2\theta (\delta_{\mu,3}\delta_{\nu,0} + \delta_{\nu,3}\delta_{\mu,0}) \ ,
\end{aligned}
\tag{2.96}
$$

where Earth's multipoles $\overline{M}^{\oplus}_{nm}$ are functions of time and include rotation and tides; and $\overline{M}^{\oplus}_{nm,T}$ are their time derivatives. Therefore, the first two terms in (2.96) describe the metric perturbation due to oscillating/rotating? multipoles and tides, while the third describes the Kerr frame-dragging effect.

Metric perturbations due to other celestial bodies are

$$
\begin{aligned}
&[h^{\ominus}_{\mu\nu}] = \sum_{nm} \overline{M}^{\ominus}_{nm} Y^m_n . \\
&\mathrm{diag}\left(r^n R^{(0)}_n, \frac{r^{n+2} R^{(0)}_n}{(r-r_\mathrm{s})^2}, r^{n+2} R^{(1)}_n, r^{n+2} R^{(1)}_n \sin^2\theta \right) \\
&+ \sum_{nm} \overline{M}^{\ominus}_{nm,T} Y^m_n \frac{r^{n+2} R^{(3)}}{r-r_\mathrm{s}} (\delta_{\mu,1}\delta_{\nu,0} + \delta_{\nu,1}\delta_{\mu,0}) \ .
\end{aligned}
\tag{2.97}
$$

where $\overline{M}^{\ominus}_{nm}$ are summed multipoles of other bodies.

We note again that multipole coefficients $\overline{M}_{nm}$ are expansion coefficients of the Newtonian potential, which are only the leading order approximations in $c \to \infty$ of exact relativistic coefficients. The first order approximations of the metric perturbations given by (2.96) and (2.97) are fully determined by multipole momenta $\overline{M}^{\oplus}_{nm}$, $\overline{M}^{\ominus}_{nm}$, Kerr parameter a, and functions $P^{(i)}_n$ and $R^{(i)}_n$.

Conclusions for WP1: In WP1 we built a scheme for including gravitational perturbations to the background of the Schwarzschild metric in the weak-field limit with the linear perturbation theory. The solutions (beyond the dominant monopole) were obtained using the RWZ formalism, i.e. the perturbations were expanded in terms of tensor spherical harmonics or normal modes. We used the $c \to \infty$ limit to find connection between our solutions and Newtonian multipole coefficients. The frame-dragging effect of the central object is taken into account by the first order term in the expansion of the Kerr metric for $a \ll 1$.

The result is a perturbed Schwarzschild metric, with perturbations incorporating effects due to Earth's multipoles, tides and rotation, and weak gravitational influences

of other Solar System objects. It is written with explicit expressions (2.96) and (2.97) for the perturbative metric. The first order approximations of the metric perturbations given by (2.96) and (2.97) are fully determined by multipole momenta $\overline{M}^{\oplus}_{nm}$, $\overline{M}^{\ominus}_{nm}$, Kerr parameter a, and functions $P_n^{(i)}$ and $R_n^{(i)}$.

2.2 Work Package 2 - Dynamics of satellites

Abstract of WP2: In WP2 we calculate satellite dynamics in perturbed space-time. We use perturbed metric derived in WP1 and perturbative Hamiltonian formalism to obtain time derivatives of 0^{th} order constants of motion. With the derivatives known, we are able to determine the time evolution of 0^{th} order constants of motion and because they are varying slowly, we apply them to analytic solutions for Schwarzschild geodesics to obtain satellites' orbits in perturbed space-time. We investigate the influence of gravitational perturbations on the orbital parameter evolution and on the satellite's position and time. We estimate the influence of gravitational perturbations on the user-satellite and inter-satellite light signal propagation.

We treat satellites as point like test-objects and neglect their effect on the space-time metric. Their trajectories are described in space-time as a curve $x^\mu(\tau)$, where τ is the proper time. The dynamics is treated in the Lagrangian and Hamiltonian formalism.

The Lagrangian function of the satellite dynamics in a space-time metric can be written as

$$L(x^\mu, \dot{x}^\mu) = \frac{1}{2} g_{\mu\nu}(x^\alpha)\dot{x}^\mu \dot{x}^\nu \,, \tag{2.98}$$

where $\dot{()} = \frac{\mathrm{d}}{\mathrm{d}\tau}$. The equations of motion are then given by the Lagrange equation

$$\frac{\mathrm{d}}{\mathrm{d}\tau}\left(\frac{\partial L}{\partial \dot{x}^\nu}\right) - \frac{\partial L}{\partial x^\nu} = 0 \,, \tag{2.99}$$

which can be rewritten in a form of the geodesic equation

$$\frac{\mathrm{d}^2 x^\mu}{\mathrm{d}\tau^2} + \Gamma^\mu_{\alpha\beta}\frac{\mathrm{d}x^\alpha}{\mathrm{d}\tau}\frac{\mathrm{d}x^\beta}{\mathrm{d}\tau} = 0 \,, \tag{2.100}$$

where $\Gamma^c_{ab} = \frac{1}{2}g^{cd}(g_{da,b} + g_{db,a} - g_{ab,d})$ are the Christoffel symbols of the second kind. Note that the metric is approximated as in 2.2: $g_{\mu\nu} = g^{(0)}_{\mu\nu} + h_{\mu\nu} + O(h^2)$.

The Hamiltonian formalism offers a more convenient way to write equations of motion. By introducing the momenta

$$p_\nu = \frac{\partial L}{\partial \dot{x}^\nu} = g_{\nu\mu}\dot{x}^\mu \,, \tag{2.101}$$

we can define the Hamiltonian

$$H(x^\mu, p_\mu) = p_\mu \dot{x}^\mu - L = \frac{1}{2} g^{\mu\nu}(x^\alpha) p_\mu p_\nu \,. \tag{2.102}$$

Taking into account that $g_{\mu\nu}$ is exactly given only up to the linear order in perturbation $h_{\mu\nu}$, we can express the inverse metric tensor $g^{\mu\nu}$ up to the same order as[3]

$$g^{\mu\nu} = g^{\mu\nu(0)} - h^{\mu\nu} + O(h^2)\,, \tag{2.103}$$

where the inverse metric perturbation $h^{\mu\nu}$ is

$$h^{\mu\nu} = g^{\mu\alpha(0)} g^{\nu\beta(0)} h_{\alpha\beta} \tag{2.104}$$

and $g^{\mu\nu(0)}$ is the inverse unperturbed metric tensor.

Using the expansion of the inverse of the metric (2.103) in the expression of the Hamiltonian H (2.102), we get

$$H = \underbrace{\frac{1}{2} g^{\mu\nu(0)} p_\mu p_\nu}_{H^{(0)}} \underbrace{- \frac{1}{2} h^{\mu\nu} p_\mu p_\nu}_{\Delta H} \tag{2.105}$$

with the unperturbed Hamiltonian $H^{(0)}$ and the perturbative part ΔH, where higher than linear orders in metric perturbations are omitted.[4]

The satellite's trajectory $(x^\nu(\tau), p_\nu(\tau))$ is then given by the Hamilton equations

$$\dot{x}^\nu = \frac{\partial H}{\partial p_\nu} \quad \text{and} \quad \dot{p}_\nu = -\frac{\partial H}{\partial x^\nu}\,, \tag{2.106}$$

which is an alternative way of writing the geodesic equation (2.100).

2.2.1 Hamiltonian formalism in the Schwarzschild space-time

The Schwarzschild metric is:

$$g_{\mu\nu} = \begin{bmatrix} -(1 - \frac{2M}{r}) & 0 & 0 & 0 \\ 0 & \frac{1}{1-2M/r} & 0 & 0 \\ 0 & 0 & r^2 & 0 \\ 0 & 0 & 0 & r^2 \sin^2\theta \end{bmatrix}\,, \tag{2.107}$$

where $M = GM_\mathrm{E}/c^2$ (M_E is the Earth mass). In Schwarzschild coordinates, the Lagrangian and the Hamiltonian are:

$$L = \frac{1}{2}\left[-\left(1 - \frac{2M}{r}\right)\dot{t}^2 + \frac{1}{1 - \frac{2M}{r}}\dot{r}^2 + r^2\left(\dot{\theta}^2 + \sin^2\theta\ \dot{\phi}^2\right)\right] \tag{2.108}$$

[3] Let us assume that we have invertible matrix A and its perturbation δA, then if $\|A^{-1}\delta A\|_2 < 1$, the inverse of $A + \Delta A$ can be given as a series $(A+\delta A)^{-1} = (1 + A^{-1}\delta A)^{-1} A^{-1} = \sum_{n=0}^{\infty} (-1)^n (A^{-1}\delta A)^n A^{-1}$, where we use $(1+x)^{-1} = \sum_{n=0}^{\infty}(-x)^n$ for $|x| < 1$. In our case we use only the first two terms in the sum.

[4] When comparing dynamics obtained by Hamiltonians H and $H^{(0)}$, it should be noted that the momenta p_μ and $p_\mu^{(0)}$ associated to the two Hamiltonians differ in interpretation; inserting the approximation of the metric $g_{\mu\nu}$ (2.2) into (2.101), it follows that $p_\nu = \underbrace{g^{(0)}_{\nu\mu}\dot{x}^\mu}_{p^{(0)}_\nu} - h_{\nu\mu}\dot{x}^\mu$.

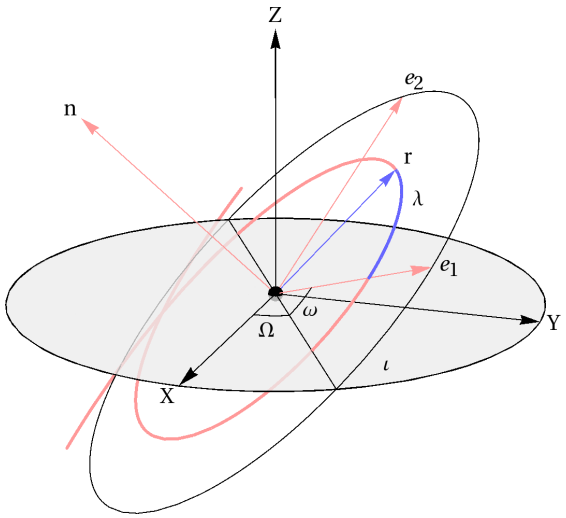

Figure 2.2: The orbital plane: $\hat{n}$ is a unit vector normal to the orbital plane, ι orbital inclination, Ω the longitude of the ascending node, ω the longitude of the apoapsis, and λ the true anomaly.

$$H = \frac{1}{2}\left[-\frac{1}{1-\frac{2M}{r}}\,p_t^2 + \left(1-\frac{2M}{r}\right)p_r^2 + \frac{1}{r^2}\left(p_\theta^2 + \frac{1}{\sin^2\theta}\,p_\phi^2\right)\right], \tag{2.109}$$

wtih the conjugate momenta:

$$p_t = \frac{\partial L}{\partial \dot{t}} = -\left(1-\frac{2M}{r}\right)\dot{t} = -E = \text{const.} \quad \text{(orbital energy)} \tag{2.110}$$

$$p_r = \frac{\partial L}{\partial \dot{r}} = \frac{1}{1-\frac{2M}{r}}\dot{r} \neq \text{const.} \tag{2.111}$$

$$p_\theta = \frac{\partial L}{\partial \dot{\theta}} = r^2\dot{\theta} \neq \text{const.} \tag{2.112}$$

$$p_\phi = \frac{\partial L}{\partial \dot{\phi}} = r^2\sin^2\theta\;\dot{\phi} = l_z = \text{const.} \quad (z\text{-component of the ang. mom.})\,. \tag{2.113}$$

Therefore, we have the coordinates q^μ and the momenta p_μ

$$(q^\mu, p_\mu) = (t, r, \theta, \phi, p_t, p_r, p_\theta, p_\phi)\,. \tag{2.114}$$

Next, we do a canonical transformation $F_2 : (q^\mu, p_\mu) \to (Q^\mu, P_\mu)$, such that (Q^μ, P_μ) are constant for the above Hamiltonian:

$$P_0 = H \quad \text{(Hamiltonian)} \tag{2.115}$$

$$P_1 = -p_t = E \quad \text{(orbital energy)} \tag{2.116}$$

$$P_2 = +\sqrt{p_\theta^2 + \frac{p_\phi^2}{\sin^2\theta}} = l \quad \text{(magnitude of the ang. mom.)} \tag{2.117}$$

$$P_3 = p_\phi = l_z \quad (z\text{-component of the ang. mom.}) \tag{2.118}$$

$$Q^0 = -\tau - \int_{r_a}^{r} \frac{dr}{\sqrt{P_1^2 - X(-2P_0 + P_2^2/r^2)}} = -\tau_a \quad \text{(proper time of the first apo. passage)} \tag{2.119}$$

$$Q^1 = -t - \int_{r_a}^{r} \frac{P_1}{X\sqrt{P_1^2 - X(-2P_0 + P_2^2/r^2)}} dr = -t_a \quad \text{(time of the first apo. passage)} \tag{2.120}$$

$$Q^2 = \int_{r_p}^{r} \frac{P_2}{r^2\sqrt{P_1^2 - X(-2P_0 + P_2^2/r^2)}} dr - \int_{\pi/2}^{\theta} \frac{P_2}{\sqrt{P_2^2 - P_3^2/\sin^2\theta}} d\theta = \omega \quad \text{(long. of the first apo. passage)} \tag{2.121}$$

$$Q^3 = \phi + \int_{\pi/2}^{\theta} \frac{P_3}{\sin^2\theta\sqrt{P_2^2 - P_3^2/\sin^2\theta}} d\theta = \Omega \quad \text{(longitude of the ascending node)}, \tag{2.122}$$

where $X = 1 - 2M/r$ and r_a the radius at the apoapsis.[5]

The above orbital parameters (Q^μ, P_μ) are used to find the analytical solutions for the orbits of the form

$$t = t(\lambda|Q^\mu, P_\mu) \quad r = r(\lambda|Q^\mu, P_\mu) \quad \theta = \theta(\lambda|Q^\mu, P_\mu) \quad \phi = \phi(\lambda|Q^\mu, P_\mu)\ , \tag{2.123}$$

where λ is the true anomaly (Kostić 2012; Gomboc 2001). With a known relation $\tau = \tau(\lambda)$, it is possible to calculate the coordinates and momenta (q^μ, p_μ) at any given proper time τ of the satellite. For geometric representation of Q^2 and Q^3 see Fig. 2.2. For detailed analysis of the canonical transformation and additional information on (Q^μ, P_μ), as well as equation of orbit, see Appendices A, A.1, and A.2, respectively.

2.2.2 Perturbative Hamiltonian

If the metric is perturbed by $h_{\mu\nu}$, we get additional ΔH to the Hamiltonian

$$\Delta H = \frac{1}{2} h^{\mu\nu} p_\mu p_\nu\ . \tag{2.124}$$

Consequently, (Q^μ, P_μ) are no longer constants of motion - they are slowly changing functions of time. Their evolution can be calculated from (Goldstein 1980):

$$\dot{Q}^\lambda = \left.\frac{\partial H}{\partial P_\lambda}\right|_{Q^\lambda, P_\lambda} = -\left.\frac{\partial \Delta H}{\partial P_\lambda}\right|_{Q^\lambda, P_\lambda} = -\frac{1}{2}\frac{\partial(h^{\mu\nu} p_\mu p_\nu)}{\partial P_\lambda} \tag{2.125}$$

$$\dot{P}_\lambda = -\left.\frac{\partial H}{\partial Q^\lambda}\right|_{Q^\lambda, P_\lambda} = \left.\frac{\partial \Delta H}{\partial Q^\lambda}\right|_{Q^\lambda, P_\lambda} = \frac{1}{2}\frac{\partial(h^{\mu\nu} p_\mu p_\nu)}{\partial Q^\lambda}\ . \tag{2.126}$$

[5] In Keplerian orbits it is customary to take the time of the periapsis passage. However, in Schwarzschild case it is better to work with the time of the apopasis passage, since this simplifies some equations.

Expanding above equations into:

$$\dot{Q}^\lambda = -\frac{1}{2}\left(\frac{\partial h^{\mu\nu}}{\partial P_\lambda}p_\mu p_\nu + h^{\mu\nu}\frac{\partial p_\mu}{\partial P_\lambda}p_\nu + h^{\mu\nu}p_\mu\frac{\partial p_\nu}{\partial P_\lambda}\right)_{Q^\lambda,P_\lambda} \tag{2.127}$$

$$\dot{P}_\lambda = \frac{1}{2}\left(\frac{\partial h^{\mu\nu}}{\partial Q^\lambda}p_\mu p_\nu + h^{\mu\nu}\frac{\partial p_\mu}{\partial Q^\lambda}p_\nu + h^{\mu\nu}p_\mu\frac{\partial p_\nu}{\partial Q^\lambda}\right)_{Q^\lambda,P_\lambda}, \tag{2.128}$$

and taking into account that perturbative metric depends only on coordinates q^μ:

$$\frac{\partial h^{\mu\nu}}{\partial P_\lambda} = \frac{\partial h^{\mu\nu}}{\partial t}\frac{\partial t}{\partial P_\lambda} + \frac{\partial h^{\mu\nu}}{\partial r}\frac{\partial r}{\partial P_\lambda} + \frac{\partial h^{\mu\nu}}{\partial \theta}\frac{\partial \theta}{\partial P_\lambda} + \frac{\partial h^{\mu\nu}}{\partial \phi}\frac{\partial \phi}{\partial P_\lambda} \tag{2.129}$$

$$\frac{\partial h^{\mu\nu}}{\partial Q^\lambda} = \frac{\partial h^{\mu\nu}}{\partial t}\frac{\partial t}{\partial Q^\lambda} + \frac{\partial h^{\mu\nu}}{\partial r}\frac{\partial r}{\partial Q^\lambda} + \frac{\partial h^{\mu\nu}}{\partial \theta}\frac{\partial \theta}{\partial Q^\lambda} + \frac{\partial h^{\mu\nu}}{\partial \phi}\frac{\partial \phi}{\partial Q^\lambda}, \tag{2.130}$$

it becomes clear, that we have to calculate all possible derivatives of the form

$$\frac{\partial p_\mu}{\partial Q^\mu}, \frac{\partial q^\mu}{\partial Q^\mu}, \frac{\partial p_\mu}{\partial P_\mu}, \frac{\partial q^\mu}{\partial P_\mu} \tag{2.131}$$

to obtain the final expressions for the derivatives (2.127) – (2.128). Detailed derivations are given in App. A.3

The Eqs. (2.127) and (2.128) can be numerically integrated to obtain the solutions for $Q^\mu(\tau|Q^\mu, P_\mu)$ and $P_\mu(\tau|Q^\mu, P_\mu)$, which are then used to replace (Q^μ, P_μ) in the analytical expressions for unperturbed orbits (2.123). In this way, the perturbed orbit is described as time-evolving unperturbed orbit:

$$\begin{aligned} t &= t(\tau|Q^\mu(\tau), P_\mu(\tau)) \qquad r = r(\tau|Q^\mu(\tau), P_\mu(\tau)) \\ \theta &= \theta(\tau|Q^\mu(\tau), P_\mu(\tau)) \qquad \phi = \phi(\tau|Q^\mu(\tau), P_\mu(\tau)) \,. \end{aligned} \tag{2.132}$$

2.2.3 Evolution of Orbits

To obtain satellite orbits, we need to calculate the evolution of orbital parameters (2.115)-(2.122), i.e. numerically solve equations (2.125) and (2.126). In doing so, we first have to calculate the metric perturbation $h_{\mu\nu}$.

In case of **Kerr contribution** metric perturbation is already well known: we use (2.67) in (2.29). We verified that non-linear terms in Kerr contribution are much smaller than linear contributions and we may neglect them. Only the rotation of the Earth's monopole is large enough for required accuracy (see also Hartle (1967), Hartle and Sharp (1967)). In fact, the perturbation due to Earth's rotation is the smallest perturbation, which we take into account. We have also confirmed that spin-spin and spin-orbit couplings between a satellite and Earth are negligible.

For all other perturbations, we use multipole expansion and the results from subsection 2.1.4 in the following way.

Calculation of multipoles: The contributions of the Moon, the Sun, Venus, and Jupiter to the metric are described by a multipole expansion, where the multipole momenta are calculated from the positions of these objects, as shown in the Appendix B.0.2. The tidal effects of the Sun and the Moon on the Earth crust and oceans were modelled with time changing Earth multipoles. The dependence of the small multipole changes on Sun's and Moon's positions is presented in the Appendix B.0.3. In both cases, the positions were obtained from the ephemerides NASA JPL's Solar System Dynamics group (2013).

The positions of celestial bodies were sampled with a time interval of 1 hour, from 1 January 2012 to 31 December 2012, however, since during the numerical integration of (2.125) and (2.126) a much finer sampling is required, we used interpolation for intermediate points. To make sure that even the weakest contributions are not lost in numerical noise, we used very accurate interpolation and integration scheme and did all the calculations in 128-bit floating point precision. Furthermore, because the calculations should also be performed as fast as possible it is best to use a higher order integration method. To meet both criteria, we used the 8-th order B-splines for interpolation and the 8-th order Runge-Kutta for integration.[6]

Results:

We set initial values of a satellite orbit: $t_a = 7$ h, $\omega = 0^\circ$, $\Omega = 0^\circ$, $a = 29600$ km, $\varepsilon = 0.007$, $\iota = 56^\circ$. We then calculated the evolution of orbital parameters for each perturbation individually as well as for the sum of all perturbations. Results are shown in Figs. 2.3 – 2.11, where we converted the conjugate momenta (E, l, l_z) into the more convenient set of parameters, i.e. major semi-axis a, eccentricity ε, and inclination ι. The graphs on the left and right side show the evolution for a period of one year and one week, respectively.

Effects of individual perturbations on orbital parameters The results for each individual perturbation show similar behavior, i.e. an oscillating and a secular contribution. As expected, the effects due to multipoles and the Moon produce the biggest changes in parameters, with the amplitudes of the oscillations of $\Delta\omega \approx 0.15^\circ - 0.35^\circ$, $\Delta\Omega \approx 0.36'' - 3.6''$, $\Delta\iota \approx 0.7'' - 7''$, $\Delta a \approx 400 - 3000$ m, and $\Delta\varepsilon \approx 2 \times 10^{-5} - 8 \times 10^{-5}$. When it comes to secular changes, the multipoles induce the biggest changes in all parameters – except in inclination. After a year, the changes fir Earth multipoles and the Moon are $\Delta\omega \approx 2^\circ - 4^\circ$, $\Delta\Omega \approx 0.5^\circ - 9.5^\circ$, $\Delta a = 0$, $\Delta\iota = 0$ (Earth), $\Delta\iota \approx 0.06^\circ$ (Moon), and $\Delta\varepsilon \approx 2 \times 10^{-5} - 8 \times 10^{-5}$.

The smallest changes in parameters come from the Kerr effect, with the amplitudes of the oscillations of $\Delta\omega \approx 12$ mas, $\Delta\omega \approx 10^{-3}$ mas, $\Delta a \approx 0.37$m, and $\Delta\varepsilon \approx 9 \times 10^{-10}$. The changes in one year are $\Delta\omega \approx -4.4$ mas, and $\Delta\Omega \approx 2.5$ mas. The remaining parameters have no secular changes.

[6] We used Intel C++ and Fortran compilers since these offer native support for 128-bit floating point precision and are thus faster than any other software multiprecision library.

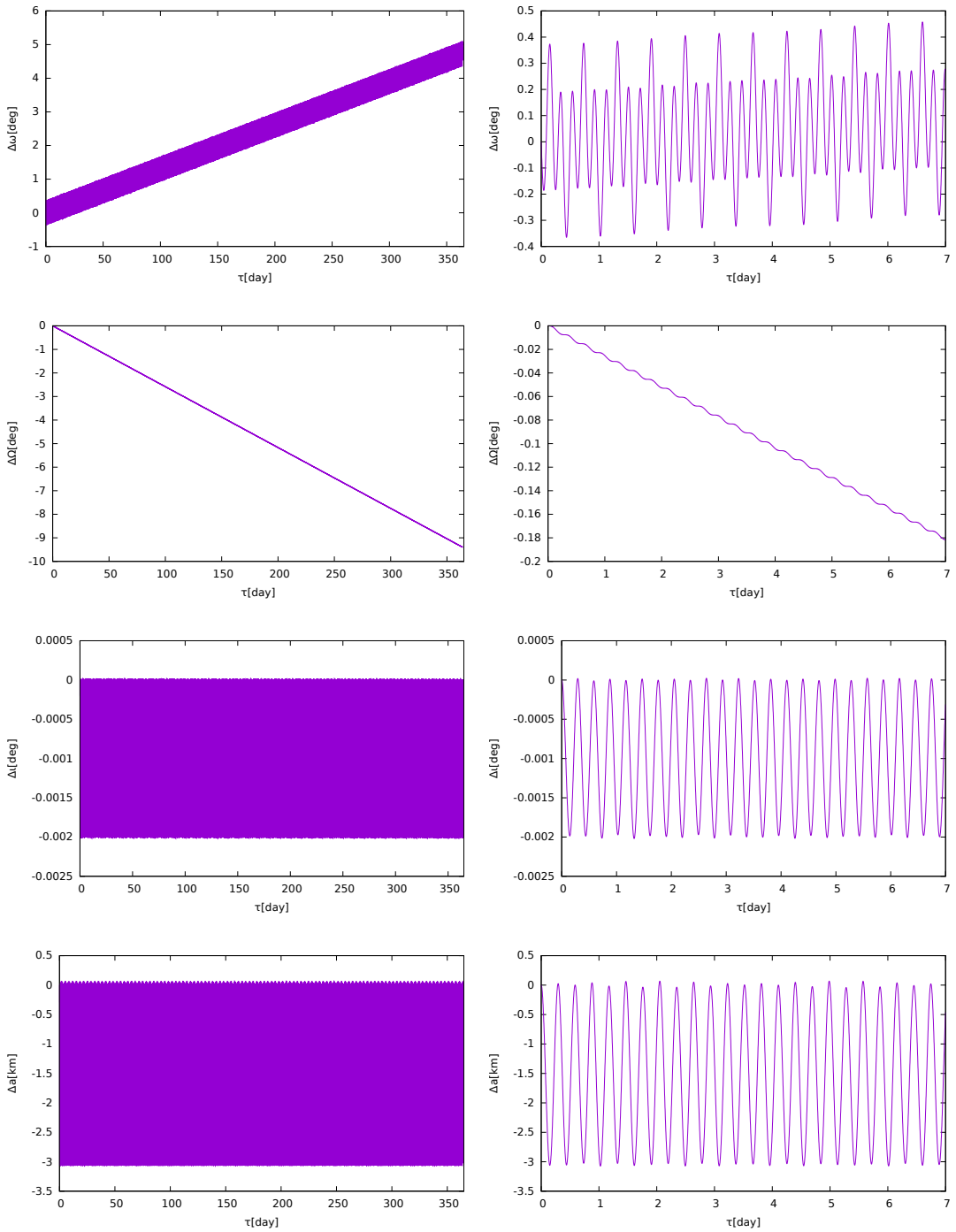

Figure 2.3: Evolution of orbital parameters due to Earth multipoles. The graphs on the left show the long-term changes of the orbital parameters in one year, while the graphs on the left show the short time-scale changes within the first 7 days. The time on x-axis counts days from 1 January 2012 at 7:00 a.m.

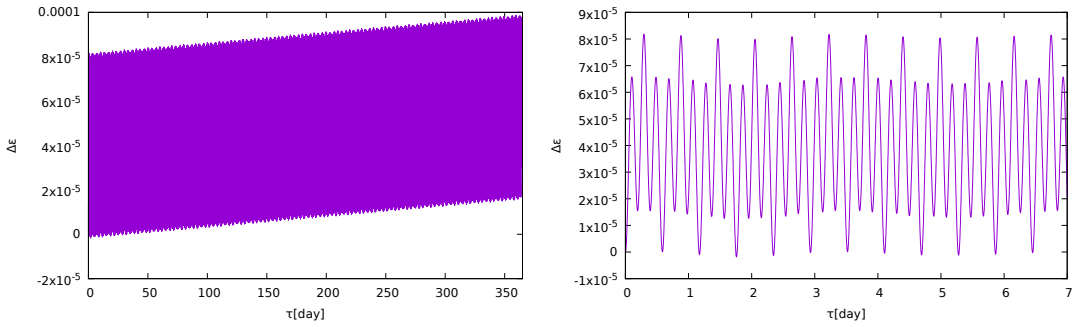

Figure 2.3: Continued.

Effects of all perturbations on orbital parameters As can be seen, there are two components, a short-term oscillating and a secular term. On average, the major semi-axis only oscillates and has no secular term, while the angles ω, Ω, and ι also have a small secular term, so the orbit can still be described as planar, whose orientation changes slowly with time.

Effects of perturbations on the position and time of the satellite Because all these changes of the orbital parameters are very small, instead of plotting the perturbed orbits (2.132), we rather plot in Figs. 2.12 and 2.13 the differences between positions[7] and Schwarzschild times (at the same proper times) of the satellite on the perturbed and unperturbed orbit. We show the differences in position and time for each perturbation, where all orbital parameters are changed at once as dictated by the solutions to (2.125) and (2.126).

The largest differences in positions ΔL and times ΔT are $\sim 10^4$ km and $\sim 10^{-10} - 10^{-9}$ s in one year, and come from the multipoles, while the smallest are ~ 20 cm and $\sim 10^{-17}$ s in one year, and come from the Kerr perturbation.

From these two figures it can be easily estimated which perturbations to include for a given accuracy of a positioning system – for a system with accuracy better than meter in one year, all perturbations down to Kerr should be included. Taking into account that the satellites are at $r \sim 30.000$ km and that the effect of Kerr perturbation is 0.5 mm per day, it would be in principle sufficient to do all the calculations in double precision. However, it turns out that some precision loss occurs when using the equations from Kostić (2012) to calculate the derivatives (2.125) - (2.131). Namely, these equations suffer from cancellation effects in case of quasi-circular orbits (which is the case for GNSS). Although we managed to get rid of the most crucial ones by replacing the energy E with $E = 1 - \eta$, where $\eta \ll 1$, the remaining ones reduce the precision by 8-10 digits. Consequently, all the calculations have to be done with 128-bit floating point numbers, to make sure that Kerr effect is not lost in numerical noise.

[7] We note that we do not measure the difference in position in length along the orbit, but by 3D distance between both positions: $\Delta L = |\vec{r}_{perturbed} - \vec{r}_{Schwarzschild}|$

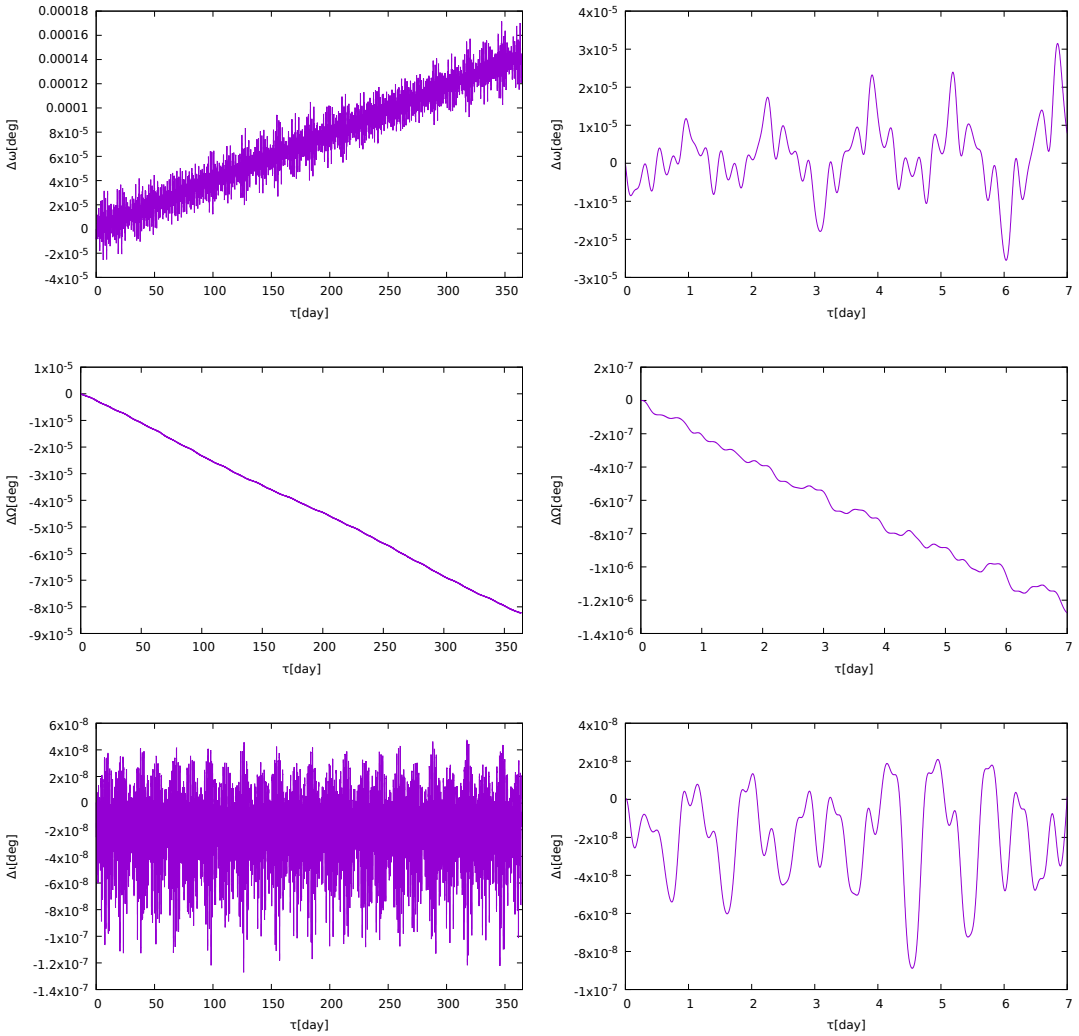

Figure 2.4: Evolution of orbital parameters due to Earth solid tides. The graphs on the left show the long-term changes of the orbital parameters in one year, while the graphs on the left show the short time-scale changes within the first 7 days. The time on x-axis counts days from 1 January 2012 at 7:00 a.m.

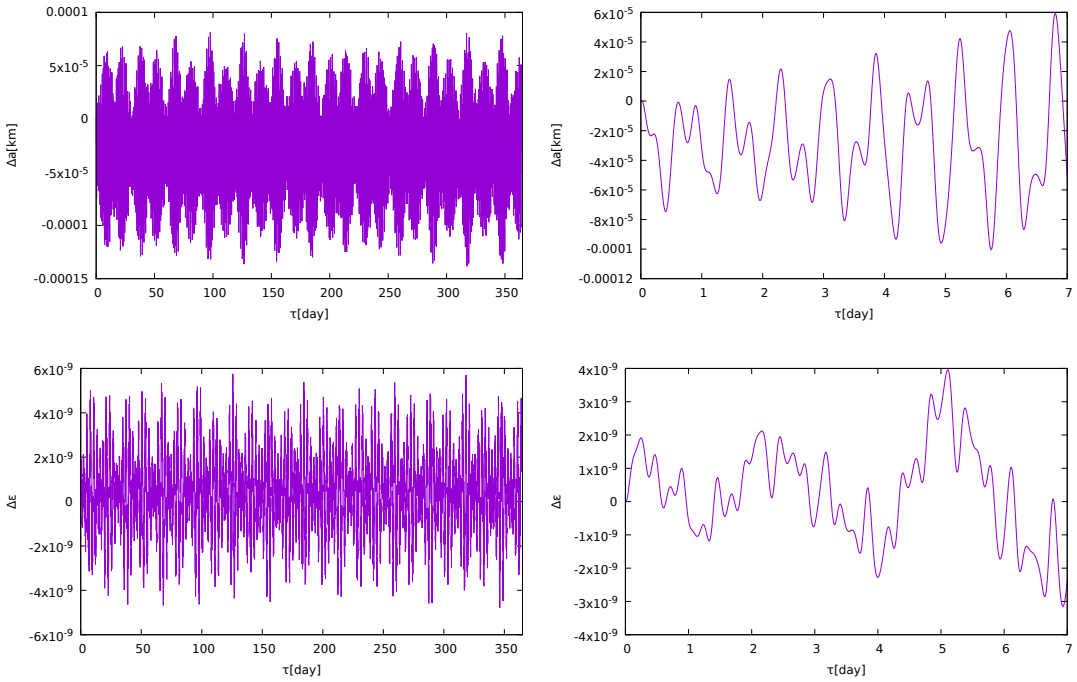

Figure 2.4: Continued.

Effects of perturbations on a light signal time-of-flight

Using results of Zschocke and Klioner (2011), we estimated the effect of gravitational perturbations on propagation of light signals (user-satellite and inter-satellite communication). The largest time delay due to Earth quadrupole perturbation is for satellites on opposite sides of Earth and amounts to 5.4×10^{-14} s. Therefore we find that effects of gravitational perturbations on signal time-of-flight are negligible in case of Galileo GNSS.

Conclusions for WP2: We calculated satellites' orbits in perturbed space-time taking into account all relevant gravitational perturbations and using Hamiltonian formalism. We make use of the Schwarzschild geodesic solution and slowly time evolving 0^{th} order constants of motion. We investigated the influence of each gravitational perturbation on the orbital parameters evolution and on the satellites position and time. We find that the influence of gravitational perturbations on the user- satellite and inter-satellite light signal propagation is negligible.

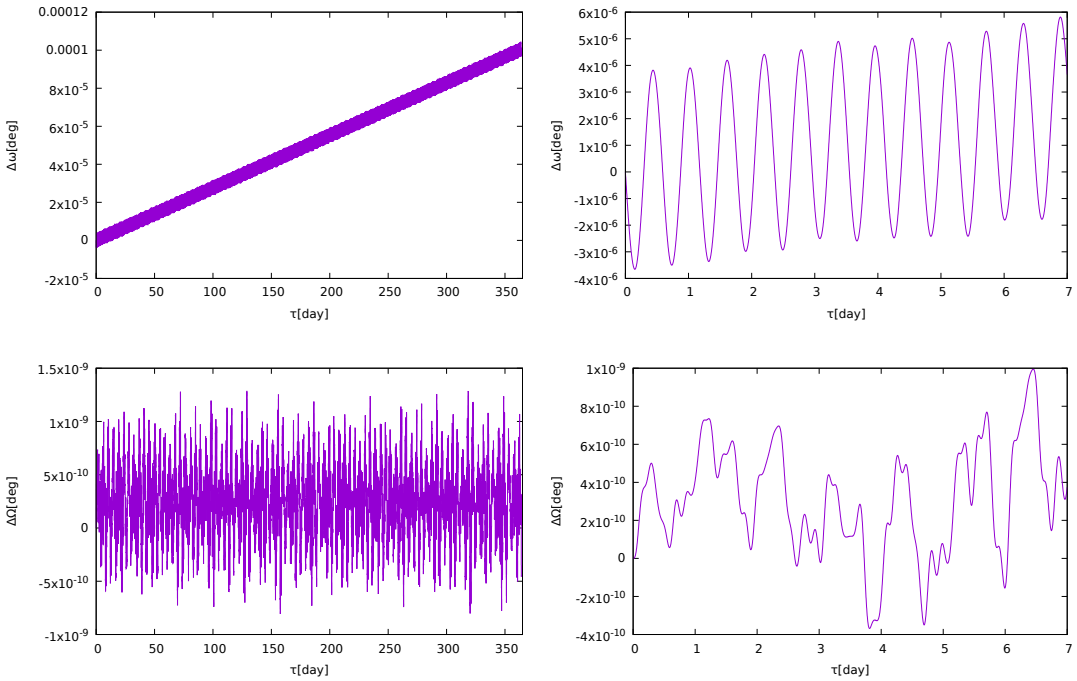

Figure 2.5: Evolution of orbital parameters due to Earth ocean tides. The graphs on the left show the long-term changes of the orbital parameters in one year, while the graphs on the left show the short time-scale changes within the first 7 days. The time on x-axis counts days from 1 January 2012 at 7:00 a.m.

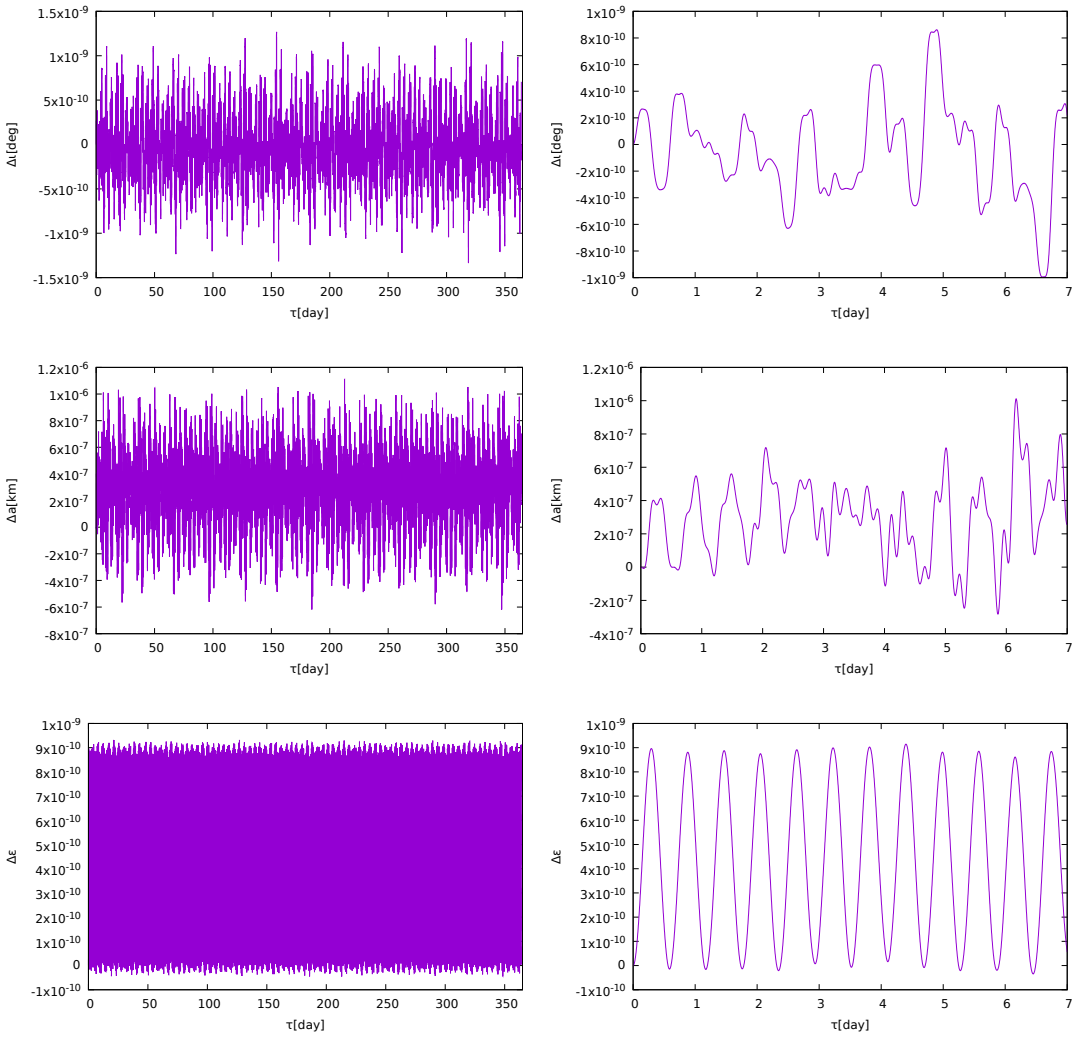

Figure 2.5: Continued.

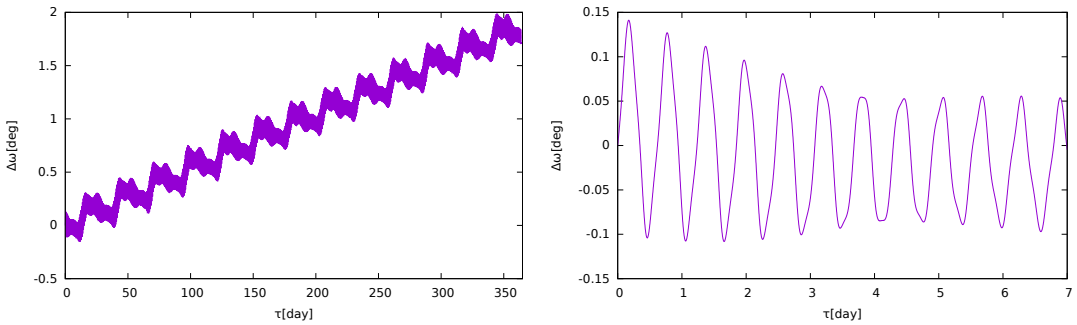

Figure 2.6: Evolution of orbital parameters due to Moon. The graphs on the left show the long-term changes of the orbital parameters in one year, while the graphs on the left show the short time-scale changes within the first 7 days. The time on x-axis counts days from 1 January 2012 at 7:00 a.m.

2.3 Work Package 3 - Determination of orbital parameters

Abstract of WP3: We use perturbed satellite orbits from Work Package 2 (including all relevant gravitational perturbations, such as Earth multipoles (up to the 6th), Earth solid and ocean tides, the Sun, the Moon, Jupiter, Venus, and the Kerr effect.) to model the relativistic positioning in gravitationally perturbed space-time and test its accuracy. We simulate a constellation of GNSS satellites as an RPS with inter-satellite links. Satellite orbits are described by their initial values of 0^{th} order constants of motion, which are, in the following, assumed to be known with only limited accuracy. By using only inter-satellite links and information on emission coordinates over several orbital periods we refine initial values of 0^{th} order constants of motion. In this way the satellites can themselves highly accurately determine and check internally in the GNSS system the system's dynamics, i.e. their own orbital parameters, and thus they constitute an Autonomous Basis of Coordinates (ABC), which is independent of any Earth based coordinate system. We study the stability of the solutions and possible degeneracies among orbital parameters.

2.3.1 Positioning in Perturbed Space-time

We simulate a constellation of four satellites moving along their time-like geodesics. The initial orbital parameters of the geodesics, i.e. initial values of 0^{th} order constants of motion, are known and their evolution due to gravitational perturbations is calculated as shown in subsections 2.2.2 and 2.2.3.

At every time-step of the simulation, each satellite emits a signal and a user on Earth receives signals from all satellites – the signals are the proper times of satellites at their emission events and constitute the emission coordinates of the user (see section 1.2). The emission coordinates determine the user's position in this particular relativistic reference frame defined by the four satellites and allow him to calculate his position

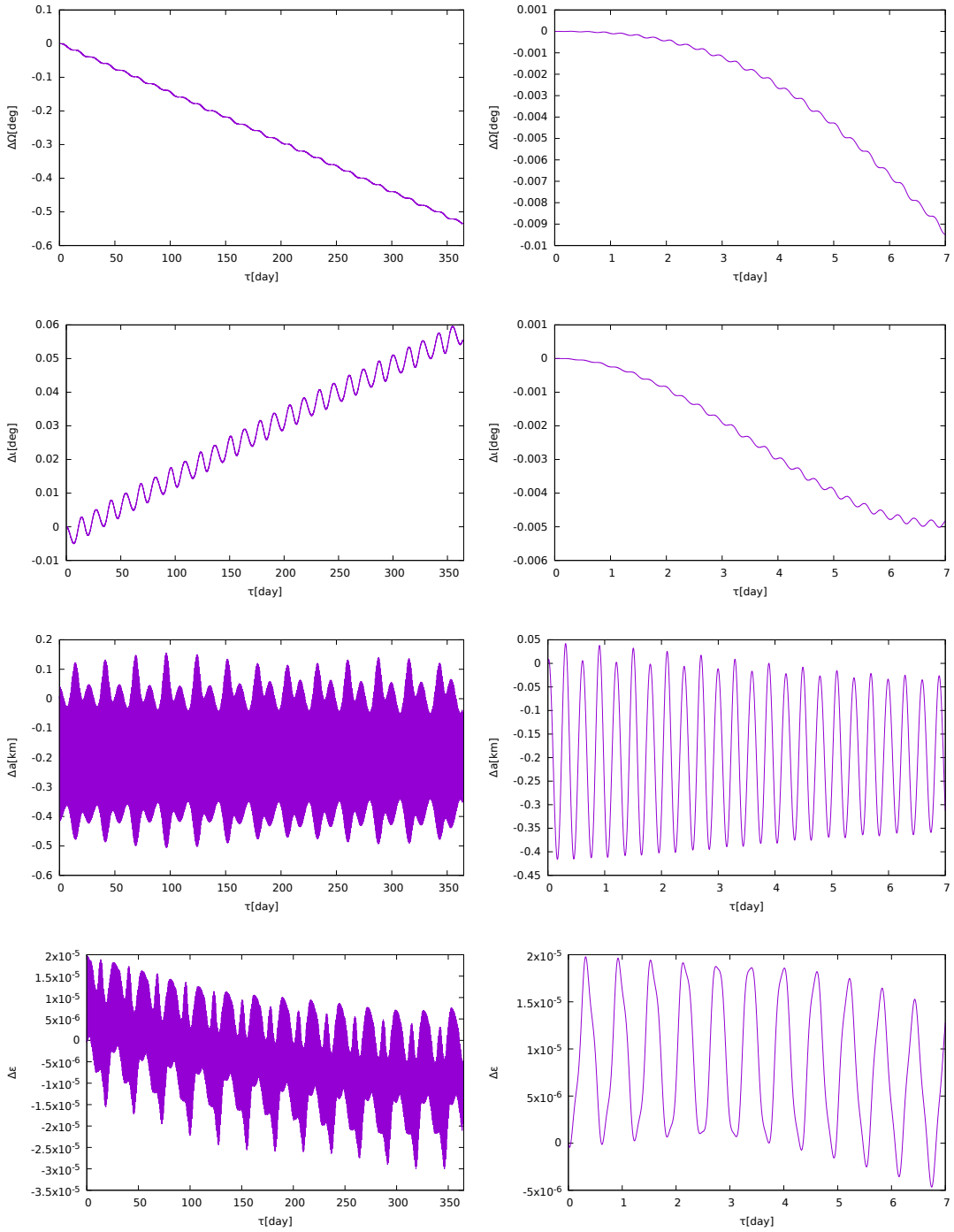

Figure 2.6: Continued.

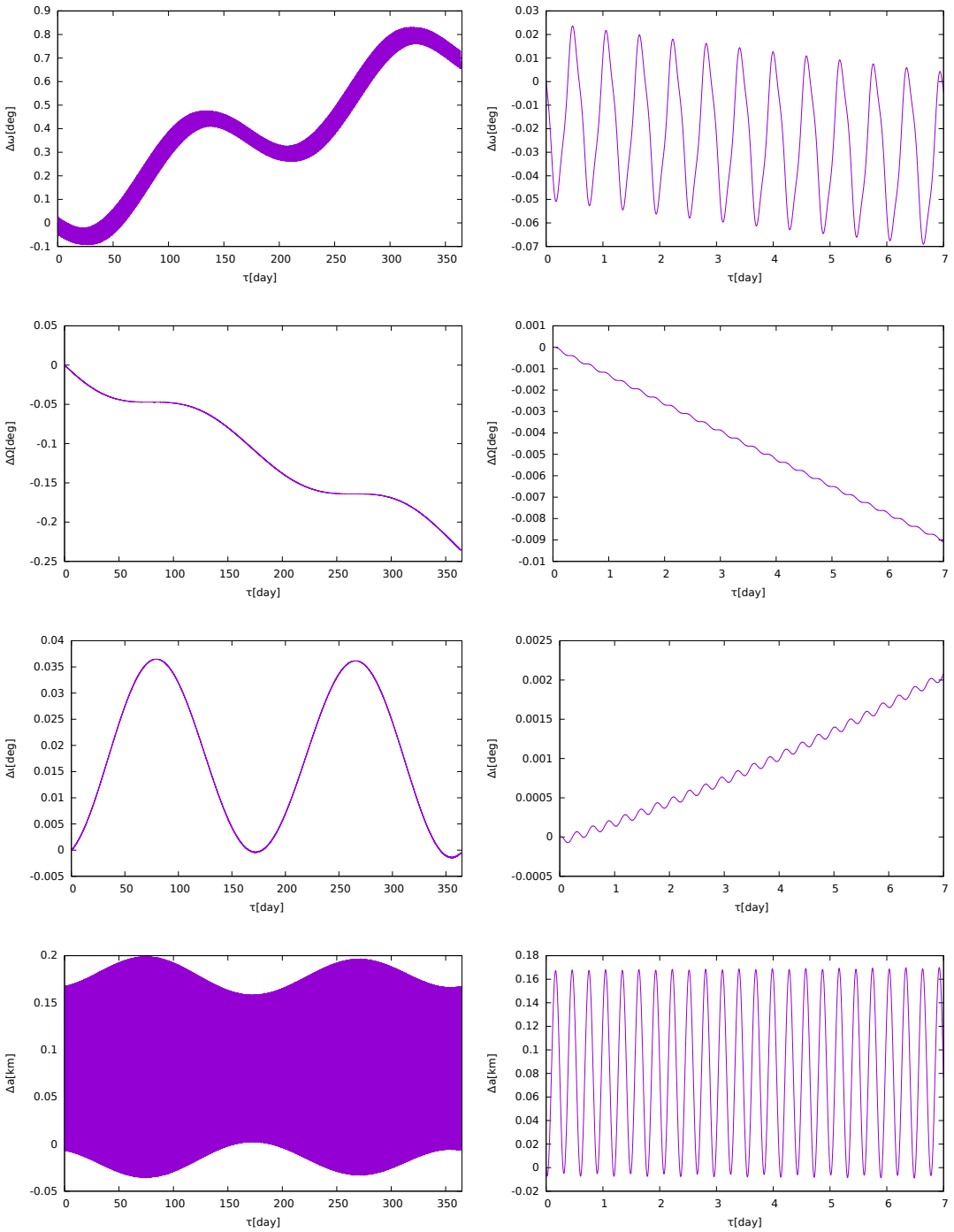

Figure 2.7: Evolution of orbital parameters due to Sun. The graphs on the left show the long-term changes of the orbital parameters in one year, while the graphs on the left show the short time-scale changes within the first 7 days. The time on x-axis counts days from 1 January 2012 at 7:00 a.m.

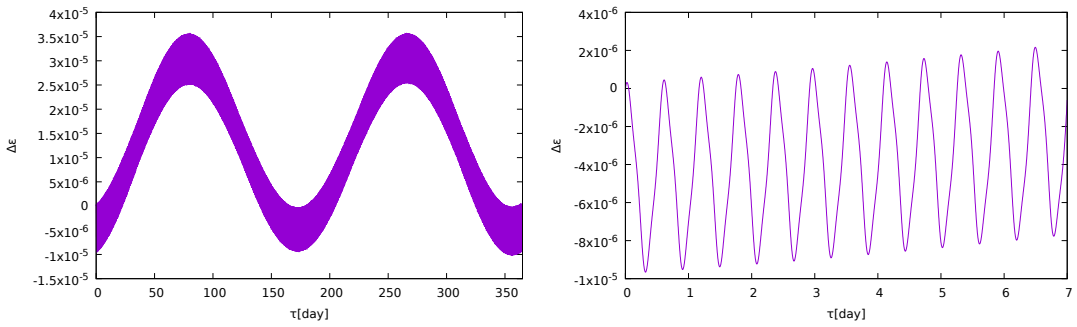

Figure 2.7: Continued.

and time in the more customary Schwarzschild coordinates. Therefore, to simulate the relativistic positioning system (RPS), we need two main algorithms: (1) determination of the emission coordinates, and (2) calculation of the Schwarzschild coordinates.

Determination of the emission coordinates The satellites' trajectories are parametrized by their true anomaly λ. The event $\mathcal{P}_o = (t_o, x_o, y_o, z_o)$ marks user's Schwarzschild coordinates at the moment of reception of the signals from four satellites. Each satellite emitted a signal at event $\mathcal{P}_i = (t_i, x_i, y_i, z_i)$, corresponding to λ_i $(i = 1, ..., 4)$. Emission coordinates of the user at $\mathcal{P}_o$ are, therefore, the proper times $\tau_i(\lambda_i)$ of the satellites at $\mathcal{P}_i$. Taking into account that the events $\mathcal{P}_o$ and $\mathcal{P}_i$ are connected with a light-like geodesic,[8] we calculate λ_i at the emission point $\mathcal{P}_i$ using the equation

$$\begin{aligned} t_o - t_i(\lambda_i | Q^\mu(\tau_i), P_\mu(\tau_i)) = \\ T_f(\vec{R}_i(\lambda_i | Q^\mu(\tau_i), P_\mu(\tau_i)), \vec{R}_o) \ , \end{aligned} \tag{2.133}$$

where $\vec{R}_i = (x_i, y_i, z_i)$ and $\vec{R}_o = (x_o, y_o, z_o)$ are the spatial vectors of the satellites and the user, respectively. The function T_f calculates the time-of-flight of light signals between $\mathcal{P}_o$ and $\mathcal{P}_i$ as shown by Čadež and Kostić (2005) and Čadež et al. (2010). The equation (2.133) is actually a system of four equations for four unknown λ_i – once the values of λ_i are determined numerically, it is straightforward to calculate τ_i from (A.38) for each satellite and thus obtain user's emission coordinates at $\mathcal{P}_o = (\tau_1, \tau_2, \tau_3, \tau_4)$.

Calculation of the Schwarzschild coordinates Here we solve the inverse problem of calculating Schwarzschild coordinates of the event $\mathcal{P}_o$ from proper times $(\tau_1, \tau_2, \tau_3, \tau_4)$ sent by the four satellites. We do this in the following way: For each satellite, we numerically solve the equation

$$\tau(\lambda_i | Q^\mu(\tau_i), P_\mu(\tau_i)) = \tau_i \ , \tag{2.134}$$

[8] The light-like geodesics are calculated in Schwarzschild space-time (see Kostić (2012)) without perturbations, because the effects of perturbations on light propagation are negligible as mentioned in subsection 2.2.3.

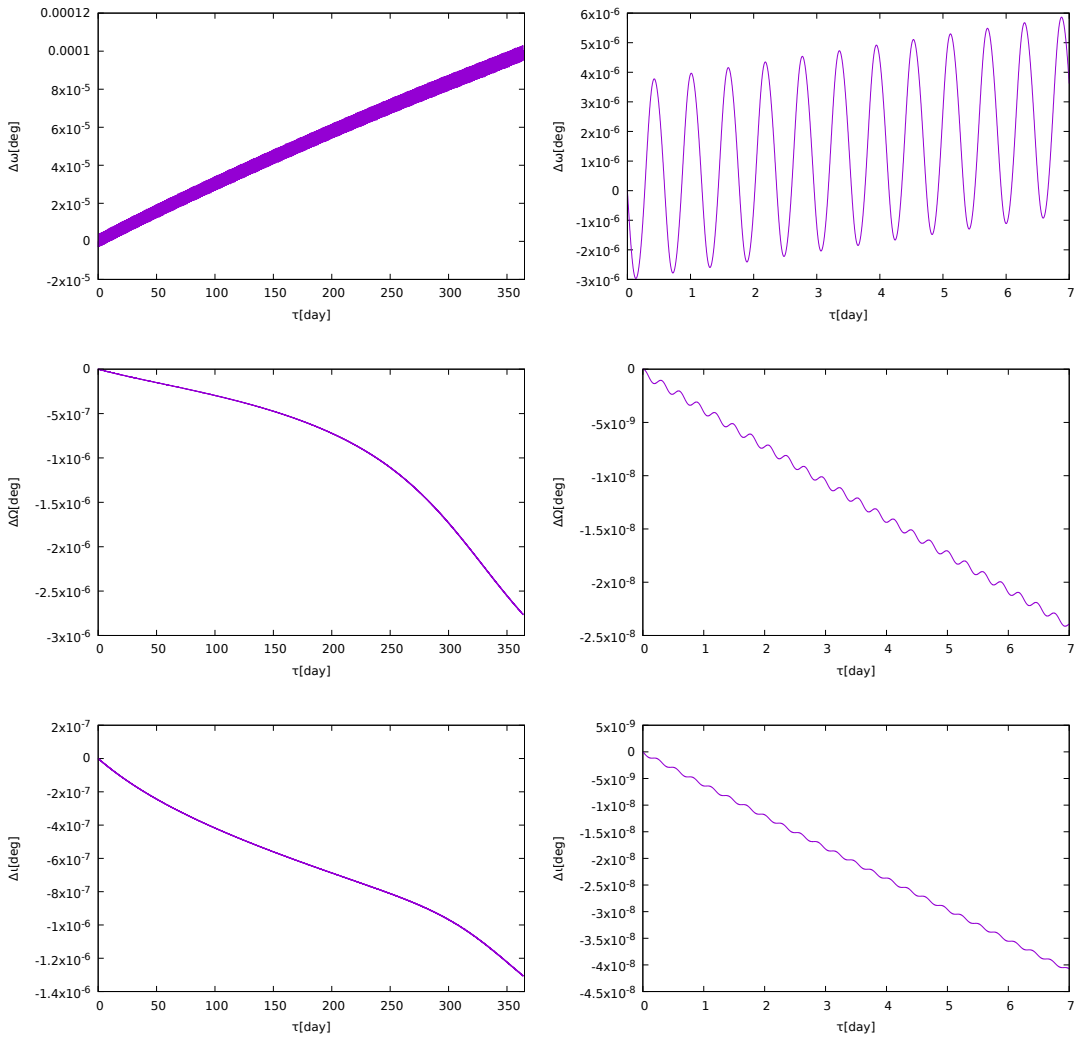

Figure 2.8: Evolution of orbital parameters due to Jupiter. The graphs on the left show the long-term changes of the orbital parameters in one year, while the graphs on the left show the short time-scale changes within the first 7 days. The time on x-axis counts days from 1 January 2012 at 7:00 a.m.

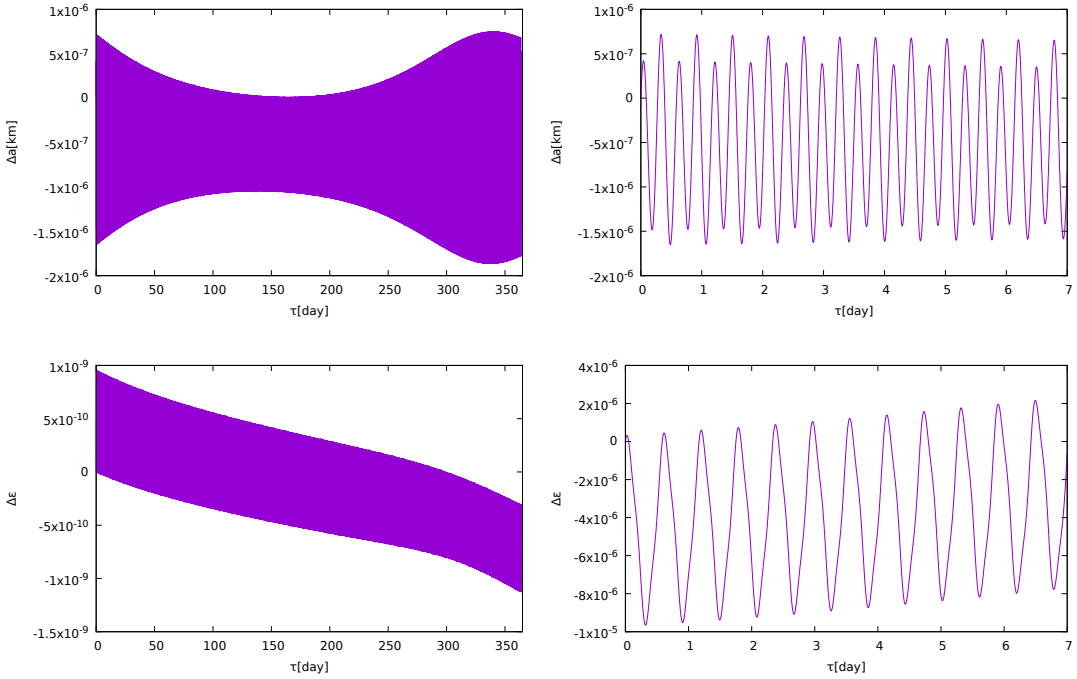

Figure 2.8: Continued.

to obtain λ_i, where $\tau(\lambda|Q^\mu(\tau), P_\mu(\tau))$ is a known function for proper time on time-like geodesics (Kostić 2012). The Schwarzschild coordinates of the satellites are then calculated from λ_i using (2.132). With the satellites' coordinates known, we can take the geometrical approach presented by Čadež et al. (2010) to calculate the Schwarzschild coordinates of the user. The final step in this method requires us again to solve (2.133), however, this time it is treated as a system of 4 equations for 4 unknown user coordinates, i.e., solving it, gives (t_o, x_o, y_o, z_o).

Results: The accuracy of these algorithms has been tested for satellites on orbits with initial parameters given in Table 2.1 and a user at coordinates $r_o = 6371$ km, $\theta_o = 43.97^\circ$, $\phi_o = 14.5^\circ$. The user's coordinates remain constant during the simulation. The relative errors, defined as

$$\epsilon_t = \frac{t_o - t_o^e}{t_o}, \ \epsilon_{x,y,z} = \frac{\vec{R}_o - \vec{R}_o^e}{\vec{R}_o} \ , \tag{2.135}$$

are of the order $10^{-32} - 10^{-30}$ for coordinate t, and $10^{-28} - 10^{-26}$ for x, y, and z;[9] here t_o^e and $\vec{R}_o^e$ are user time and coordinates as calculated from the emission coordinates. Using

[9]Note that these numbers represent the accuracy of the numerical methods used. In a real system, the accuracy would be much lower due to numerous effects, e.g. non-gravitational perturbations, atmospheric effects, clock errors...

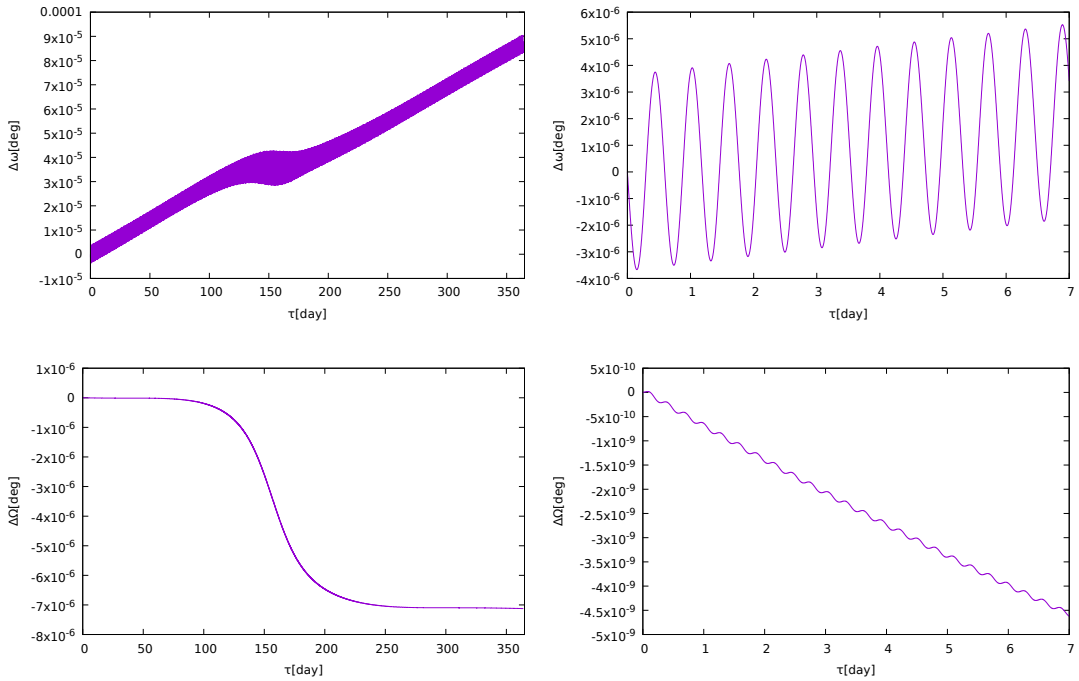

Figure 2.9: Evolution of orbital parameters due to Venus. The graphs on the left show the long-term changes of the orbital parameters in one year, while the graphs on the left show the short time-scale changes within the first 7 days. The time on x-axis counts days from 1 January 2012 at 7:00 a.m.

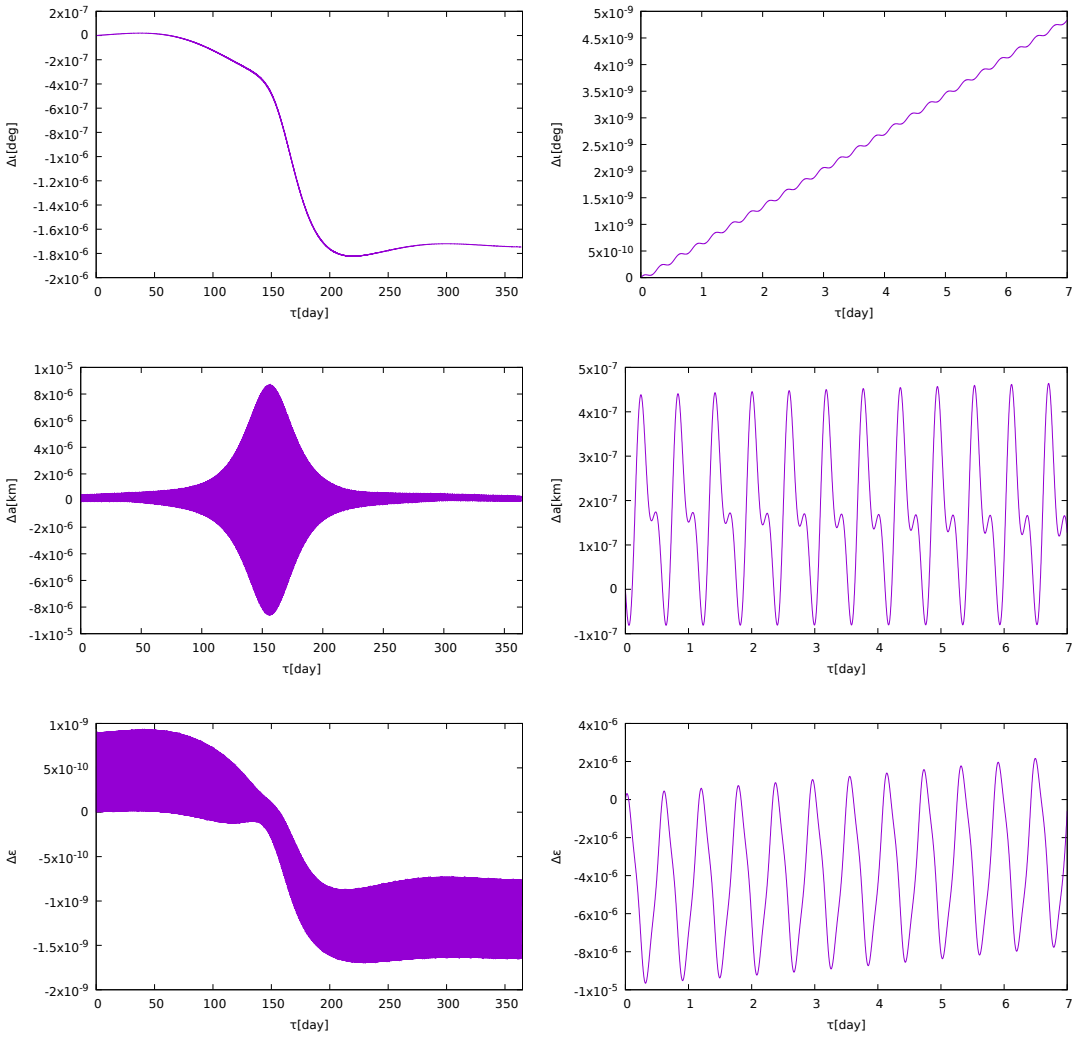

Figure 2.9: Continued.

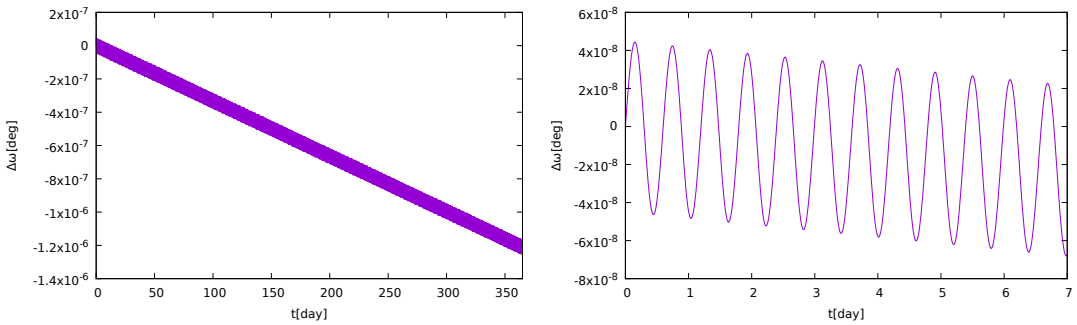

Figure 2.10: Evolution of orbital parameters due to Kerr. The graphs on the left show the long-term changes of the orbital parameters in one year, while the graphs on the left show the short time-scale changes within the first 7 days. The time on x-axis counts days from 1 January 2012 at 7:00 a.m.

Table 2.1: Orbital parameters for 4 satellites: longitude of ascending node (Ω), longitude of the first apogee passage (ω), inclination (ι), major semi-axis (a), eccentricity (ε), and time of apogee passage (t_a).

#	Ω [°]	ω [°]	ι [°]	a [km]	ε	t_a [s]
1	0	270	45	30000	0.007	0
2	0	315	45	30000	0.007	0
3	0	275	135	30000	0.007	0
4	0	320	135	30000	0.007	0

a laptop[10] for calculations, the user's position (with such errors) was determined in 0.04 s, where we assumed that (1) in real applications of the positioning the true values of orbital parameters would be transmitted to the user together with the emission coordinates, so to account for this in our simulations, we calculated the evolution of parameters from their initial values before starting the positioning, and (2) the position of the user is completely unknown, i.e., we do not start from the last known position. If we did, the times for calculating the position would be even shorter.

2.3.2 Autonomous Basis of Coordinates - ABC

To construct an autonomous coordinate system, we apply the idea of the Autonomous Basis of Coordinates (ABC) presented in Čadež et al. (2011) (see 2.2.3) to a perturbed satellite system, i.e. we simulate the motion of a pair of satellites along their perturbed orbits and their inter-satellite communication.

[10]With the following configuration: Intel(R) Core(TM) i7-3610QM CPU @ 2.30GHz, 8GB RAM, Intel C/C++/Fortran compiler 13.0.1.

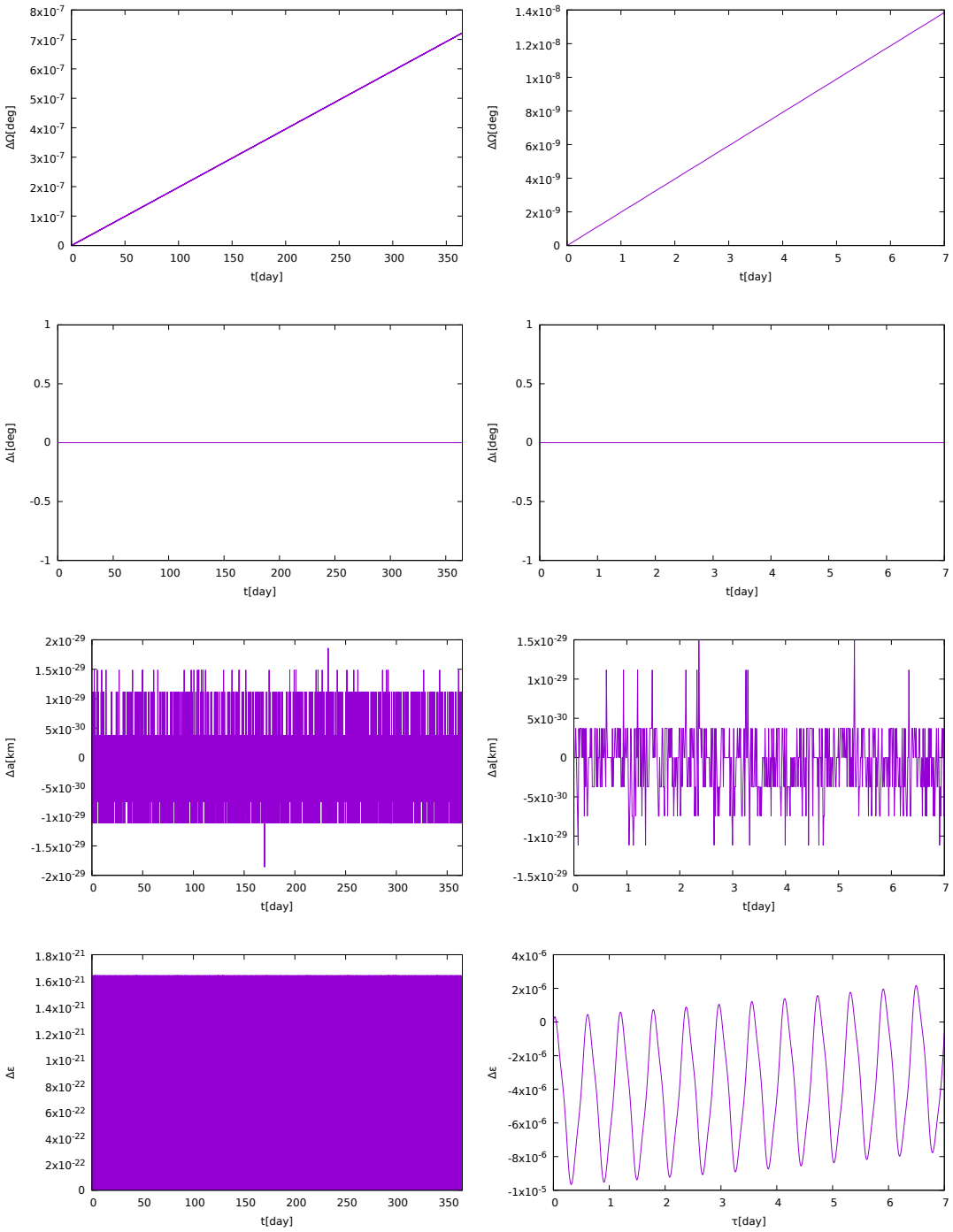

Figure 2.10: Continued.

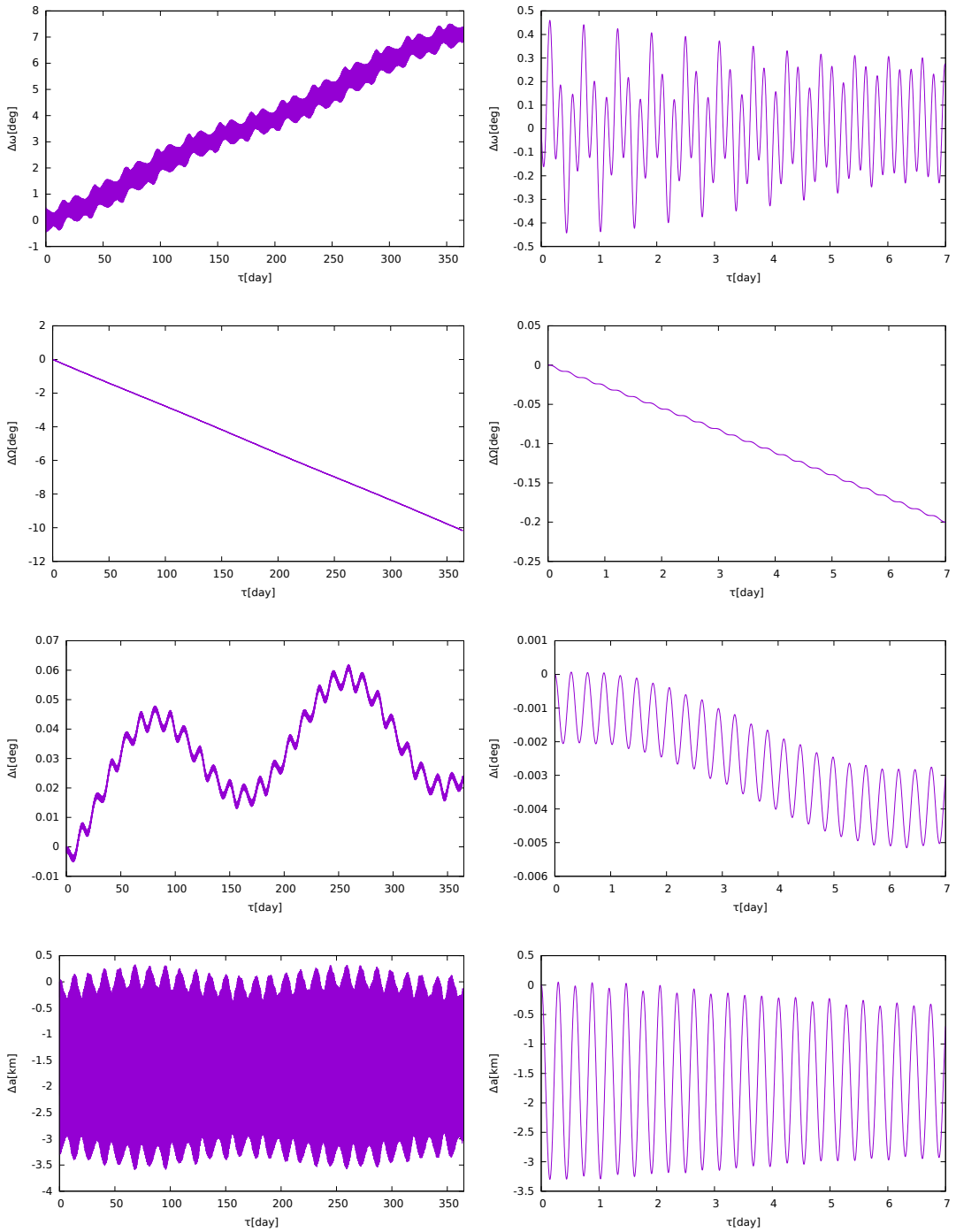

Figure 2.11: Evolution of orbital parameters due to sum of all perturbations (Earth multipoles, Earth solid tide, ocean tide, the Moon, the Sun, Venus, Jupiter, and Kerr effect). The graphs on the left show the long-term changes of the orbital parameters in one year, while the graphs on the left show the short time-scale changes within the first 7 days. The time on x-axis counts days from 1 January 2012 at 7:00 a.m.

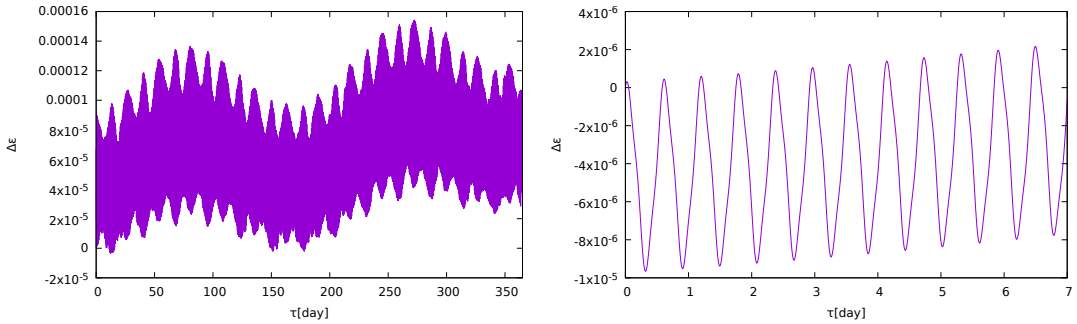

Figure 2.11: Continued.

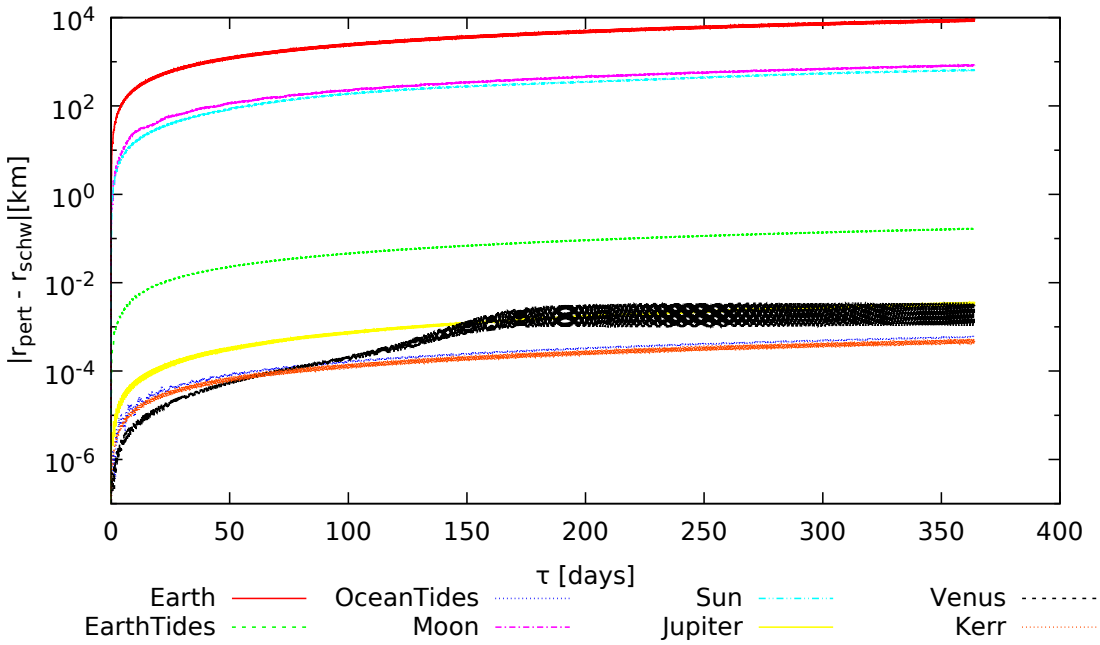

Figure 2.12: The differences in the position ΔL of the satellite due to each gravitational perturbation. The time on x-axis counts days from 1 January 2012 at 7:00 a.m.. The initial values of parameters are: $t_a = 7$ h, $\omega = 0^\circ$, $\Omega = 0^\circ$, $a = 29602$ km, $\varepsilon = 0.007$, $\iota = 56^\circ$.

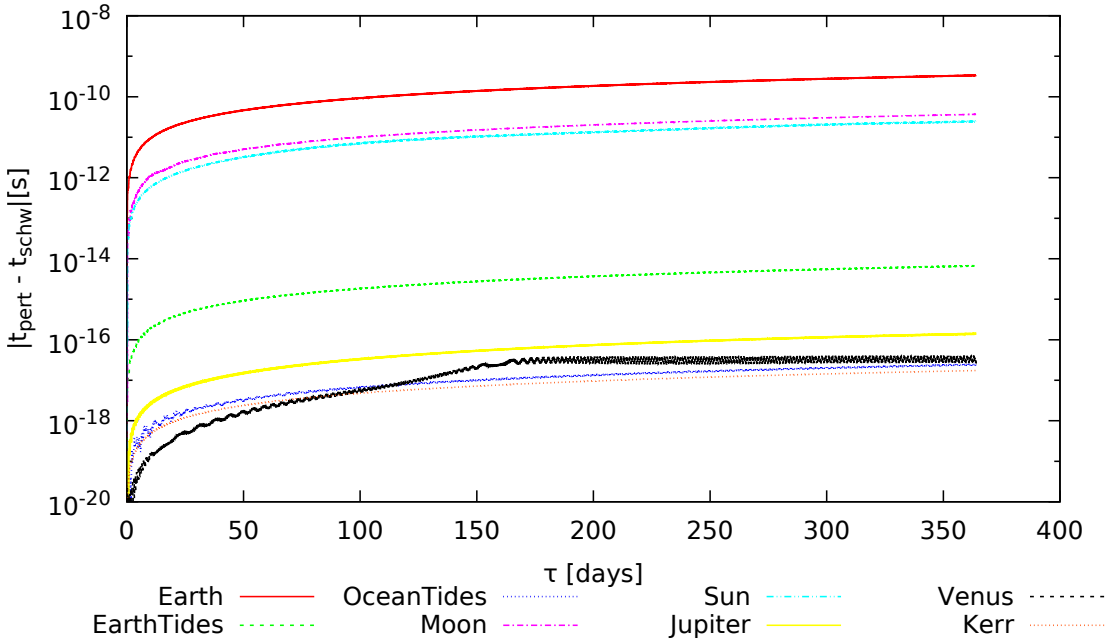

Figure 2.13: The differences of the Schwarzschild times ΔT of the satellite due to each gravitational perturbation. The time on x-axis counts days from 1 January 2012 at 7:00 a.m.. Axes on red and gray plots have the same units. The initial values of parameters are: $t_a = 7$ h, $\omega = 0^\circ$, $\Omega = 0^\circ$, $a = 29602$ km, $\varepsilon = 0.007$, $\iota = 56^\circ$.

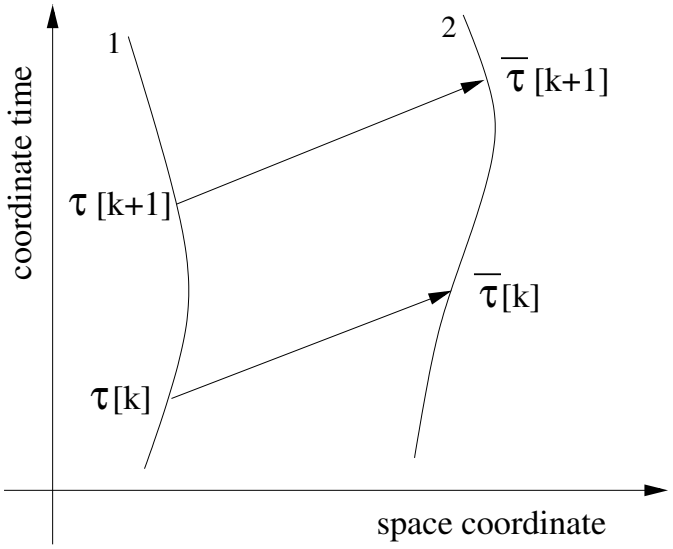

Figure 2.14: A pair of satellites exchanging their proper times. At every time-step k, the satellite 1 sends the proper time of emission $\tau[k]$ to the satellite 2, which receives it at the time of reception $\overline{\tau}[k]$. The emission and reception event pairs are connected with a light-like geodesic.

At each time-step of the simulation, both satellites exchange emission coordinates as shown in Fig. 2.14, where, for clarity, only communication from satellite 1 to satellite 2 is plotted. These events of emission at proper time τ of the first satellite and reception at $\overline{\tau}$ of the second satellite are connected with a light-like geodesic, i.e. the difference between the coordinate times of emission $t_1(\tau)$ and reception $t_2(\overline{\tau})$ must be equal to the time-of-flight of a light signal between the two satellites (cf. (2.133))

$$T_f = t_2(\overline{\tau}) - t_1(\tau) \ . \tag{2.136}$$

However, this is only true if we know the exact values of the initial orbital parameters of each satellite, as well as their evolution.

When constructing the relativistic positioning system, it is reasonable to assume that the initial orbital parameters $(Q^\mu(0), P_\mu(0))$ are not known very precisely. In the following we therefore assume that they are known only with limited accuracy and to improve their values, we use the following method. We assume that the satellites have some initial orbital parameters $(Q^\mu(0), P_\mu(0))$, we let them evolve with time according to gravitational perturbations, and calculate satellite orbits, simulate their communication and calculate the left hand side of (2.136) for all communication pairs. We then compare these values to the right hand side values derived for "true" initial orbital parameters, and sum the differences between left hand side and right hand side for all communication

events into an action

$$
\begin{aligned}
S(Q^\mu(0), P_\mu(0)) = \sum_k \big(& t_1(\tau[k]|Q^\mu(\tau[k]), P_\mu(\tau[k])) - \\
& t_2(\overline{\tau}[k]|Q^\mu(\overline{\tau}[k]), P_\mu(\overline{\tau}[k])) - \\
& T_f(\vec{R}_1(\tau[k]|Q^\mu(\tau[k]), P_\mu(\tau[k])), \\
& \vec{R}_2(\overline{\tau}[k]|Q^\mu(\overline{\tau}[k]), P_\mu(\overline{\tau}[k])))\big)^2 \ ,
\end{aligned}
\tag{2.137}
$$

which has a minimum value (close to zero) for the true initial values of orbital parameters. By changing initial values of orbital parameters and finding the minimum of the action S we can thus find or at least come very close to the true initial values.

For the 2×6 orbital parameters that we have ($Q^\mu(0), P_\mu(0)$ for both satellites), this becomes a problem of finding a minimum of a 12D function. Because the orbital parameters depend on time, their time evolution has to be recalculated (as presented in Sec. 2.2.2 and Sec. 2.2.3) at every step of the minimization (for each set of initial values of orbital parameters), which makes the minimization process very slow.

To speed up the process, the minimization was done in two stages. In the first stage, we use the PRAXIS minimization method (Brent 1973) implemented in the NLOPT library (Johnson 2013) to determine the parameters within double precision. The resulting values are then used as initial values for the second stage, where we use the simplex method to "polish" the parameters within 128-bit quad precision.[11] In Figs. 2.15 – 2.16 we plot the values of the action and the orbital parameters during the first and the second stage of the minimization process, respectively.

The number of time-steps along the orbits was sufficiently large ($k = 1 \ldots 433$) to cover approximately two orbits. The initial values of the orbital parameters used as starting point in the minimization differ from the true values by an amount which induces the error of $\sim 2-3$ km in the satellites' positions. At the beginning of the minimization, the value of the action is $S \approx 10^{24}(r_g/c)^2$, at the end of the first stage it is $2 \times 10^{10}(r_g/c)^2$, and at the end of the second stage it drops to $8 \times 10^{-24}(r_g/c)^2$. The relative errors of the orbital parameters ($Q^\mu(0), P_\mu(0)$) after the minimization are of the order of 10^{-22}.[12]

By repeating the minimization procedure for all possible pairs of satellites, we can reconstruct the orbital parameters of every satellite in the system **without tracking the satellites from Earth** and thus obtain an autonomous coordinate system.

2.3.3 Degeneracies

We investigated possible degeneracies between orbital parameters by scanning the action S: We take two satellites on orbits with known initial orbital parameters. Then we

[11] Quad precision is required if the resulting parameters are used in (2.132), where cancellation effects become significant in case of quasi-circular orbits.

[12] Better safe than sorry... so, again, we note that these numbers represent the accuracy of the numerical methods used. In a real system, the accuracy would be much lower due to numerous effects, e.g. non-gravitational perturbations, atmospheric effects, clock errors...

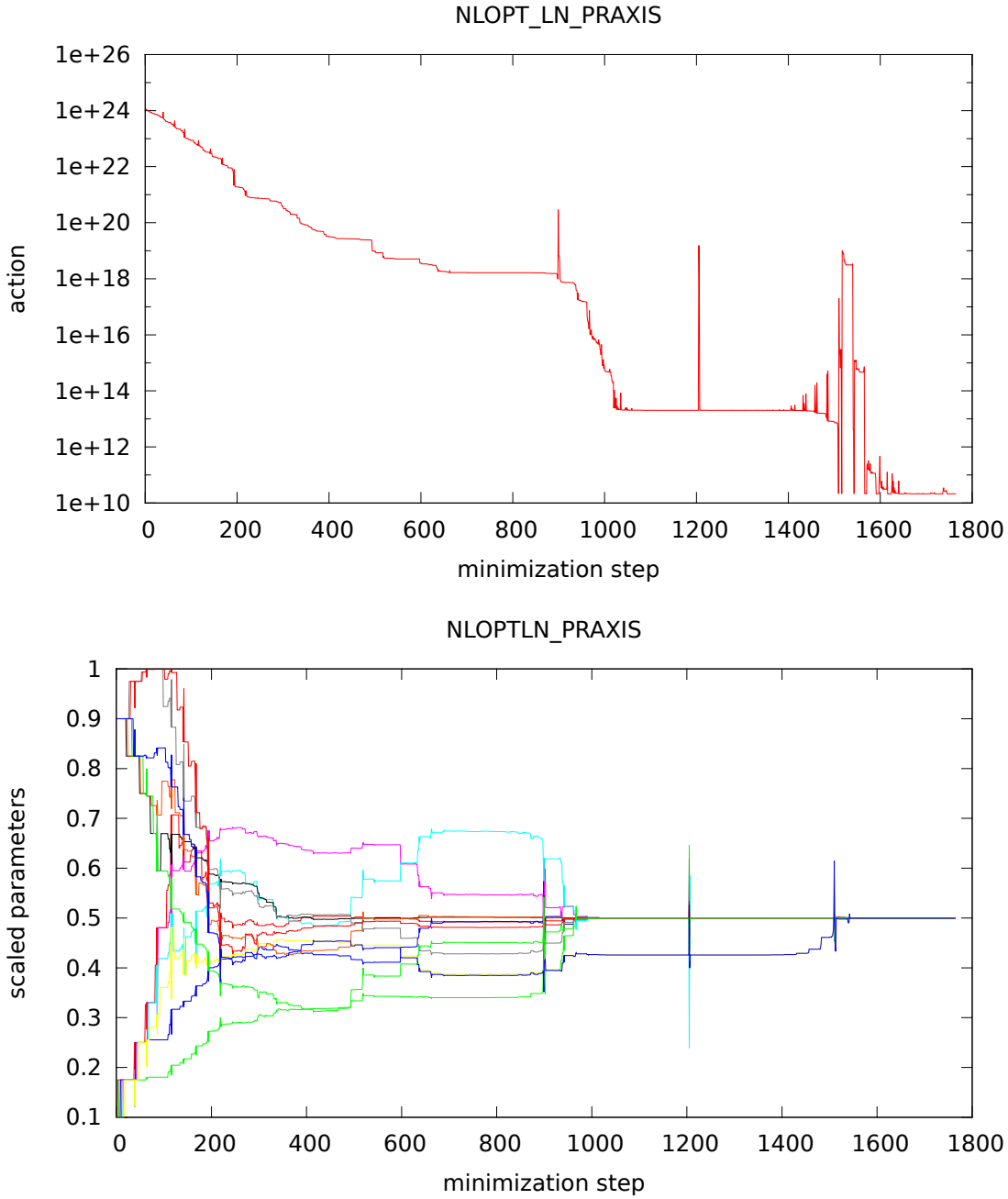

Figure 2.15: The action $S(Q^\mu(0), P_\mu(0))$ (top) and the orbital parameters (bottom) during the first stage of the minimization process. The parameters are scaled in the interval $[0, 1]$, corresponding to the absolute errors $\{\Delta a, \Delta\varepsilon, \Delta\omega, \Delta\Omega, \Delta\iota, \Delta t_a\} = \{10\text{ km}, 2.815125 \times 10^{-5}, 1.689075 \times 10^{-2}, 1.12605 \times 10^{-2}, 3.37815 \times 10^{-3}, 0.2\text{ s}\}$, so that the action is symmetric in that interval. The true values are at 0.5.

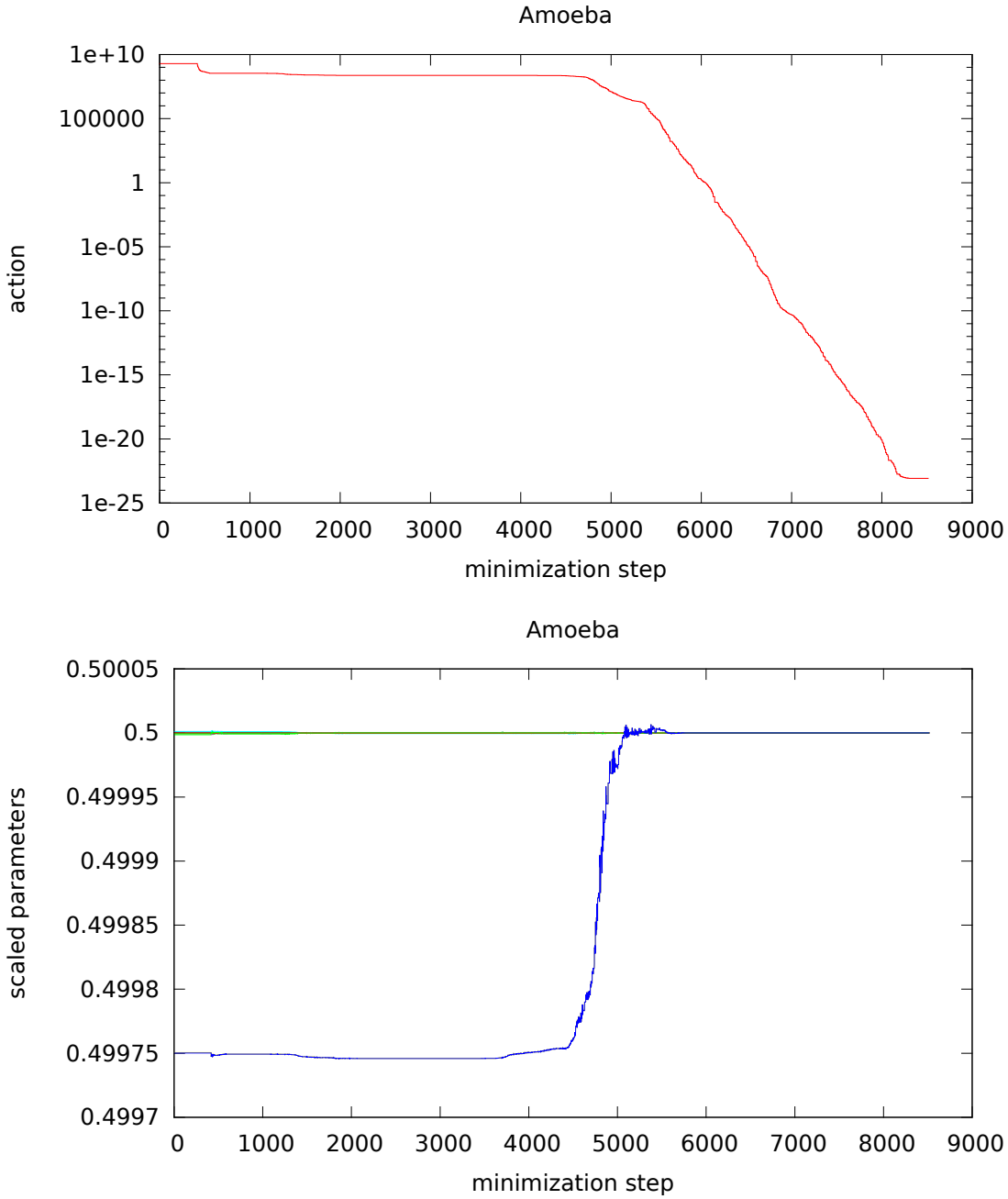

Figure 2.16: The action $S(Q^\mu(0), P_\mu(0))$ (top) and the orbital parameters (bottom) during the second stage of the minimization process. The parameters are scaled in the interval $[0, 1]$, corresponding to the absolute errors $\{\Delta a, \Delta\varepsilon, \Delta\omega, \Delta\Omega, \Delta\iota, \Delta t_a\} = \{10\text{ km}, 2.815125 \times 10^{-5}, 1.689075 \times 10^{-2}, 1.12605 \times 10^{-2}, 3.37815 \times 10^{-3}, 0.2\text{ s}\}$, so that the action is symmetric in that interval. The true values are at 0.5.

change two of them (one for the first satellite and one for the second) and calculate corresponding action S (2.137). We repeat this for different values of this pair of orbital parameters in order to scan the action S in their parameter space in the surroundings of their true values. In case there is no degeneracy between these two orbital parameters, we expect to find one well defined minimum of S - a "well". In case of a degeneracy, we will get more than one point in which S reaches minimum, i.e. more pairs of these two orbital parameters give minimum in S, therefore the problem is degenerate.

We checked whether a certain point is a minimum by calculating the Hessian matrix. Let f be a function of n variables

$$f(x_1, x_2, \cdots, x_n), f \in \mathbb{R} \ . \tag{2.138}$$

If all second order partial derivatives of the function f exist, we can define the Hessian matrix:

$$H(f)_{ij}(\vec{x}) = D_i D_j f(\vec{x}) \tag{2.139}$$

where $\vec{x} = (x_1, x_2, \cdots, x_n)$ and D_i is the differential operator of variable i. Thus

$$H(f) = \begin{bmatrix} \frac{\partial^2 f}{\partial x_1^2} & \frac{\partial^2 f}{\partial x_1 \partial x_2} & \cdots & \frac{\partial^2 f}{\partial x_1 \partial x_n} \\ \frac{\partial^2 f}{\partial x_2 \partial x_1} & \frac{\partial^2 f}{\partial x_2^2} & \cdots & \frac{\partial^2 f}{\partial x_2 \partial x_n} \\ \vdots & \vdots & \ddots & \vdots \\ \frac{\partial^2 f}{\partial x_n \partial x_1} & \frac{\partial^2 f}{\partial x_n \partial x_2} & \cdots & \frac{\partial^2 f}{\partial x_n^2} \end{bmatrix} . \tag{2.140}$$

For a function f of $n > 2$ variables we investigate eigenvalues of the Hessian matrix in a critical point $\vec{P} = (p_1, p_2, \cdots, p_n)$ (local minimum, local maximum or saddle). If the Hessian matrix is positive - all its eigenvalues are positive - then the function f has a local minimum in point $\vec{P}$.

Degeneracies in unperturbed, Schwarzschild metric First we considered unperturbed, Schwarzschild metric, which is spherically symmetric. True orbital parameters of both satellites are:

- satellite 1: $\Omega_1 = 20°, \omega_1 = 120°, \iota_1 = 40°, a_1 = 30025$ km$, \varepsilon = 0.008, t_{a1} = 7.04$ h$, \tau_{a1} = 0$,
- satellite 2: $\Omega_2 = 20°, \omega_2 = 120°, \iota_2 = 80°, a_2 = 30025$ km$, \varepsilon_2 = 0.008, t_{a2} = t_{a1} = 7.04$ h$, \tau_{a2} = 0$.

Action S is calculated for one orbit.

Scanning the action S we find that parameters: ι_1-ι_2, Ω_1-Ω_2, and t_{a1}-t_{a2} are degenerate. In the scanning region in the vicinity of their true values, the action S has a shape of a "valley" (Fig. 2.17,2.18, 2.19). Degenerate points lie on a line $x = y$, which is understandable if we think of spherical symmetry of Schwarzschild metric. Changing ι and Ω of both satellites' orbital planes by the same amount, i.e. keeping the same orientation

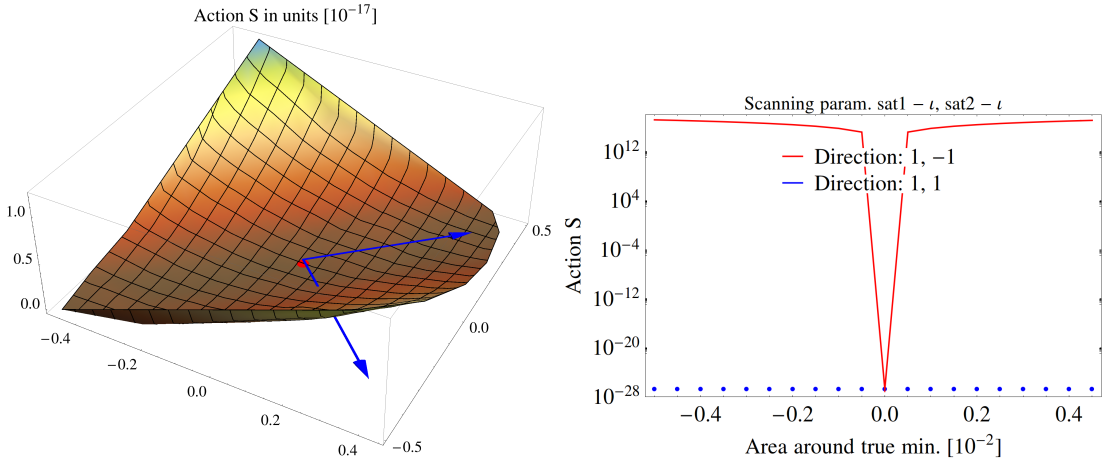

Figure 2.17: Left: 2D scan of action S for ι_1-ι_2 pairs in case of unperturbed, Schwarzschild metric. Blue arrows show the direction of eigenvectors of the Hessian matrix. Right: Section of action S along the eigenvector directions for ι_1-ι_2 pairs. It is evident that there is a degeneracy along the direction marked '1,1'. '$\pm$0.5' on horizontal axes corresponds to $\pm$0.01 rad.

of one satellite with respect to the other, means moving along one of the Hessian matrix eigenvector direction (see Fig. 2.17,2.18, 2.19) and does not make a difference in action S . No difference in action S is expected also if t_a of both satellites are changed by the same amount.

Other orbital parameters are not degenerate as can be seen in Figures: 2.20-2.23.

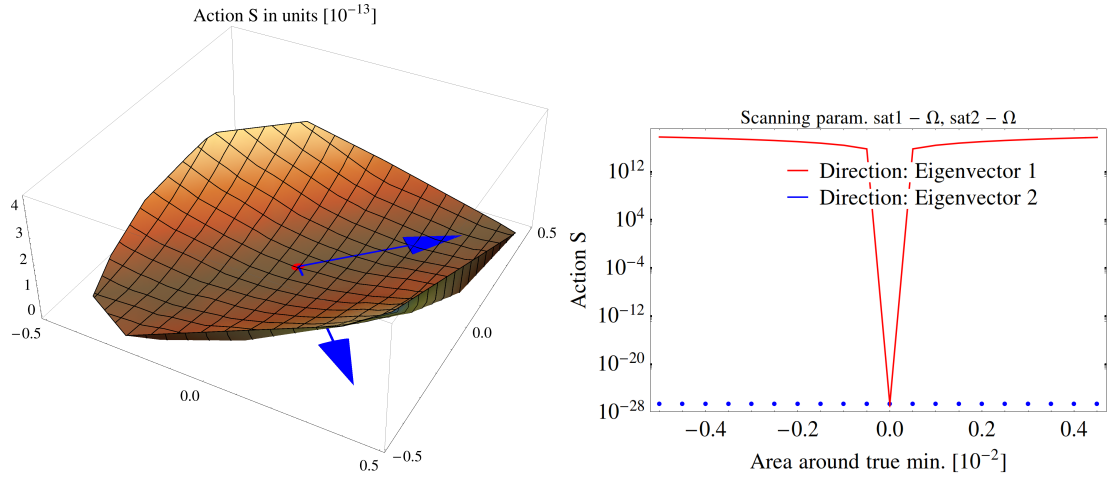

Figure 2.18: Left: 2D scan of action S for Ω_1-Ω_2 pairs in case of unperturbed, Schwarzschild metric. Blue arrows show the direction of eigenvectors of the Hessian matrix. Right: Section of action S along the eigenvector directions for Ω_1-Ω_2 pairs. It is evident that there is a degeneracy along the direction marked 'Eigenvector 2'. '± 0.5' on horizontal axes corresponds to $\pm 2 \cdot 10^{-4}$ rad.

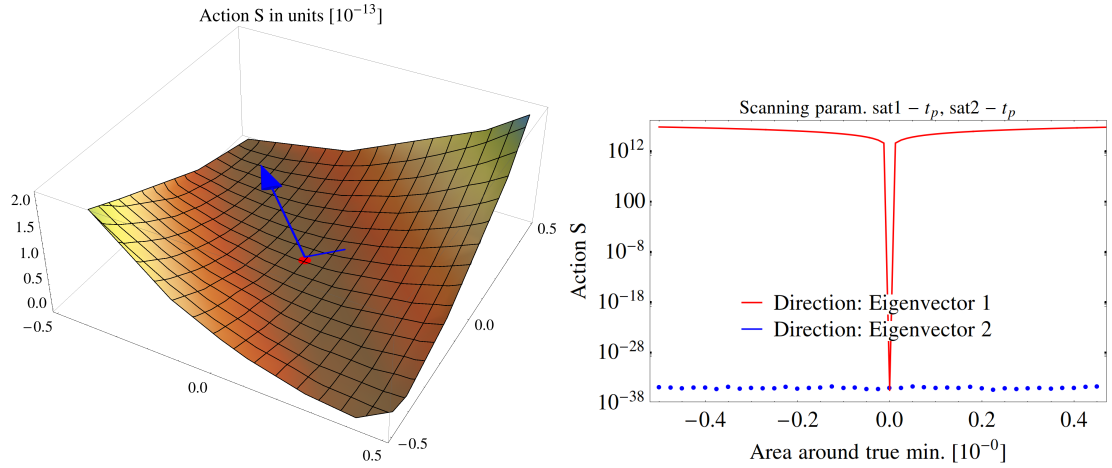

Figure 2.19: Left: 2D scan of action S for t_{a1}-t_{a2} pairs in case of unperturbed, Schwarzschild metric. Blue arrows show the direction of eigenvectors of the Hessian matrix. Right: Section of action S along the eigenvector directions for t_{a1}-t_{a2} pairs. It is evident that there is a degeneracy along the direction marked 'Eigenvector 2'. '± 0.5' on horizontal axes corresponds to $\pm 5 \cdot 10^7\, r_g/c = 7.5 \cdot 10^{-4}$ s.

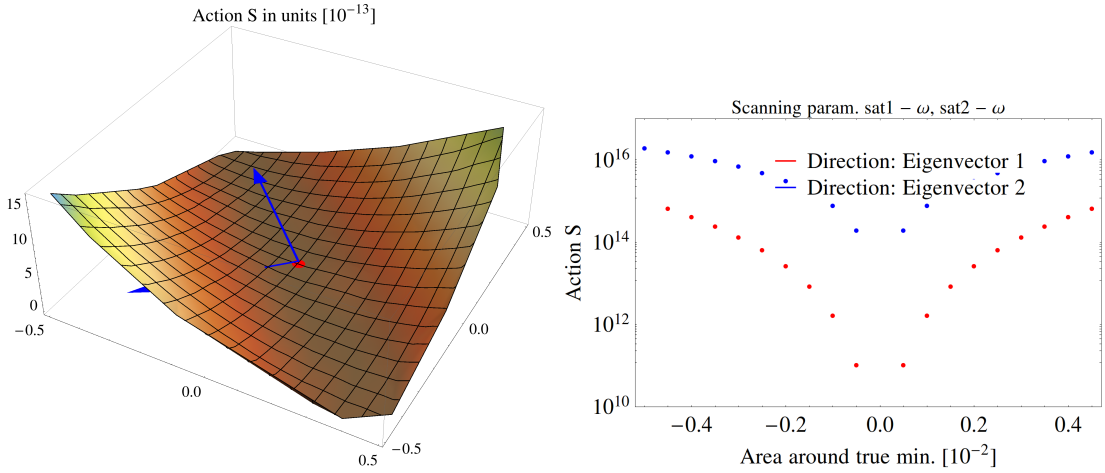

Figure 2.20: Left: 2D scan of action S for ω_1-ω_2 pairs in case of unperturbed, Schwarzschild metric. Blue arrows show the direction of eigenvectors of the Hessian matrix. Right: Section of action S along the eigenvector directions for Ω_1-Ω_2 pairs. It is evident that there is no degeneracy. '± 0.5' on horizontal axes corresponds to $\pm 1 \cdot 10^{-4}$ rad.

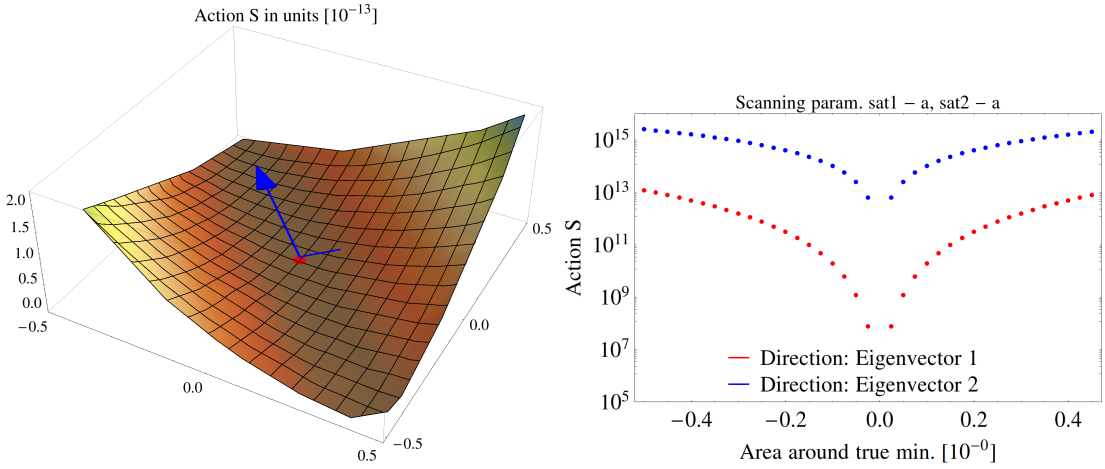

Figure 2.21: Left: 2D scan of action S for a_1-a_2 pairs in case of unperturbed, Schwarzschild metric. Blue arrows show the direction of eigenvectors of the Hessian matrix. Right: Section of action S along the eigenvector directions for a_1-a_2 pairs. It is evident that there is no degeneracy. '± 0.5' on horizontal axes corresponds to $\pm 2 \cdot 10^6\, r_{\mathrm{g}} = \pm 8900$ m.

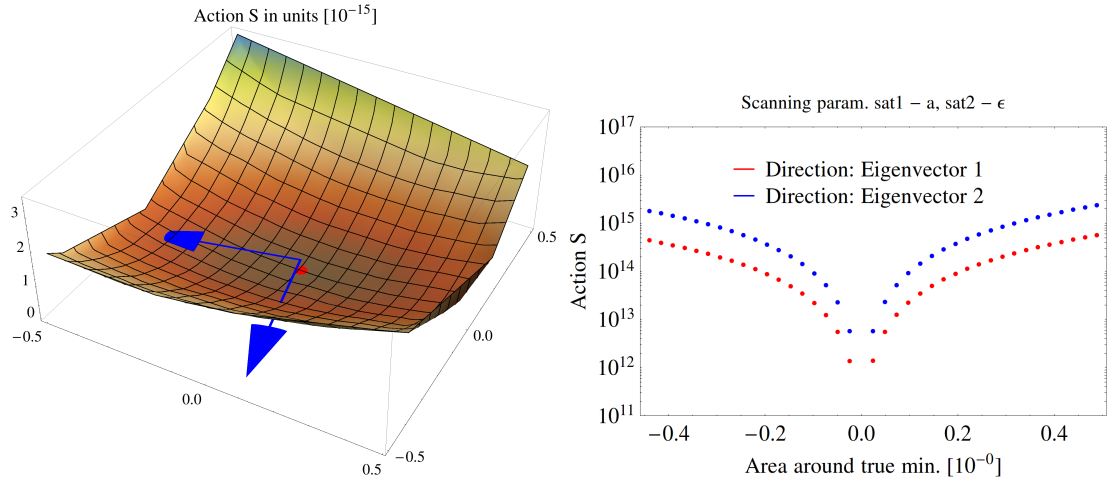

Figure 2.22: Left: 2D scan of action S for a_1-ε_2 pairs in case of unperturbed, Schwarzschild metric. Blue arrows show the direction of eigenvectors of the Hessian matrix. Right: Section of action S along the eigenvector directions for a_1-ε_2 pairs. It is evident that there is no degeneracy. '± 0.5' on horizontal a_1 axis corresponds to $\pm 2 \cdot 10^6\, r_{\mathrm{g}} = \pm 8900$ m, '± 0.5' on ε_2 axis corresponds to ± 0.07.

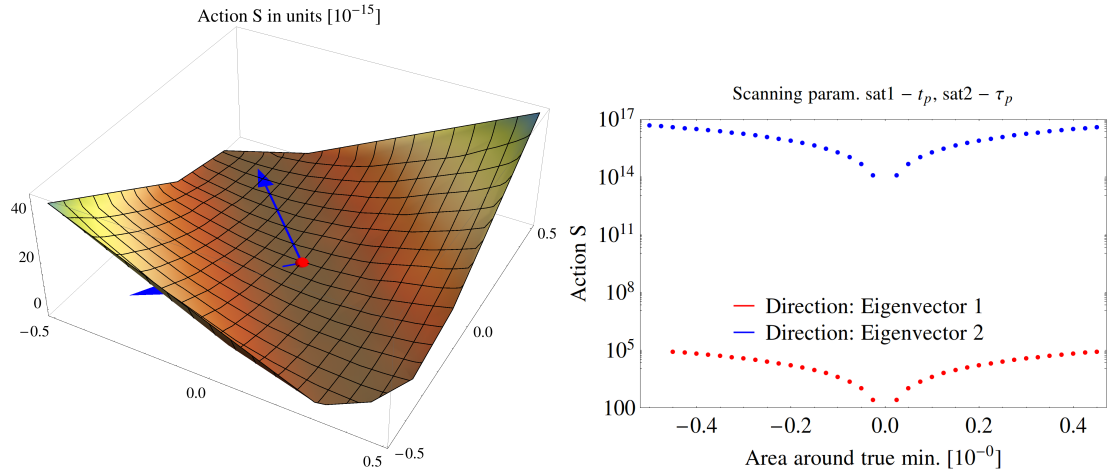

Figure 2.23: Left: 2D scan of action S for t_{a1}-τ_{a2} pairs in case of unperturbed, Schwarzschild metric. Blue arrows show the direction of eigenvectors of the Hessian matrix. Right: Section of action S along the eigenvector directions for t_{a1}-τ_{a2} pairs. It is evident that there is no degeneracy. '± 0.5' on horizontal axes corresponds to $\pm 5 \cdot 10^7\, r_{\mathrm{g}}/c = 7.5 \cdot 10^{-4}$ s.

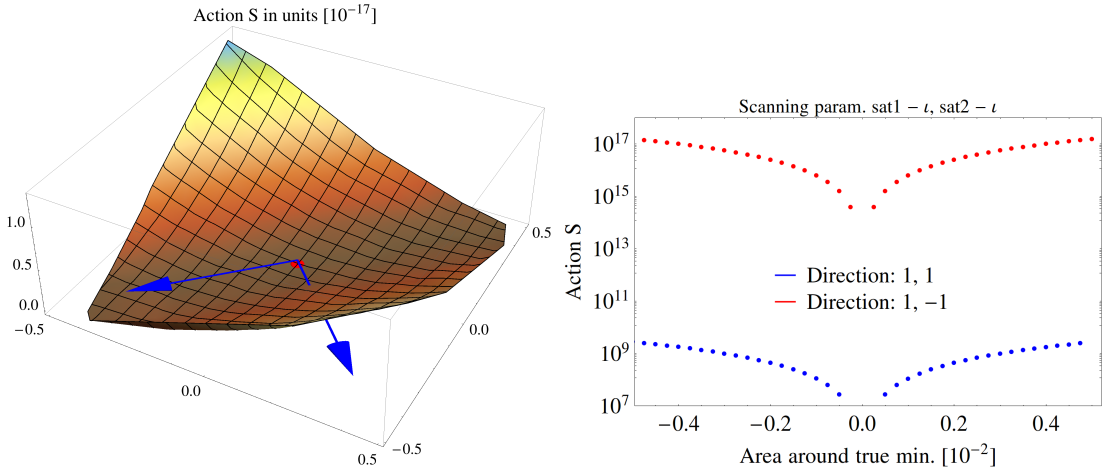

Figure 2.24: Left: 2D scan of action S for ι_1-ι_2 pairs in case of metric perturbed by Earth multipoles, Earth tides and ocean tides. Blue arrows show the direction of eigenvectors of the Hessian matrix. Right: Section of action S along the eigenvector directions for ι_1-ι_2 pairs. It is evident that there is no degeneracy. '$\pm$0.5' on horizontal axes corresponds to $\pm$0.01 rad.

Degeneracies in perturbed metric We then repeated our analysis for the case of perturbed metric. First we include only Earth multipoles, Earth tides and ocean tides. Since the metric is no longer spherically symmetric, above three degeneracies dissapear as is evident in Fig. 2.24-Fig. 2.26. We also repeated our analysis for the case of metric including all gravitational perturbations. Results for ι_1-ι_2 and Ω_1-Ω_2 pairs are shown in Fig. 2.28-Fig. 2.29.

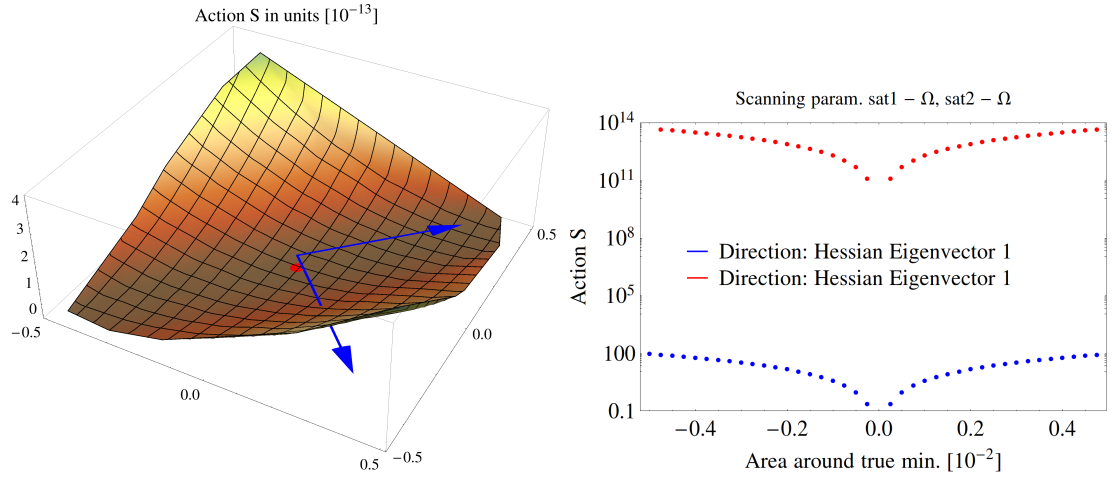

Figure 2.25: Left: 2D scan of action S for Ω_1-Ω_2 pairs in case of metric perturbed by Earth multipoles, Earth tides and ocean tides. Blue arrows show the direction of eigenvectors of the Hessian matrix. Right: Section of action S along the eigenvector directions for Ω_1-Ω_2 pairs. It is evident that there is no degeneracy. '$\pm$0.5' on horizontal axes corresponds to $\pm 2 \cdot 10^{-4}$ rad.

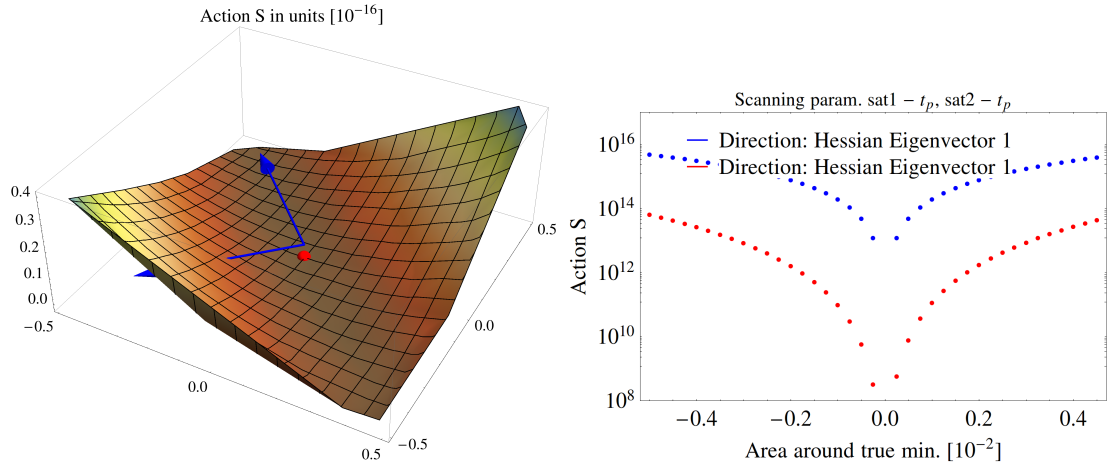

Figure 2.26: Left: 2D scan of action S for t_{a1}-t_{a2} pairs in case of metric perturbed by Earth multipoles, Earth tides and ocean tides. Blue arrows show the direction of eigenvectors of the Hessian matrix. Right: Section of action S along the eigenvector directions for t_{a1}-t_{a2} pairs. It is evident that there is no degeneracy. '$\pm$0.5' on horizontal axes corresponds to $\pm 5 \cdot 10^7\, r_g/c = 7.5 \cdot 10^{-4}$ s.

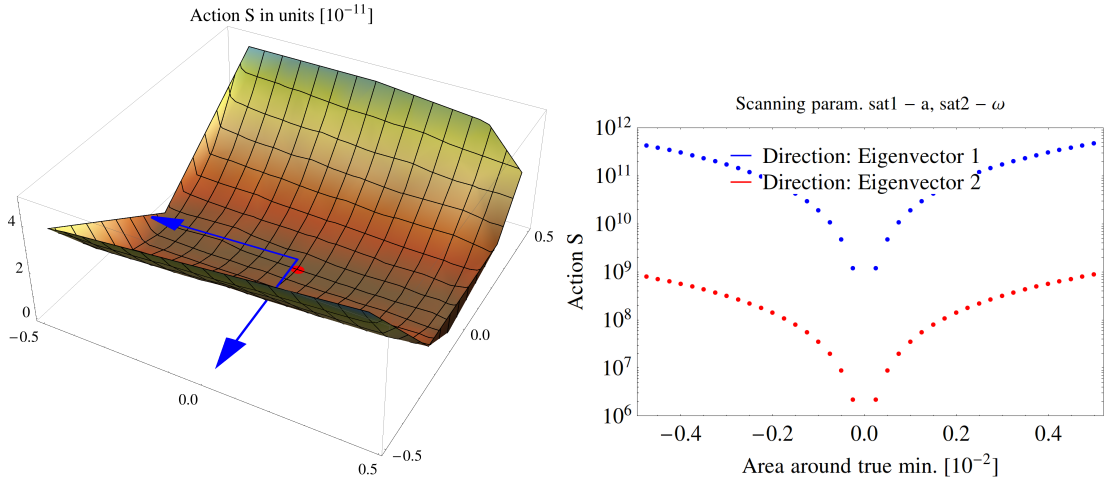

Figure 2.27: Left: 2D scan of action S for a_1-ω_2 pairs in case of metric perturbed by Earth multipoles, Earth tides and ocean tides. Blue arrows show the direction of eigenvectors of the Hessian matrix. Right: Section of action S along the eigenvector directions for a_1-ω_2 pairs. It is evident that there is no degeneracy. '± 0.5' on horizontal a_1 axis corresponds to $\pm 2 \cdot 10^4\, r_{\mathrm{g}} = \pm 89$ m, '± 0.5' on ω_2 axis corresponds to $\pm 1 \cdot 10^{-4}$ rad.

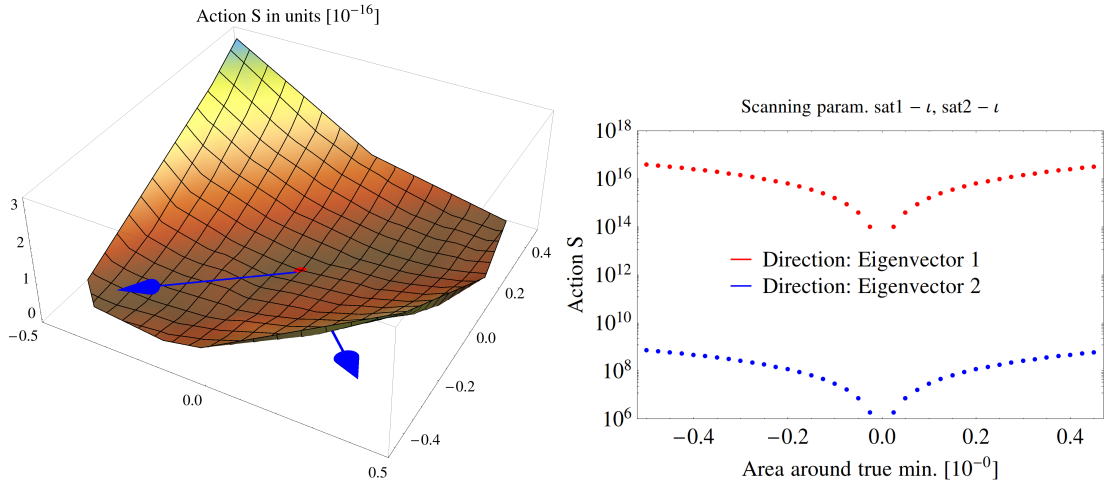

Figure 2.28: Left: 2D scan of action S for ι_1-ι_2 pairs in case of metric including all gravitational perturbations. Blue arrows show the direction of eigenvectors of the Hessian matrix. Right: Section of action S along the eigenvector directions for ι_1-ι_2 pairs. It is evident that there is no degeneracy. '± 0.5' on horizontal axes corresponds to ± 1 rad.

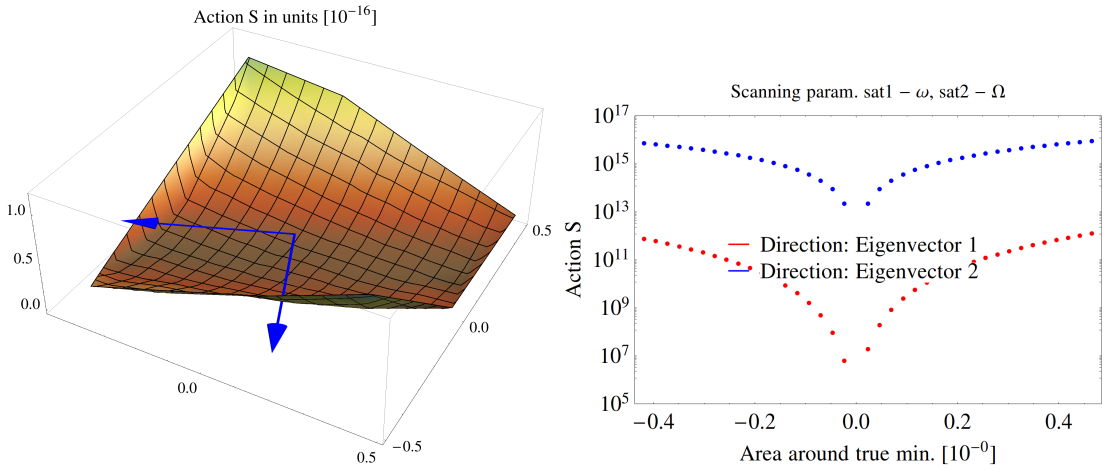

Figure 2.29: Left: 2D scan of action S for ω_1-Ω_2 pairs in case of metric including all gravitational perturbations. Blue arrows show the direction of eigenvectors of the Hessian matrix. Right: Section of action S along the eigenvector directions for ω_1-Ω_2 pairs. It is evident that there is no degeneracy. '± 0.5' on horizontal ω_1 axis corresponds to ± 0.01 rad, '± 0.5' on Ω_2 axis corresponds to $\pm 2 \cdot 10^{-2}$ rad.

To summarize: there are degeneracies in the case of spherically symmetric Earth in pairs of orbital parameters which preserve relative orientation of two satellites. As soon as perturbations are present (Earth multipoles etc.) degeneracies disappear.

Conclusions for WP3: In WP3 we have shown how to construct a relativistic GNSS in a perturbed Schwarzschild space-time including all relevant gravitational perturbations. We find that a user, which receives proper times of four satellites, can determine its position in such RPS with accuracy of the order of $10^{-32} - 10^{-30}$ for coordinate t, and $10^{-28} - 10^{-26}$ for coordinates x, y, and z. We simulated inter-satellite links and built a model of the ABC system, independent of terrestrial reference frames. We showed that using only inter-satellite links and minimizing action S (2.137) for 2x6 orbital parameters, such a system can determine orbital parameters of satellites with accuracy of 10^{-22}. We investigated possible degeneracies in action S and found that in perturbed metric there is no degeneracy between orbital parameters present.

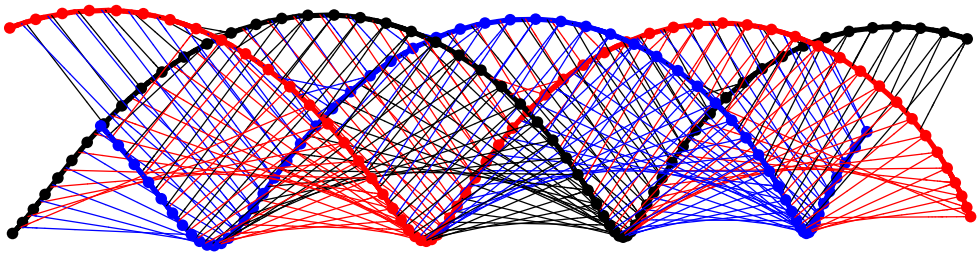

Figure 2.30: Mapping the space-time with three satellites.

2.4 Work Package 4 - Determination of gravitational parameters

Abstract of WP4: When the satellites exchange communication, they actually scan the space-time around Earth (see Fig. 2.30). In this work package we try to determine whether such mapping could be used to find/measure the properties of the sources responsible for the space-time curvature. In a similar way as in Work Package 3, we simulate a constellation of GNSS satellites with inter-satellite links and assume that in addition to initial values of orbital parameters also gravitational perturbation coefficients are known only with limited accuracy. We investigate if action S (2.137) has a well defined minimum also in this case. We vary 2×6 orbital parameters + 14 gravitational parameters and use several numerical methods to find the minimum of action. We investigate to which level of accuracy it would be possible to refine values of gravitational parameters by this method. We discuss prospects and limitations of using GNSS constellation of satellites to probe the space-time around Earth, i.e. to measure gravitational perturbations, and how this influences possible scientific applications.

As in subsection 2.3.2, we construct a model of the RPS with inter-satellite links, and assume that the initial orbital parameters $(Q^\mu(0), P_\mu(0))$ and gravitational parameters (e.g. mass of the Moon) are not known very precisely. Giving the satellites some initial orbital parameters $(Q^\mu(0), P_\mu(0))$ we let them evolve with time according to gravitational perturbations. We calculate satellite orbits, simulate their communication, and calculate the action S according to (2.137). We repeat this for various values of orbital and gravitational parameters to scan the parameter space and investigate whether the action S has a well defined minimum.

2.4.1 Minimum of the action S and refinement of gravitational parameters

We take two satellites on orbits with the following initial orbital parameters:

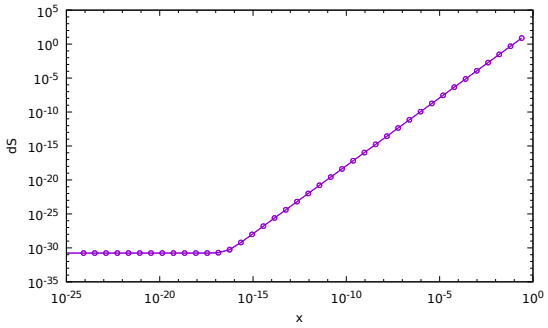

Figure 2.31: Action S as a function of relative offset of Earth's angular velocity $\Omega_\oplus$ from its true value. Value 1 on x axis corresponds to $\Delta\Omega_\oplus/\Omega_\oplus = 0.000014$. Knee in S is at $\sim 10^{-16}$, which corresponds to $\Delta\Omega_\oplus/\Omega_\oplus \sim 10^{-21}$.

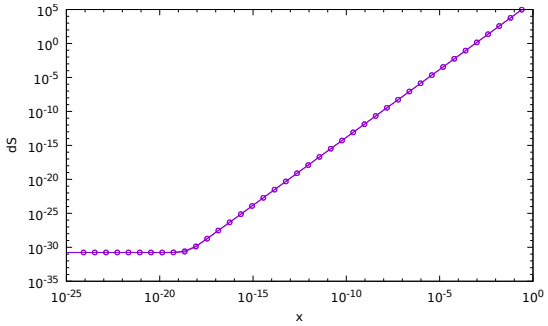

Figure 2.32: Action S as a function of relative offset of Earth's multipole M_{20} from its true value. Value 1 on x axis corresponds to $\Delta M_{20}/M_{20} = 0.00007$. Knee in S is at $\sim 10^{-18}$, which corresponds to $\Delta M_{20}/M_{20} \sim 7 \cdot 10^{-23}$.

- satellite 1: $\Omega_1 = 0^\circ$, $\omega_1 = 0^\circ$, $\iota_1 = 60^\circ$, $a_1 = 30025$ km, $\varepsilon = 0.007$, $t_{a1} = 7.04$ h,
- satellite 2: $\Omega_2 = 120^\circ$, $\omega_2 = 20^\circ$, $\iota_2 = 60^\circ$, $a_2 = 30025$ km, $\varepsilon_2 = 0.008$, $t_{a2} = t_{a1} = 7.04$ h.

First, we vary each of 14 gravitational parameters individually and calculate action S. We find that in all cases the minimum of the action S is well defined and deep[13].

To investigate how accurately one could determine gravitational parameters by this method, we calculate action S as a function of a relative offset of the gravitational parameter from its true value. Results are shown in Figs. 2.31 – 2.44.

In all cases, the action stays more or less constant to some relative offset, and after it, it starts increasing. Position of this "knee" determines how accurately it is possible to determine a given gravitational parameter with this method, namely, for offsets below

[13]Depth of the minimum depends on the numerical precision, e.g. if we do all calculations in double precision, then the minimum is displaced from the true value, and is not as deep as in case of quad precision.

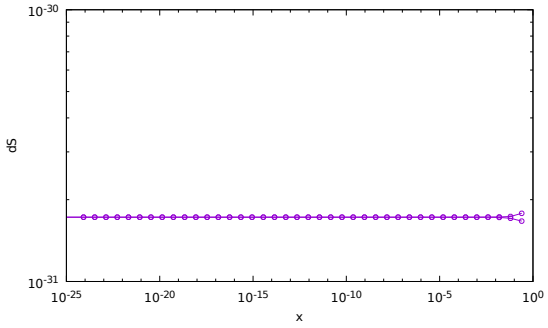

Figure 2.33: Action S as a function of relative offset of Earth's multipole $Re\{M_{21}\}$ from its true value. Value 1 on x axis corresponds to $\Delta Re\{M_{21}\}/Re\{M_{21}\} = 5 \cdot 10^{-18}$. Knee in S lies above that value, therefore it is not possible to refine this parameter using the method of action minimization.

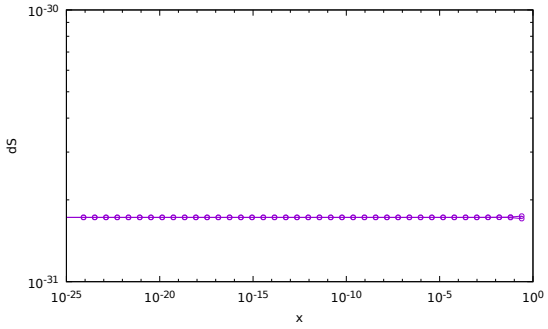

Figure 2.34: Action S as a function of relative offset of Earth's multipole $Im\{M_{21}\}$ from its true value. Value 1 on x axis corresponds to $\Delta Im\{M_{21}\}/Im\{M_{21}\} = 8 \cdot 10^{-19}$. Knee in S lies above that value, therefore it is not possible to refine this parameter using the method of action minimization.

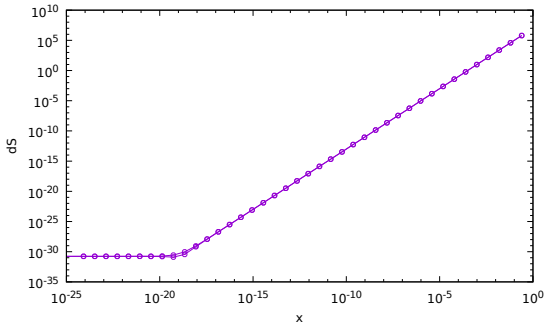

Figure 2.35: Action S as a function of relative offset of Earth's multipole $Re\{M_{22}\}$ from its true value. Value 1 on x axis corresponds to $\Delta Re\{M_{22}\}/Re\{M_{22}\} = 0.02$. Knee in S is at $\sim 10^{-18}$, which corresponds to $\Delta Re\{M_{22}\}/Re\{M_{22}\} \sim 2 \cdot 10^{-20}$.

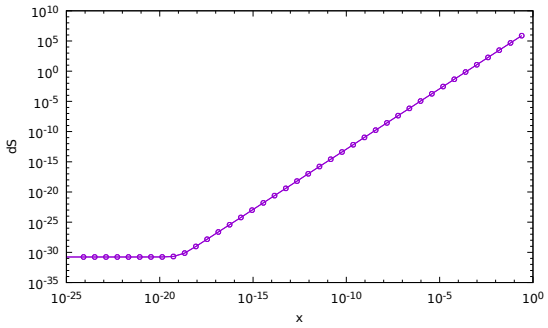

Figure 2.36: Action S as a function of relative offset of Earth's multipole $Im\{M_{22}\}$ from its true value. Value 1 on x axis corresponds to $\Delta Im\{M_{22}\}/Im\{M_{22}\} = 0.04$. Knee in S is at $\sim 10^{-18}$, which corresponds to $\Delta Im\{M_{22}\}/Im\{M_{22}\} \sim 4 \cdot 10^{-20}$.

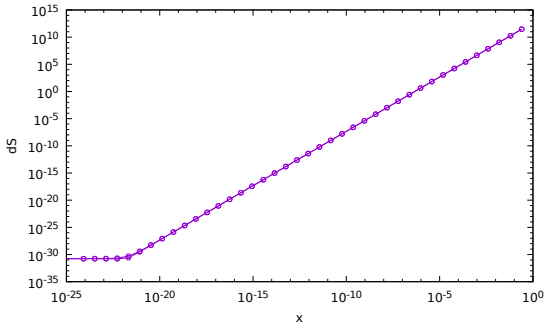

Figure 2.37: Action S as a function of relative offset of the Moon's mass $M_{\leftmoon}$ from its true value. Value 1 on x axis corresponds to $\Delta M_{\leftmoon}/M_{\leftmoon} = 1$. Knee in S is at $\sim 10^{-21}$, which corresponds to $\Delta M_{\leftmoon}/M_{\leftmoon} \sim 10^{-21}$.

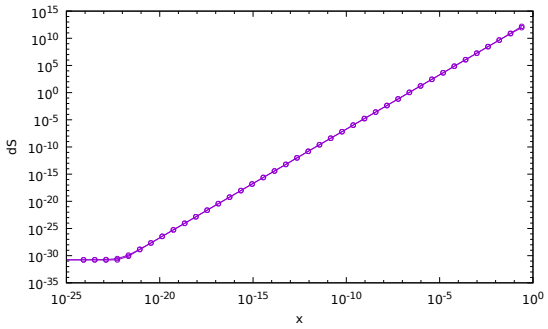

Figure 2.38: Action S as a function of relative offset of the Moon's distance $r_{\leftmoon}$ from its true value. Value 1 on x axis corresponds to $\Delta r_{\leftmoon}/r_{\leftmoon} = 1$. Knee in S is at $\sim 10^{-21}$, which corresponds to $\Delta r_{\leftmoon}/r_{\leftmoon} \sim 10^{-21}$.

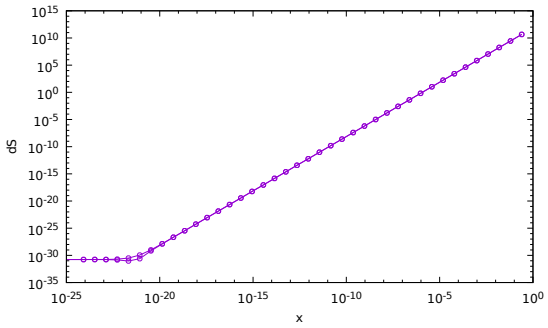

Figure 2.39: Action S as a function of relative offset of the Sun's mass $M_\odot$ from its true value. Value 1 on x axis corresponds to $\Delta M_\odot/M_\odot = 1$. Knee in S is at $\sim 10^{-21}$, which corresponds to $\Delta M_\odot/M_\odot \sim 10^{-21}$.

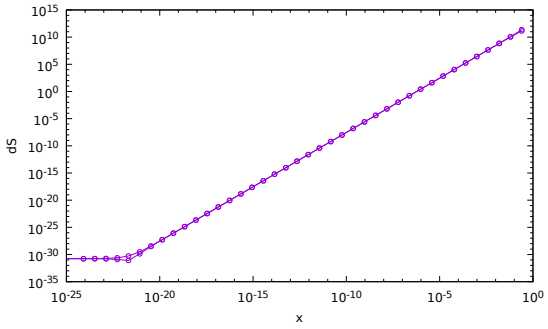

Figure 2.40: Action S as a function of relative offset of the Sun's distance $r_\odot$ from its true value. Value 1 on x axis corresponds to $\Delta r_\odot/r_\odot = 1$. Knee in S is at $\sim 10^{-21}$, which corresponds to $\Delta r_\odot/r_\odot \sim 10^{-21}$.

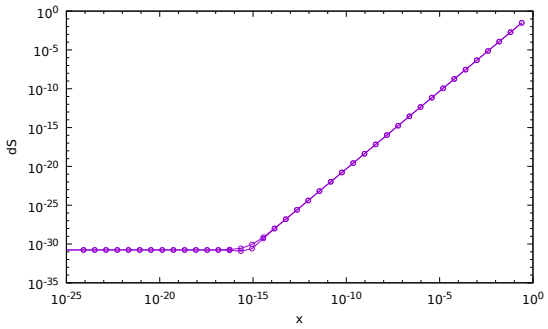

Figure 2.41: Action S as a function of relative offset of Venus' mass M_φ from its true value. Value 1 on x axis corresponds to $\Delta M_\varphi/M_\varphi = 1$. Knee in S is at $\sim 10^{-14}$, which corresponds to $\Delta M_\varphi/M_\varphi \sim 10^{-14}$.

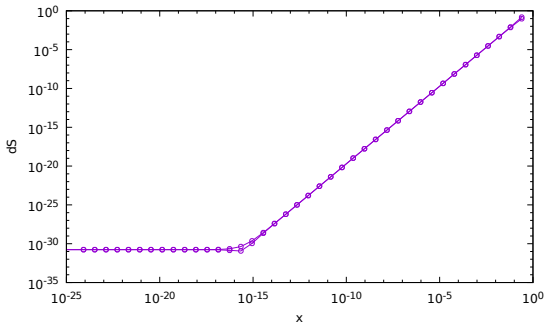

Figure 2.42: Action S as a function of relative offset of the Venus' distance $r_{♀}$ from its true value. Value 1 on x axis corresponds to $\Delta r_{♀}/r_{♀} = 1$. Knee in S is at $\sim 10^{-15}$, which corresponds to $\Delta r_{♀}/r_{♀} \sim 10^{-15}$.

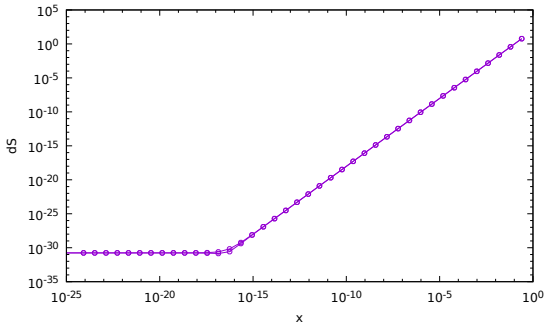

Figure 2.43: Action S as a function of relative offset of Jupiter's mass $M_{♃}$ from its true value. Value 1 on x axis corresponds to $\Delta M_{♃}/M_{♃} = 1$. Knee in S is at $\sim 10^{-14}$, which corresponds to $\Delta M_{♃}/M_{♃} \sim 10^{-14}$.

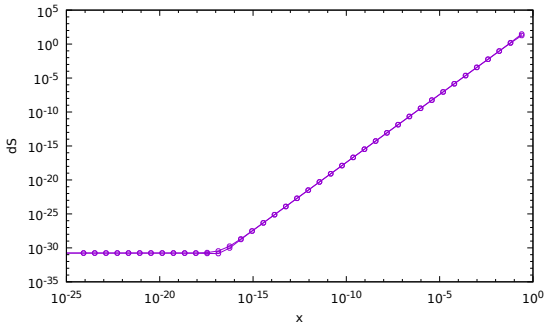

Figure 2.44: Action S as a function of relative offset of the Jupiter's distance $r_{♃}$ from its true value. Value 1 on x axis corresponds to $\Delta r_{♃}/r_{♃} = 1$. Knee in S is at $\sim 10^{-16}$, which corresponds to $\Delta r_{♃}/r_{♃} \sim 10^{-16}$.

the knee value, this method is not sensitive. These limiting (knee) values for different gravitational perturbations are given in Table 2.2. Table 2.2 also gives values of action S and change in position ΔL for some representative offsets in gravitational parameters.[14]

Based on these results (Figs. 2.31 – 2.44 and Table 2.2) we can conclude that, *in principle*, it is possible to refine the gravitational parameters to a very high degree[15] just by finding the minimum of the action.[16]

Table 2.2: Influence of gravitational parameter variation on the action S and satellite's position. Columns are: gravitational parameter, its relative change, corresponding value of action S and change in satellite's position ΔL, knee value order of magnitude.

parameter P	$\frac{\Delta P}{P}$	$S\ [(\frac{r_g}{c})^2]$	ΔL [m]	$(\frac{\Delta P}{P})_{\text{knee}}$
$\Omega_\oplus$	$1.4 \cdot 10^{-8}$	$1.1 \cdot 10^{-6}$	0.00048	10^{-21}
$M_{2,0}$	$7 \cdot 10^{-8}$	1.5	0.1	$7 \cdot 10^{-23}$
Re $M_{2,1}$	$5 \cdot 10^{-21}$	$1 \cdot 10^{-31}$	$8 \cdot 10^{-24}$	$> 5 \cdot 10^{-18}$
Im $M_{2,1}$	$8 \cdot 10^{-22}$	$1 \cdot 10^{-31}$	$4 \cdot 10^{-21}$	$> 8 \cdot 10^{-19}$
Re $M22$	0.00002	10	0.38	$2 \cdot 10^{-20}$
Im $M22$	0.00004	12	0.002	$4 \cdot 10^{-20}$
$M_{☾}$	0.001	$4.6 \cdot 10^6$	140	10^{-21}
$r_{☾}$	0.001	$2 \cdot 10^7$	261	10^{-21}
$M_\odot$	0.001	71000	113	10^{-21}
$r_\odot$	0.001	$2.8 \cdot 10^6$	220	10^{-21}
$M_♀$	0.001	$4.2 \cdot 10^{-7}$	0.00008	10^{-14}
$r_♀$	0.001	$1.5 \cdot 10^{-6}$	0.00016	10^{-15}
$M_♃$	0.001	0.000086	0.00046	10^{-14}
$r_♃$	0.001	0.0003	0.00084	10^{-16}

2.4.2 Finding the minimum

We used different minimization methods. When working in double precision, we used the following algorithms from NLopt library (Johnson 2013): gradient-based (LBFGS, NEWTON, MMA, SLSQP), gradient-free (COBYLA, BOBYQA, NEWUOA, PRAXIS, Nelder-Mead Simplex, Sbplx), and global (DIRECT, DIRECT-L, CRS, MLSL, StoGO, ISRES, ESCH). For global minimization, we also used Multinest (Feroz and Hobson 2008; Feroz et al. 2009, 2013) and Pswarm (Vaz and Vicente 2007, 2009; Le Thi et al. 2012). For quad precision, we implemented the following methods, which we found most promising based on their performance in double precision: gradient-based BFGS, and

[14] ΔL has been calculated in the same way as in Sec. 2.2.3, Fig. 2.12.

[15] At this point, we have to note again, that these numbers represent the accuracy of the numerical methods used. In a real system, the accuracy would be much lower due to numerous effects, e.g. non-gravitational perturbations, atmospheric effects, clock errors...

[16] Except for the $M_{2,1}$ multipole, which is already known with great accuracy.

gradient-free simplex, powell, and praxis. In Figs. 2.45 – 2.51 we show only a tiny fraction of all the countless combinations and tests which we performed.

Minimization approaches From the analysis of action in Figs. 2.31 – 2.42 it follows that it is reasonable to do minimization only with those parameters, which are relevant at current value of action; i.e. we start with the fewest possible parameters, which produce the largest errors in the action, and as the minimization progresses and the action is lowered, we include more and more parameters. In this way it is possible to speed up the whole process. (Basically, it is best to have dimensions of equal size.) Note, however, that gradient-based methods are unaffected by dimension sizes, so we may just include all the parameters at the very beginning of the minimization.

This behaviour can be observed in Figs. 2.50 – 2.51, where we added 5 gravitational parameters (Earth rotation frequency and 4 quadrupoles) to the orbital ones, and used gradient-based method BFGS for minimization. In both plots we can see the horizontal lines, which correspond to the gravitational parameters – the method never modifies these parameters while searching for the minimum. Nevertheless, even though the method correctly ignores the small parameters and the final action is much lower than the initial one, the method did not reach the minimum.

In Figs. 2.45 – 2.49 we added only one gravitational parameter (Earth rotation frequency) to the orbital parameters in minimization. In this case, gradient-free methods approach the true minimum, and the most successful ones manage to minimize all but two parameters (both times of apoapsis passage). The still high values of the final action clearly show, that the true minimum has not been reached yet.

We performed numerous other tests with different initial points, and have found out that the final values of parameters can be different. Although we did many scans of action and did not find any other local minima,[17] we also used global minimizers just to be sure that this is not an issue. An example of global minimization is in Fig. 2.49.

We also found out that the results are independent of number of orbits or number of communication pairs per orbit.[18]

Finally, we have confirmed that it is not possible to decouple minimization of the orbital parameters from minimization of the gravitational parameters, i.e. it is not possible to first minimize wrt. orbital parameters and afterwards wrt. gravitational parameters. As soon as a gravitational parameter is changed from its true value, also the minimum in the orbital parameters shifts from its correct position.

Speed of calculations vs. accuracy In previous sections it was shown that we have to work with 128-bit precision (quad precision) floating point numbers in order to not lose any significant digits for the weakest perturbations. However, doing calculations in quad precision is extremely slow. For example, just by replacing double precision with quad precision variables, the calculations slow down by a factor of 30. Furthermore, if

[17] Except if we extend the interval for ω and Ω so that the periodic nature of these angles starts to show.

[18] In the previous Ariadna studies this was not the case!

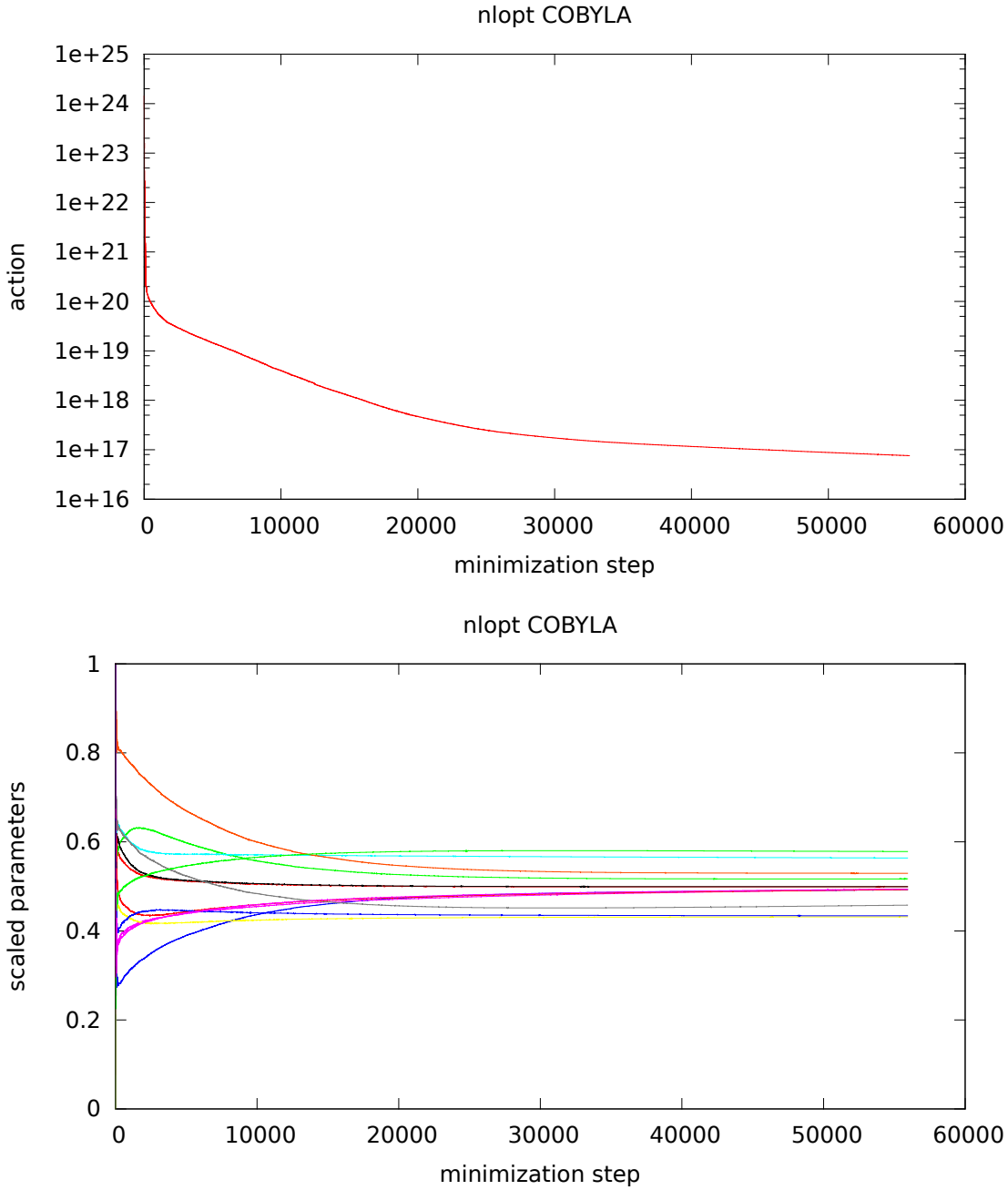

Figure 2.45: The action $S(Q^\mu(0), P_\mu(0))$ (top) and the orbital parameters (bottom) during the minimization process. The parameters are scaled in the interval $[0, 1]$, corresponding to the absolute errors $\{\Delta a, \Delta\varepsilon, \Delta\omega, \Delta\Omega, \Delta\iota, \Delta t_a\} = \{10 \text{ km}, 2.815125 \times 10^{-5}, 1.689075 \times 10^{-2}, 1.12605 \times 10^{-2}, 3.37815 \times 10^{-3}, 0.2 \text{ s}\}$, so that the action is symmetric in that interval. The true values are at 0.5.

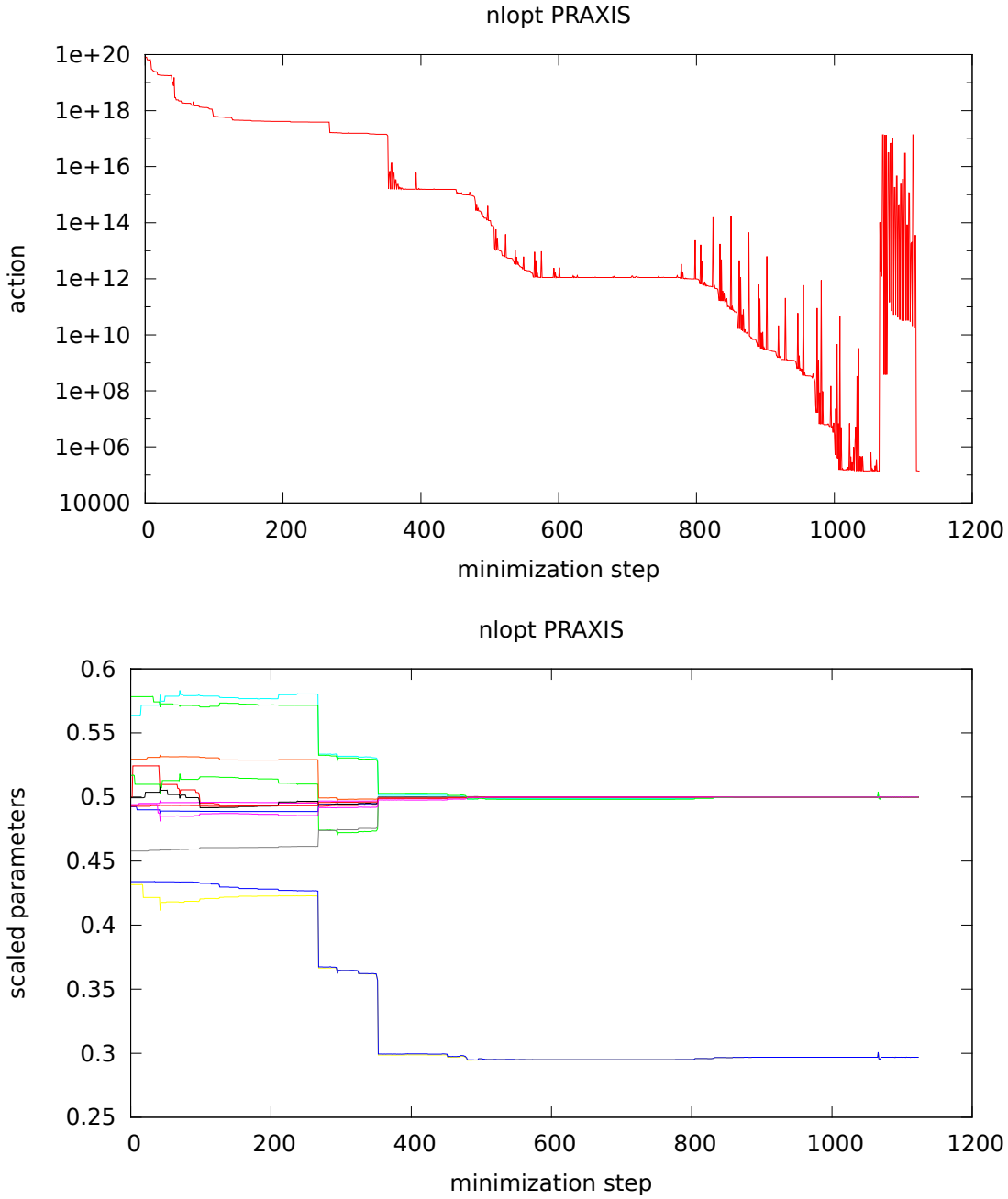

Figure 2.46: The action $S(Q^\mu(0), P_\mu(0))$ (top) and the orbital parameters (bottom) during the minimization process. The parameters are scaled in the interval $[0, 1]$, corresponding to the absolute errors $\{\Delta a, \Delta\varepsilon, \Delta\omega, \Delta\Omega, \Delta\iota, \Delta t_a\} = \{10 \text{ km}, 2.815125 \times 10^{-5}, 1.689075 \times 10^{-2}, 1.12605 \times 10^{-2}, 3.37815 \times 10^{-3}, 0.2 \text{ s}\}$, so that the action is symmetric in that interval. The true values are at 0.5.

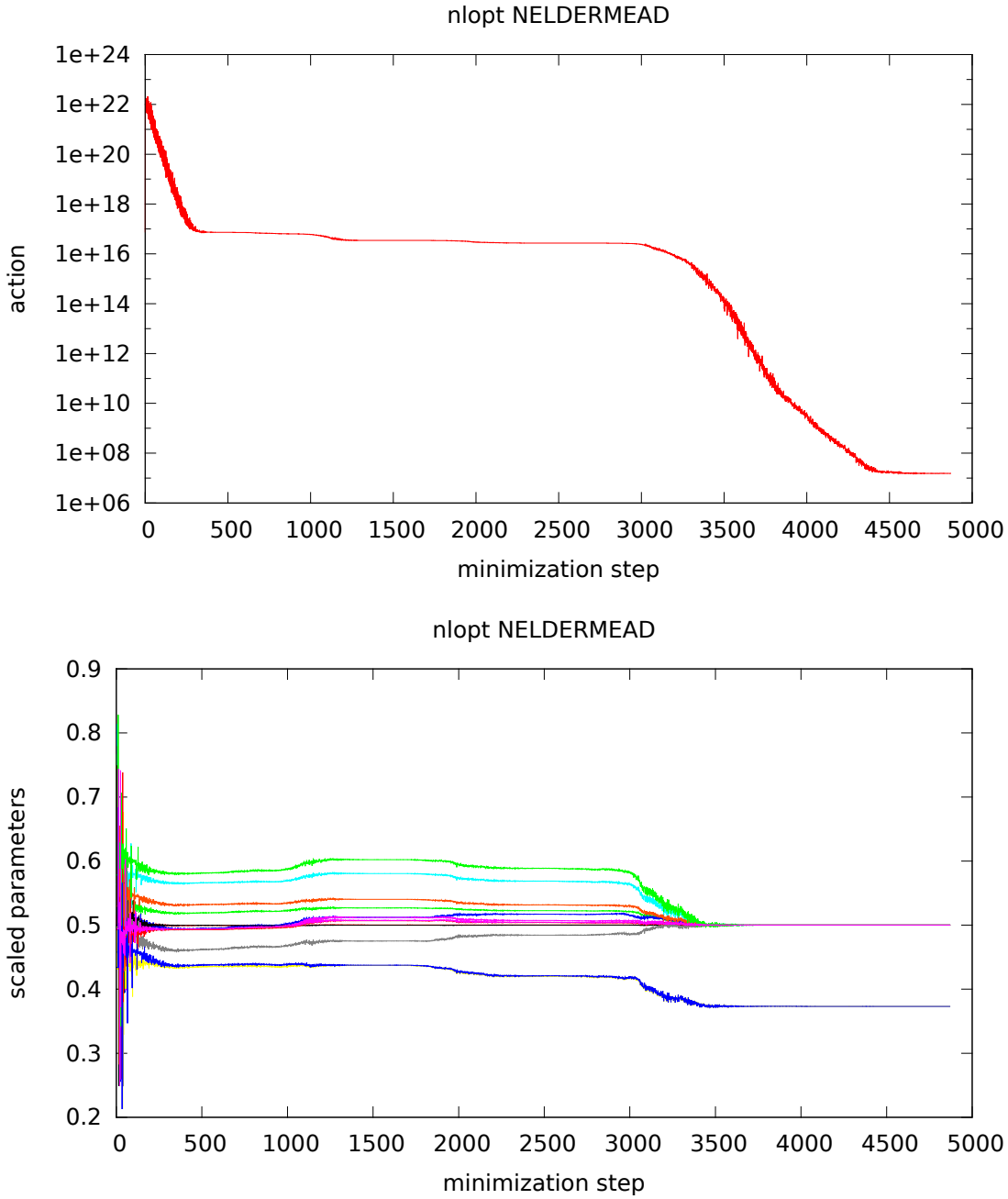

Figure 2.47: The action $S(Q^\mu(0), P_\mu(0))$ (top) and the orbital parameters (bottom) during the minimization process. The parameters are scaled in the interval $[0, 1]$, corresponding to the absolute errors $\{\Delta a, \Delta\varepsilon, \Delta\omega, \Delta\Omega, \Delta\iota, \Delta t_a\} = \{10 \text{ km}, 2.815125 \times 10^{-5}, 1.689075 \times 10^{-2}, 1.12605 \times 10^{-2}, 3.37815 \times 10^{-3}, 0.2 \text{ s}\}$, so that the action is symmetric in that interval. The true values are at 0.5.

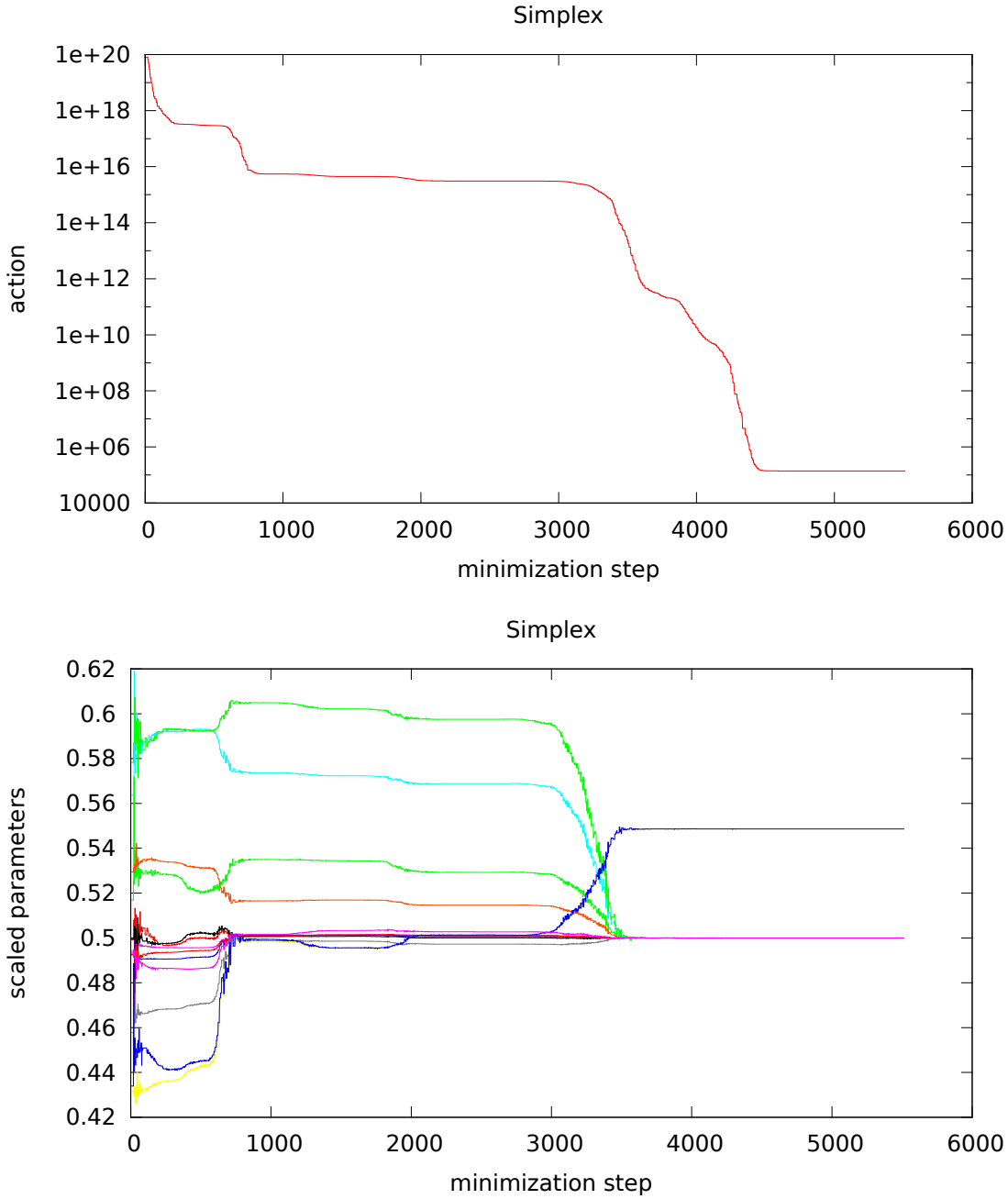

Figure 2.48: The action $S(Q^\mu(0), P_\mu(0))$ (top) and the orbital parameters (bottom) during the minimization process. The parameters are scaled in the interval $[0, 1]$, corresponding to the absolute errors $\{\Delta a, \Delta\varepsilon, \Delta\omega, \Delta\Omega, \Delta\iota, \Delta t_a\} = \{10\text{ km}, 2.815125 \times 10^{-5}, 1.689075 \times 10^{-2}, 1.12605 \times 10^{-2}, 3.37815 \times 10^{-3}, 0.2\text{ s}\}$, so that the action is symmetric in that interval. The true values are at 0.5.

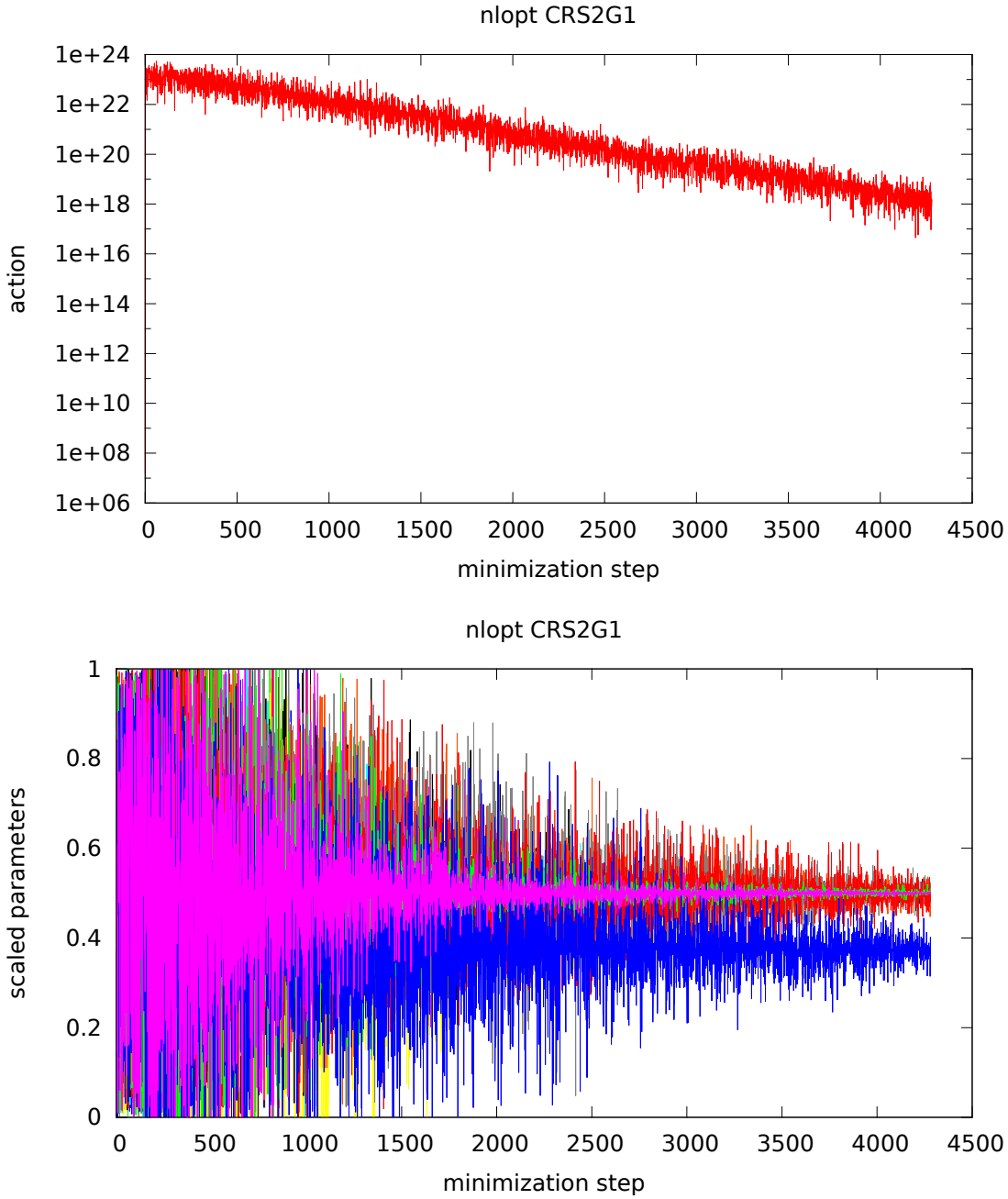

Figure 2.49: The action $S(Q^\mu(0), P_\mu(0))$ (top) and the orbital parameters (bottom) during the minimization process. The parameters are scaled in the interval $[0, 1]$, corresponding to the absolute errors $\{\Delta a, \Delta\varepsilon, \Delta\omega, \Delta\Omega, \Delta\iota, \Delta t_a\} = \{10 \text{ km}, 2.815125 \times 10^{-5}, 1.689075 \times 10^{-2}, 1.12605 \times 10^{-2}, 3.37815 \times 10^{-3}, 0.2 \text{ s}\}$, so that the action is symmetric in that interval. The true values are at 0.5.

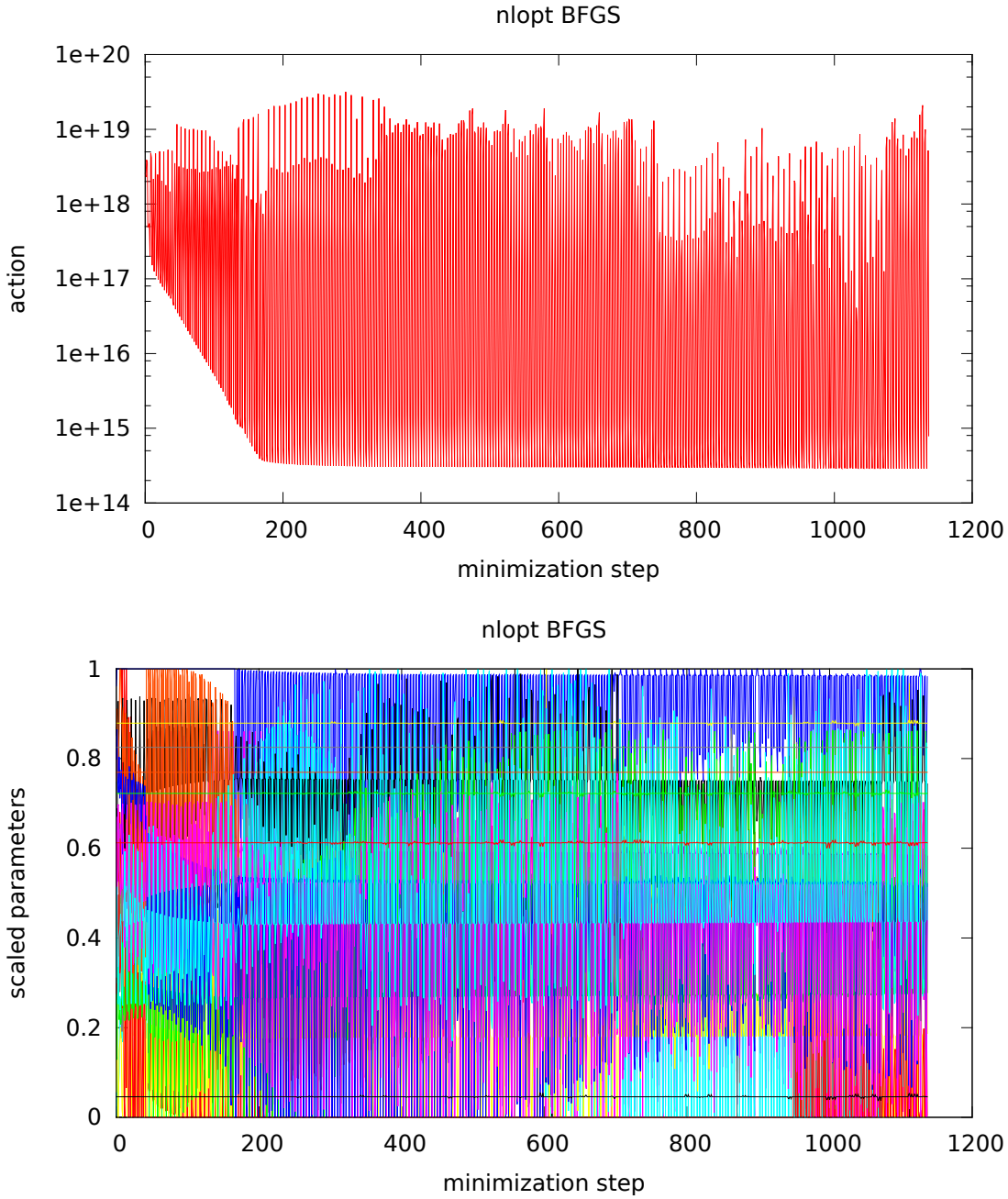

Figure 2.50: The action $S(Q^\mu(0), P_\mu(0))$ (top) and the orbital parameters (bottom) during the minimization process. The parameters are scaled in the interval $[0, 1]$, corresponding to the absolute errors $\{\Delta a, \Delta\varepsilon, \Delta\omega, \Delta\Omega, \Delta\iota, \Delta t_a\} = \{10 \text{ km}, 2.815125 \times 10^{-5}, 1.689075 \times 10^{-2}, 1.12605 \times 10^{-2}, 3.37815 \times 10^{-3}, 0.2 \text{ s}\}$, so that the action is symmetric in that interval. The true values are at 0.5.

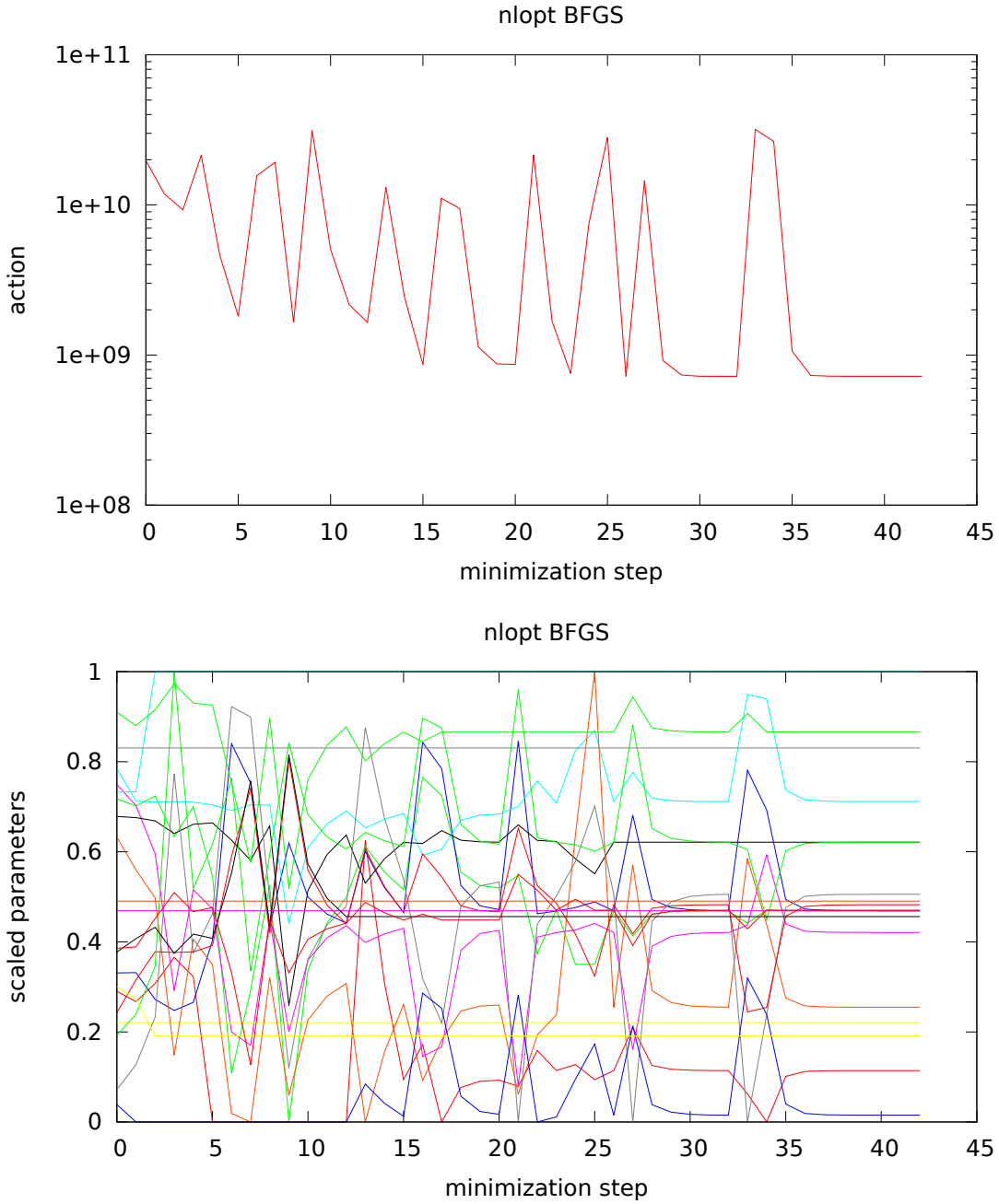

Figure 2.51: The action $S(Q^\mu(0), P_\mu(0))$ (top) and the orbital parameters (bottom) during the minimization process. The parameters are scaled in the interval $[0, 1]$, corresponding to the absolute errors $\{\Delta a, \Delta\varepsilon, \Delta\omega, \Delta\Omega, \Delta\iota, \Delta t_a\} = \{10 \text{ km}, 2.815125 \times 10^{-5}, 1.689075 \times 10^{-2}, 1.12605 \times 10^{-2}, 3.37815 \times 10^{-3}, 0.2 \text{ s}\}$, so that the action is symmetric in that interval. The true values are at 0.5.

we reduce the step-size in the numerical integrator to get the output in quad precision, the time of calculation increases by an additional factor of 30. In the end, it takes 140 seconds to calculate only one action (one step) for a duration of 10 orbits, if the Earth rotation and quadrupoles are the only gravitational parameters included in the minimization. But to do minimization, thousands of action calculations are required, which would take tens of days. And because the number of calculations quickly increases with number of dimensions, it could take months to do only one single minimization test! This is why we put a lot of effort into reducing the calculation times. Here are a few things that we tried:

- Since we found out that the number of orbits and communication pairs per orbit does not affect the end result, we decided to mostly work with only 2 orbits and used only 36 communication pairs per orbit, i.e. we simulated the satellites for 2 periods and let them communicate only every 10°.

- Calculation of planetary perturbations requires data from ephemerides, which we have to interpolate. This is a very slow process, especially if the number of interpolations required is very large – which it is, if we want the results in quad precision. Minimizing the action wrt. planetary parameters (their mass and distance) slows down the calculations by an order of magnitude (or more!), therefore we only include the Earth multipoles in the minimization.

- To speed up calculation of an action, the orbits of the satellites and the summation of the communication pairs are calculated in parallel.

- We tried 2 parallel minimization methods (Multinest and Pswarm), however they are global minimization methods, which are always slower than local methods (even if parallel). Furthermore, they are implemented only for double precision.

- Working with double precision variables. Although this is very fast (and this is why we did many tests with it), the precision loss is too severe, so at some point we had to abandon double precision.

- Use gradient-based minimizers. These require much less steps to find the minimum. The problem is, though, that we do not have an analytic expression for gradient of the action, so we have to calculate it numerically, which takes a very long time. Consequently, calculations of the action are very slow, and in the end, the benefits of the fewer minimization steps are gone. Furthermore, since we calculate the gradient numerically, the minimizer typically stops after a small number of steps due to cancellation errors in gradient computations.

- We used quad precision variables, but increased the integrator step-size so that its output is accurate only to double precision. In this way we were able to maintain all the 16-17 digits of double precision in all the internal computations. This is how Figs. 2.45 – 2.51 were obtained.

- Finally, as it turned out that the equations used in the Hamiltonian formalism (Sec. 2.2 and App. A) are prone to cancellation errors (e.g. some derivatives lose 10 digits!), we decided not to use it for the WP4 minimization, but rather implemented an integrator of the geodesic equation (2.100). The equations involved in this integrator are very meek compared to the Hamiltonian ones and the mere number of them is much lower, so in the end we not only got rid of the cancellation errors, but also gained some speed-up in calculations.

For all the reasons mentioned above, we never performed minimization on *all* $30 - 40$ parameters. It is simply impossible, at least with the hardware that we have at our disposal.

Although none of the tested methods were able to find the minimum when the gravitational parameters were included, the results of all the analysis done clearly show that the action has one minimum for the true values of the gravitational parameters, and if we find a way to get to the minimum, the gravitational parameters can be determined with unprecedented accuracy. But to get there, we would most likely need some non-generic minimizers written especially for this minimization problem, as well as use much better equipment for numerical computations.

2.4.3 Degeneracies

In a similar way as in subsection 2.3.3, we studied possible degeneracies between different gravitational parameters. Some results for the case of metric perturbed by Earth multipoles, Earth tides and ocean tides are presented in Figures 2.52-2.55. We find no degeneracy in action S between gravitational parameters.

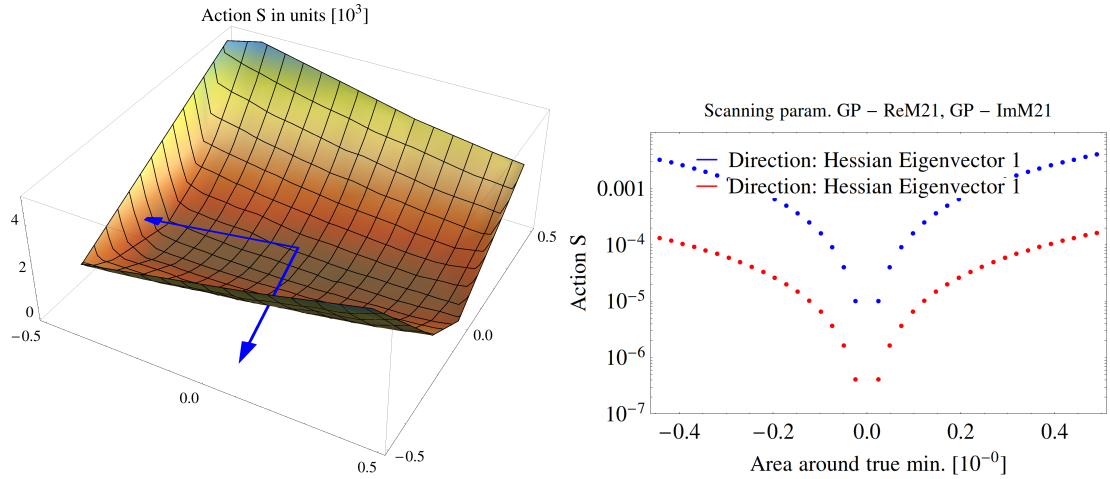

Figure 2.52: Left: 2D scan of action S for Re $M_{2,1}$ and Im $M_{2,1}$ pairs in case of metric perturbed by Earth multipoles, Earth tides and ocean tides. Blue arrows show the direction of eigenvectors of the Hessian matrix. Right: Section of action S along the eigenvector directions for Re $M_{2,1}$ and Im $M_{2,1}$ pairs. It is evident that there is no degeneracy. '± 0.5' on horizontal Re $M_{2,1}$ axis corresponds to $\pm 3.79 \cdot 10^{17}$ m^{5}s^{-2}, '± 0.5' on Im $M_{2,1}$ axis corresponds to $\pm 2.42 \cdot 10^{18}$ m^{5}s^{-2}.

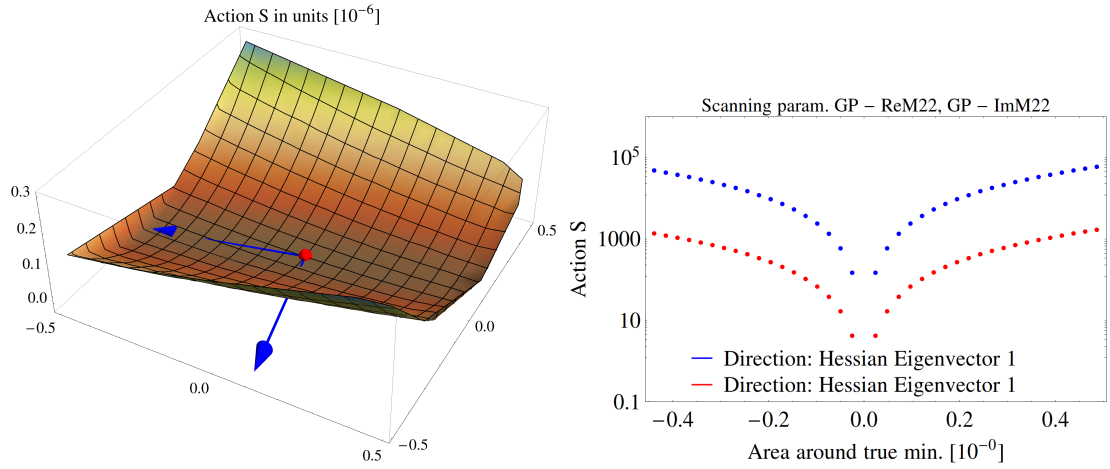

Figure 2.53: Left: 2D scan of action S for Re $M_{2,2}$ and Im $M_{2,2}$ pairs in case of metric perturbed by Earth multipoles, Earth tides and ocean tides. Blue arrows show the direction of eigenvectors of the Hessian matrix. Right: Section of action S along the eigenvector directions for Re $M_{2,2}$ and Im $M_{2,2}$ pairs. It is evident that there is no degeneracy. '± 0.5' on horizontal Re $M_{2,2}$ axis corresponds to $\pm 1.98 \cdot 10^{21}$ m^{5}s^{-2}, '± 0.5' on Im $M_{2,2}$ axis corresponds to $\pm 2.27 \cdot 10^{21}$ m^{5}s^{-2}.

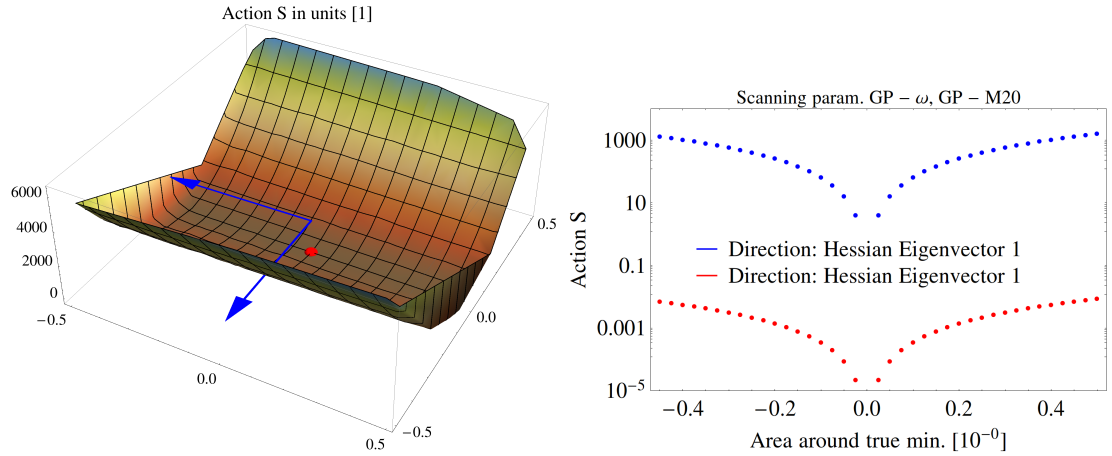

Figure 2.54: Left: 2D scan of action S for $\Omega_\oplus$ and $M_{2,0}$ pairs in case of metric perturbed by Earth multipoles, Earth tides and ocean tides. Blue arrows show the direction of eigenvectors of the Hessian matrix. Right: Section of action S along the eigenvector directions for $\Omega_\oplus$ and $M_{2,0}$ pairs. It is evident that there is no degeneracy. '± 0.5' on horizontal $\Omega_\oplus$ axis corresponds to $\pm 1.02 \cdot 10^{-9}$ s^{-1}, '± 0.5' on $M_{2,0}$ axis corresponds to $\pm 1.94 \cdot 10^{21}$ m^{5}s^{-2}.

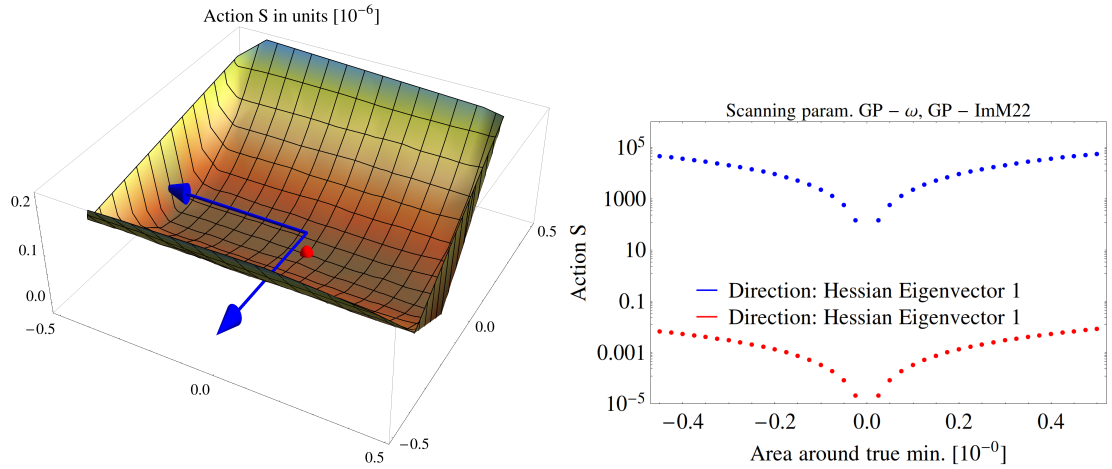

Figure 2.55: Left: 2D scan of action S for $\Omega_\oplus$ and Im $M_{2,2}$ pairs in case of metric perturbed by Earth multipoles, Earth tides and ocean tides. Blue arrows show the direction of eigenvectors of the Hessian matrix. Right: Section of action S along the eigenvector directions for $\Omega_\oplus$ and Im $M_{2,2}$ pairs. It is evident that there is no degeneracy. '± 0.5' on horizontal $\Omega_\oplus$ axis corresponds to $\pm 1.02 \cdot 10^{-9}$ s^{-1}, '± 0.5' on Im $M_{2,2}$ axis corresponds to $\pm 2.27 \cdot 10^{21}$ m^{5}s^{-2}

Conclusions for WP4: In WP4 we simulated a constellation of GNSS satellites with inter-satellite links and assumed that in addition to initial values of orbital parameters also gravitational perturbation coefficients are known only with limited accuracy. We used action S (2.137) and found that it has a well defined minimum also in these cases. By varying each gravitational parameter individually we found that the minimum in action S is pronounced and narrow enough to *theoretically* allow the refinement of gravitational parameters (e.g. Earth multipoles, mass of the Moon) to very high accuracies (see Table 2.2). We then varied orbital and gravitational parameters, and used several numerical methods to find the minimum of action. Although none of the tested methods were able to find the minimum when the gravitational parameters were included, the results of all the analysis done in WP4 clearly show that the action has one minimum for the true values of the gravitational parameters, and if we find a way to get to the minimum, the gravitational parameters can be determined with unprecedented accuracy. Their accuracy is therefore not limited by this method, but rather by other effects (e.g. non-gravitational perturbations, clock noise, atmospheric effects). We investigated possible degeneracies between gravitational parameters and found none.

Chapter 3

Summary

In this project we continued work done under two ESA Ariadna projects carried out in 2010 and 2011 (Čadež et al. 2010, 2011; Delva et al. 2011). It was shown there that GNSS could be modelled in general relativity, and that RPS and ABC concepts are feasible, stable and highly accurate in the case that space-time around Earth is described with Schwarzschild metric, i.e. idealized, spherically symmetric Earth and no other celestial objects.

For a high accuracy GNSS, several gravitational perturbations have to be taken into account in order to get a more realistic model. From Fig. 2.1 we can see that at the GNSS (Galileo, GPS) altitudes relevant gravitational perturbations are (in approximative order of decreasing magnitude) due to: Earth multipoles, the Moon, the Sun, Earth solid tide[1], Venus, Jupiter, Earth ocean tide, and Kerr effect due to Earth's rotation.

Our work and results can be divided in the following Work Packages:

- In WP1 we built a scheme for including all relevant gravitational perturbations (Earth multipoles up to the 6^{th}, Earth solid and ocean tides, the Sun, the Moon, Jupiter, Venus, and the Kerr effect) to the background of the Schwarzschild metric in the weak-field limit with the linear perturbation theory. We used the Regge-Wheeler-Zerilli formalism, i.e., expand perturbations in terms of tensor spherical harmonics, and found connection between our solutions and Newtonian multipole coefficients in the $c \to \infty$ limit. We took into account also the frame-dragging effect of the Earth by the first order term in the expansion of the Kerr metric for $a \ll 1$. The result is a perturbed Schwarzschild metric, with perturbations incorporating effects due to Earth's multipoles, tides and rotation, and weak gravitational influences of other Solar System objects. It is written to the first order with explicit expressions (2.96) and (2.97) and fully determined by multipole momenta $\overline{M}^{\oplus}_{nm}$, $\overline{M}^{\ominus}_{nm}$, Kerr parameter a, and functions $P_n^{(i)}$ and $R_n^{(i)}$.

[1] We note that effects of Earth tides were not part of the original proposal of this project. Since their effects are comparable or even larger than effects of some other gravitational perturbations included in the project, we decided to include also tides to have a complete description of gravitational perturbations.

- In WP2 we calculated satellite dynamics in perturbed space-time. We use perturbed metric derived in WP1 and perturbative Hamiltonian formalism to obtain time derivatives of 0^{th} order constants of motion. With the derivatives known, we were able to determine the time evolution of 0^{th} order constants of motion and because they are varying slowly, we applied them to analytic solutions for Schwarzschild geodesics to calculate orbits of satellites in perturbed space-time. We investigated the influence of individual gravitational perturbations on the orbital parameters evolution (Fig. 2.3 - 2.10) and on the satellite's position and time (Fig. 2.12 - 2.13). We also calculated orbital parameter evolution due to all gravitational perturbations together (Fig. 2.11). We estimated the influence of gravitational perturbations on the user-satellite and inter-satellite light signal time-of-flight and found it to be negligible.

- In WP3 we used perturbed satellite orbits from WP2 to model the relativistic positioning in gravitationally perturbed space-time and test its accuracy. We found that a user, which receives proper times of four satellites, can determine its position in an RPS with accuracy of the order of $10^{-32} - 10^{-30}$ for coordinate t, and $10^{-28} - 10^{-26}$ for coordinates x, y, and z. We then simulated inter-satellite links and built a model of an ABC system. We assumed that the initial values of 0^{th} order constants of motion are known with limited accuracy and showed that a system of two satellites, using only inter-satellite links and minimizing action S (2.137) for 2x6 orbital parameters, can determine their orbital parameters with accuracy of 10^{-22}. We also investigated possible degeneracies between orbital parameters. We found that degeneracies between ι_1-ι_2, Ω_1-Ω_2, and $t_{\text{a}1}$-$t_{\text{a}2}$ exist in unperturbed, Schwarzschild metric (Fig. 2.17-2.19), but they disappear in the perturbed, non-spherically symmetric metric (Fig. 2.24-Fig. 2.26).

- In WP 4 we used a similar procedure as in WP3 to simulate a constellation of GNSS satellites with inter-satellite links and assumed that in addition to initial values of 0^{th} order constants of motion also gravitational perturbation coefficients are known only with limited accuracy. We investigated the behaviour of the action S (2.137) and found that it has a well defined minimum also in these cases. By varying each gravitational parameter individually we found that the minimum in action S is pronounced and narrow enough to *theoretically* allow the refinement of gravitational parameters to very high accuracies (see Table 2.2). We then varied orbital and gravitational parameters, and used several numerical methods to find the minimum of action. Although none of the tested methods were able to find the minimum when the gravitational parameters were included, the results of all the analysis done in WP4 clearly show that the action has one minimum for the true values of the gravitational parameters, and if we find a way to get to the minimum, the gravitational parameters can be determined with unprecedented accuracy. But to get there, we would most likely need some non-generic minimizers written especially for this minimization problem, as well as use much better equipment for numerical computations. We investigated possible degeneracies between

gravitational parameters and found none.

- We presented our work and results of this project at two international meetings. The first one was the ESA - Faculty of Mathematics and Physics (University of Ljubljana) workshop *Relativistic Positioning Systems and Their Scientific Applications*, which we organized from 19$^{\text{th}}$ to 21$^{\text{st}}$ Sep 2012 at Brdo near Kranj in Slovenia (http://rgnss.fmf.uni-lj.si/workshop). We co-edited the workshop proceedings, which were published as a special issue of the ESA Advanced Concepts Team publication *Acta Futura*, Issue 7 (http://www.esa.int/gsp/ACT/doc/ACTAFUTURA/AF07/ACT-BOK-AF07.pdf). The second meeting was the 4$^{\text{th}}$ International Colloquium *Scientific and Fundamental Aspects of the Galileo Programme*, held from 4$^{\text{th}}$ to 6$^{\text{th}}$ Dec 2013 in Prague, Czech Republic, where we co-chaired the session on Relativistic Positioning.

Results of our work are very promising. We find that positioning in an RPS with gravitational perturbations is feasible, highly accurate and stable. Our results show that it is also possible to use RPS with inter-satellite links as an ABC and that a system of satellites can determine their own dynamics, and any additional satellite can be used to increase accuracy of the system and to probe gravitational field. Namely, we find that if we individually vary gravitational parameters, action S has a very well defined minimum and *theoretically* allows refinement of most gravitational parameters to highly accurate values. This indicates that RPS with inter-satellite links may have big scientific potential in various areas of gravimetry, geology, astronomy etc. Namely, as quoted in Table2.2, it would be theoretically possible with the action minimization to determine gravitational parameters, such as Earth multipoles, celestial objects' masses and distances. We note however, that *in practice* there are several difficulties:

- Theoretically possible highly accurate values of gravitational parameters may not be achievable due to effects not considered in this project, e.g. non-gravitational perturbations, clock-noise, atmospheric effects etc.

- Existence and efficiency of numerical multi-dimensional minimization methods which would allow fast and highly precise convergence to the action minimum.

- Minimization problems are expected to be even more severe in cases, where we would like to minimize action in all orbital and gravitational parameters at the same time.

Nevertheless, a system with inter-satellite links and action minimization offers a new, independent way of probing space-time in the vicinity of Earth and measuring the gravitational influence of not only Earth and its multipoles and tides, but also gravitational parameters (e.g. mass and distance) of other celestial bodies. The concept of RPS GNSS has the potential to measure gravitational perturbations to unprecedented

accuracies, which could bring yet unforeseen and various scientific applications, and therefore deserves further studies.

The main reason to further develop a concept of RPS with inter-satellite links is in the accuracy and lower costs of such a system. Namely, although we are not experts on this, we expect that the cost of on-board transmitters and receivers is much lower than the cost of building, running and maintaining ground-based stations to track satellites in order to determine their positions in some terrestrial reference frame. The link between terrestrial reference frames and ABC can be obtained by placing several receivers at the known terrestrial positions, the cost of which is again expected to be low compared to cost of ground-based tracking. All the heavy computations would be preformed in ground-based computing facility. In addition, there would be no need to synchronize satellite clocks to a time-scale realized on the ground.

Next steps should, in our opinion, include:

- Study of more suitable numerical methods for highly accurate and faster minimization of action S.
- Study of the influence of non-gravitational perturbations (e.g. Solar radiation pressure, Earth albedo) on an RPS performance and orbital and gravitational parameters determination.
- Tests on real satellite data: use data of real satellites' orbits, compare them with predictions by a model, and from residuals 'measure' perturbing effects (gravitational and non-gravitational).
- Feasibility study focused on ground-based infrastructure and on-board hardware required for implementing the ABC system.

List of all software and relevant papers is given in App. C.

Bibliography

M. Abramowitz and I. A. Stegun. *Handbook of Mathematical Functions*. Dover, New York, fifth edition, 1964.

T. D. Allison. *Perturbations of test mass motion in the Schwarzschild spacetime using the method of Hamilton and Jacobi*. PhD thesis, Colorado Univ., Boulder., 1989.

G. Arfken. *Mathematical Methods for Physicists*. Academic Press, Orlando, third edition, 1985.

N. Ashby. Relativity in the global positioning system. *Living Reviews in Relativity*, 6 (1):43, 2003. URL http://www.livingreviews.org/lrr-2003-1.

T. Backdahl and M. Herberthson. Explicit multipole moments of stationary axisymmetric spacetimes. *Classical and Quantum Gravity*, 22:3585, 2005. URL doi:10.1088/0264-9381/22/17/017.

E. Berti, V. Cardoso, and A. O. Starinets. Quasinormal modes of black holes and black branes. *Classical and Quantum Gravity*, 26(16):163001, 2009. URL http://stacks.iop.org/0264-9381/26/i=16/a=163001.

R. Biancale. Updates to the iers conventions (2010): Chapter 6 geopotential: Harmonic coefficients of the main waves of fes2004, August 2012. URL http://tai.bipm.org/iers/convupdt/convupdt_c6.html. Accessed: 10. September 2013.

M. Blagojević, J. Garecki, F. W. Hehl, and Y. N. Obukhov. Real null coframes in general relativity and GPS type coordinates. *Phys. Rev. D*, 65(4):044018–+, Feb. 2002. doi: 10.1103/PhysRevD.65.044018.

R. Brent. *Algorithms for Minimization Without Derivatives*. Dover Books on Mathematics. Dover Publications, 1973. ISBN 9780486419985. URL http://books.google.si/books?id=6Ay2biHG-GEC.

A. Čadež, U. Kostić, and P. Delva. Mapping the spacetime metric with a global navigation satellite system, european space agency, the advanced concepts team, ariadna final report (09/1301). Technical report, European Space Agency, 2010.

A. Čadež, U. Kostić, and P. Delva. Mapping the spacetime metric with a global navigation satellite system-extension study: Recovery of orbital constants using intersatellite links, european space agency, the advanced concepts team, ariadna final report (09/1301 ccn). Technical report, European Space Agency, 2011.

B. Coll. A principal positioning system for the Earth. In N. Capitaine and M. Stavinschi, editors, *Journées 2002 - systèmes de référence spatio-temporels. Astrometry from ground and from space, Bucharest, 25 - 28 September 2002, edited by N. Capitaine and M. Stavinschi, Bucharest: Astronomical Institute of the Romanian Academy, Paris: Observato*, volume 14, pages 34–38, 2003.

B. Coll and J. A. Morales. Symmetric frames on Lorentzian spaces. *Journal of Mathematical Physics*, 32(9):2450, 1991. ISSN 00222488. doi: 10.1063/1.529173.

P. Delva, U. Kostić, and A. Čadež. Numerical modeling of a Global Navigation Satellite System in a general relativistic framework. *Advances in Space Research*, 47:370–379, Jan. 2011. doi: 10.1016/j.asr.2010.07.007.

A. T. Doodson. The harmonic development of the tide-generating potential. *Proceedings of the Royal Society of London. Series A, Containing Papers of a Mathematical and Physical Character*, 100(704):pp. 305–329, 1921. ISSN 09501207. URL http://www.jstor.org/stable/93989.

A. Einstein, L. Infeld, and B. Hoffmann. The Gravitational Equations and the Problem of Motion. *The Annals of Mathematics*, 39(1):65–100, 1938. ISSN 0003486X. doi: 10.2307/1968714. URL http://dx.doi.org/10.2307/1968714.

F. Feroz and M. P. Hobson. Multimodal nested sampling: an efficient and robust alternative to Markov Chain Monte Carlo methods for astronomical data analyses. *MNRAS*, 384:449–463, Feb. 2008. doi: 10.1111/j.1365-2966.2007.12353.x.

F. Feroz, M. P. Hobson, and M. Bridges. MULTINEST: an efficient and robust Bayesian inference tool for cosmology and particle physics. *MNRAS*, 398:1601–1614, Oct. 2009. doi: 10.1111/j.1365-2966.2009.14548.x.

F. Feroz, M. P. Hobson, E. Cameron, and A. N. Pettitt. Importance Nested Sampling and the MultiNest Algorithm. *ArXiv e-prints*, June 2013.

R. Geroch. Multipole moments. i. curved space. *J. Math. Phys.*, 11(6):1955–1961, 1970. doi: 10.1063/1.1665348. URL http://dx.doi.org/10.1063/1.1665348.

H. Goldstein. *Classical Mechanics*. Addison-Wesley Publishing Company, Reading, MA, 2nd edition, 1980.

A. Gomboc. *Rapid Luminosity Changes Due to Interaction with a Black Hole*. PhD thesis, Faculty of Mathematics and Physics, University in Ljubljana, Jadranska 19, 1000 Ljubljana, Slovenia, September 2001.

V. Gurzadyan, J. Makino, M. J. Rees, G. Meylan, R. Ruffini, and J. A. Wheeler. *Black Holes, Gravitational Waves and Cosmology*. Advances in Astronomy and Astrophysics Series. Cambridge Scientific Publishers Limited, 2005. ISBN 9781904868255. URL http://books.google.si/books?id=CGp7AAAACAAJ.

R. Hansen. Multipole moments of stationary space-times. *J. Math. Phys.*, 15:46–52, 1974. doi: 10.1063/1.1666501.

J. B. Hartle. Slowly Rotating Relativistic Stars. I. Equations of Structure. *Astrophysical Journal*, 150:1005, Dec. 1967. doi: 10.1086/149400.

J. B. Hartle and D. H. Sharp. Variational Principle for the Equilibrium of a Relativistic, Rotating Star. *Astrophysical Journal*, 147:317, Jan. 1967. doi: 10.1086/149002.

S. Johnson. *The NLopt nonlinear-optimization package*, 2013. http://ab-initio.mit.edu/nlopt.

U. Kostić. Analytical time-like geodesics in Schwarzschild space-time. *General Relativity and Gravitation*, 44:1057–1072, Apr. 2012. doi: 10.1007/s10714-012-1328-5.

H. Le Thi, A. Vaz, and L. Vicente. Optimizing radial basis functions by d.c. programming and its use in direct search for global derivative-free optimization. *TOP*, 20(1):190–214, 2012. ISSN 1134-5764. doi: 10.1007/s11750-011-0193-9. URL http://dx.doi.org/10.1007/s11750-011-0193-9.

F. Lemoine and G. S. F. Center. *Geopotential Model EGM96*. NASA technical paper. National Aeronautics and Space Administration, Goddard Space Flight Center, 1998. URL http://books.google.si/books?id=Ny8rAAAAIAAJ.

F. Lyard, F. Lefevre, T. Letellier, and O. Francis. Modelling the global ocean tides: modern insights from FES2004. *Ocean Dynamics*, 56:394–415, Dec. 2006. doi: 10.1007/s10236-006-0086-x.

C. Ma, M. Feissel, and I. E. R. Service. *Definition and Realization of the International Celestial Reference System by VLBI Astrometry of Extragalactic Objects*. IERS technical note. Central Bureau of IERS, Observatoire de Paris, 1997. URL http://books.google.si/books?id=yJp0nQEACAAJ.

D. McCarthy and P. Seidelmann. *Time: From Earth Rotation to Atomic Physics*. Wiley, 2009. ISBN 9783527627950. URL http://www.scribd.com/doc/23721477/TIME-%E2%80%93-From-Earth-Rotation-to-Atomic-Physics.

O. Montenbruck and E. Gill. *Satellite Orbits: Models, Methods, Applications*. Springer Verlag, 2005.

T. Moyer. *Formulation for Observed and Computed Values of Deep Space Network Data Types for Navigation*. JPL Deep-Space Communications and Navigation Series. John Wiley & Sons, 2005. ISBN 9780471726173. URL http://books.google.si/books?id=Ql8Ge563QGUC.

A. Nagar and L. Rezzolla. Gauge-invariant non-spherical metric perturbations of Schwarzschild black-hole spacetimes. *Classical and Quantum Gravity*, 22(16):R167, 2005. URL http://stacks.iop.org/0264-9381/22/i=16/a=R01.

NASA JPL's Solar System Dynamics group. HORIZONS system Web-Interface, 2013. URL http://ssd.jpl.nasa.gov/horizons.cgi.

H.-P. Nollert. Quasinormal modes: the characteristic 'sound' of black holes and neutron stars. *Classical and Quantum Gravity*, 16(12):R159, 1999. URL http://stacks.iop.org/0264-9381/16/i=12/a=201.

J.-F. Pascual-Sánchez. Introducing relativity in global navigation satellite systems. *Ann. Phys. (Leipzig)*, 16:258–273, April 2007.

G. Petit and B. Luzum. IERS Conventions, IERS Technical Note No. 36. Technical report, International Earth Rotation and Reference Systems Service, 2010.

H. Quevedo. Multipole moments in general relativity -static and stationary vacuum solutions. *Fortschritte der Physik/Progress of Physics*, 38:733840, 1990. doi: 10.1002/prop.2190381002.

T. Regge and J. A. Wheeler. Stability of a Schwarzschild Singularity. *Phys. Rev.*, 108:1063–1069, Nov 1957. doi: 10.1103/PhysRev.108.1063. URL http://link.aps.org/doi/10.1103/PhysRev.108.1063.

C. Rovelli. GPS observables in general relativity. *Phys. Rev. D*, 65:044017, Jan 2002. doi: 10.1103/PhysRevD.65.044017. URL http://link.aps.org/doi/10.1103/PhysRevD.65.044017.

P. K. Seidelmann, G. Britain., and U. S. N. Observatory. *Explanatory supplement to the astronomical almanac*. University Science Books, Mill Valley, Calif. :, [rev. ed.]. edition, 1992. ISBN 0935702687.

J. Souchay. *The International Celestial Reference System and Frame: ICRS Center Report for 2001-2004*. IERS technical note. Verlag des Bundesamtes für Kartographie und Geodäsie, 2006. ISBN 9783898888028. URL http://books.google.si/books?id=U7mztgAACAAJ.

F. Stacey and P. Davis. *Physics of the Earth*. Cambridge University Press, 2008.

A. Tarantola, L. Klimes, J. M. Pozo, and B. Coll. Gravimetry, Relativity, and the Global Navigation Satellite Systems. *ArXiv e-prints*, 2009:35, 5 2009.

W. Torge. *Geodesy*. Walter de Gruyter, 2001.

U.S. Nautical Almanac Office. *Astronomical Almanac for the Year 2013 and Its Companion, the Astronomical Almanac Online*. Astronomical Almanac For The Year. U.S. Government Printing Office, 2012. ISBN 9780707741284. URL http://books.google.si/books?id=7fl_-DLwJ8YC.

A. Čadež and U. Kostić. Optics in the Schwarzschild spacetime. *Phys. Rev. D*, 72(10): 104024, Nov. 2005. doi: 10.1103/PhysRevD.72.104024.

D. A. Varshalovich, A. N. Moskalev, and V. K. Khersonskii. *Quantum Theory of Angular Momentum: Irreducible Tensors, Spherical Harmonics, Vector Coupling Coefficients, 3 Nj Symbols*. World Scientific Publishing Company, Incorporated, 1988. ISBN 9789971501075. URL http://books.google.ru/books?id=zPxlQgAACAAJ.

A. I. Vaz and L. N. Vicente. A particle swarm pattern search method for bound constrained global optimization. *J. of Global Optimization*, 39(2):197–219, Oct. 2007. ISSN 0925-5001. doi: 10.1007/s10898-007-9133-5. URL http://dx.doi.org/10.1007/s10898-007-9133-5.

A. I. F. Vaz and L. N. Vicente. Pswarm: A hybrid solver for linearly constrained global derivative-free optimization. *Optimization Methods Software*, 24(4-5):669–685, Aug. 2009. ISSN 1055-6788. doi: 10.1080/10556780902909948. URL http://dx.doi.org/10.1080/10556780902909948.

C. V. Vishveshwara. Stability of the Schwarzschild Metric. *Phys. Rev. D*, 1:2870–2879, May 1970. doi: 10.1103/PhysRevD.1.2870. URL http://link.aps.org/doi/10.1103/PhysRevD.1.2870.

S. Wolfram. *The Mathematica book*. Wolfram media, Cambridge University Press, 3rd edition, 1996.

F. J. Zerilli. Gravitational Field of a Particle Falling in a Schwarzschild Geometry Analyzed in Tensor Harmonics. *Phys. Rev. D*, 2:2141–2160, Nov 1970. doi: 10.1103/PhysRevD.2.2141. URL http://link.aps.org/doi/10.1103/PhysRevD.2.2141. See erratum by Zerilli in Appendix A-7 of Gurzadyan et al. (2005).

S. Zschocke and S. A. Klioner. On the efficient computation of the quadrupole light deflection. *Classical and Quantum Gravity*, 28(1):015009, 2011. URL http://stacks.iop.org/0264-9381/28/i=1/a=015009.

Appendix A

Canonical transformation

For the transformation $F_2 : (q^\mu, p_\mu) \rightarrow (Q^\mu, P_\mu)$, it is best to take the characteristic function F_2 such that $F_2 = F_2(q^\mu, P_\mu, \tau) = W(q^\mu, P_\mu) - H\tau$, so that p_μ and Q^μ following from this F_2 are (Goldstein 1980):

$$p_\mu = \frac{\partial F_2}{\partial q^\mu} = \frac{\partial W}{\partial q^\mu} \tag{A.1}$$

$$Q^k = \frac{\partial F_2}{\partial P_\mu} \ . \tag{A.2}$$

The Hamiltonian is therefore

$$H = \frac{1}{2}\left(g^{\mu\nu}\frac{\partial W}{\partial q^\mu}\frac{\partial W}{\partial q^\nu}\right) \ . \tag{A.3}$$

Because H satisfies the Staeckel conditions, the Hamilton-Jacobi equations are completely separable, so the function W is simply

$$W = W_t(t) + W_r(r) + W_\theta(\theta) + W_\phi(\phi) \ . \tag{A.4}$$

Since coordinates t and ϕ are cyclic and therefore the momenta p_t and p_ϕ are constant, it is reasonable to keep them also after the canonical transformation:

$$P_1 = -p_t = E = \text{const.} \tag{A.5}$$

$$P_3 = p_\phi = l_z = \text{const.} \tag{A.6}$$

Also due to the cyclic nature of the coordinates, the corresponding functions W_μ are very simple (Goldstein 1980):

$$W_t = p_t t = -P_1 t \tag{A.7}$$

$$W_\phi = p_\phi \phi = P_3 \phi \ . \tag{A.8}$$

With these, it is possible to write the Hamiltonian as

$$H = \frac{1}{2}\left(-\frac{1}{1-2M/r}P_1^2 + \left(1-\frac{2M}{r}\right)\left(\frac{\partial W}{\partial r}\right)^2 + \frac{1}{r^2}\left[\left(\frac{\partial W}{\partial \theta}\right)^2 + \frac{1}{\sin^2\theta}P_3^2\right]\right) \ . \tag{A.9}$$

The expression in the square parenthesis depends only on θ, and is therefore constant (Goldstein 1980). If we label this constant as P_2, we get an expression for $\partial W/\partial\theta$:

$$\left(\frac{\partial W}{\partial \theta}\right)^2 = p_\theta^2 = P_2^2 - \frac{P_3^2}{\sin^2\theta} \ . \tag{A.10}$$

Having in mind equations (A.1), (A.6), and (A.10), it is easy to see that P_2 is the magnitude of the angular momentum:

$$P_2^2 = p_\theta^2 + \frac{p_\phi^2}{\sin^2\theta} = l^2 = \text{const.} \tag{A.11}$$

If we use all the constants to write H

$$H = \frac{1}{2}\left(-\frac{1}{1-2M/r}P_1^2 + \left(1-\frac{2M}{r}\right)\left(\frac{\partial W}{\partial r}\right)^2 + \frac{P_2^2}{r^2}\right), \tag{A.12}$$

and take into account that H itself is constant

$$P_0 = H = \begin{cases} -\frac{1}{2}, & \text{time-like} \\ 0, & \text{light-like} \end{cases} \tag{A.13}$$

we get the expression for $\partial W/\partial r$:

$$\left(\frac{\partial W}{\partial r}\right)^2 = p_r^2 = \frac{1}{1-2M/r}\left[\frac{P_1^2}{1-2M/r} - \frac{P_2^2}{r^2} + 2P_0\right] \ . \tag{A.14}$$

Now we can write the function W from (A.4)

$$W = -P_1 t + P_3\phi + \int_{r_a}^{r}\frac{\partial W}{\partial r}dr + \int_{\pi/2}^{\theta}\frac{\partial W}{\partial\theta}d\theta \ , \tag{A.15}$$

and finally

$$W = -P_1 t + P_3\phi - \int_{r_a}^{r}\frac{1}{X}\sqrt{P_1^2 - X\left(\frac{P_2^2}{r^2} - 2P_0\right)}dr - \int_{\pi/2}^{\theta}\sqrt{P_2^2 - \frac{P_3^2}{\sin^2\theta}}d\theta \ , \tag{A.16}$$

where $X = 1 - 2M/r$ and r_a the apoapsis.[1]

The new coordinates Q^μ after the canonical transformation F_2 are obtained from (A.2) and (A.16):

$$Q^0 = \frac{\partial F_2}{\partial P_0} = -\tau - \int_{r_a}^{r}\frac{1}{\sqrt{P_1^2 - X(P_2^2/r^2 - 2P_0)}}dr = \text{const.} \tag{A.17}$$

[1]The signs of the square roots are chosen so that if the satellite starts at apoapsis, it approaches Earth.

$$Q^1 = \frac{\partial W}{\partial P_1} = -t - \int_{r_a}^{r} \frac{P_1}{X\sqrt{P_1^2 - X(P_2^2/r^2 - 2P_0)}} dr = \text{const.} \tag{A.18}$$

$$Q^2 = \frac{\partial W}{\partial P_2} = \int_{r_a}^{r} \frac{P_2}{r^2\sqrt{P_1^2 - X(P_2^2/r^2 - 2P_0)}} dr - \int_{\pi/2}^{\theta} \frac{P_2}{\sqrt{P_2^2 - P_3^2/\sin^2\theta}} d\theta = \text{const.} \tag{A.19}$$

$$Q^3 = \frac{\partial W}{\partial P_3} = \phi + \int_{\pi/2}^{\theta} \frac{P_3}{\sin^2\theta\sqrt{P_2^2 - P_3^2/\sin^2\theta}} d\theta = \text{const.} \ . \tag{A.20}$$

A.1 Physical meaning of Q^μ

The integral in (A.18) measures time since apoapsis, so the difference between time and this integral equals the time of the first apoapsis passage, i.e. $Q^1 = -t_a$. Similarly, $Q^0 = -\tau_a$ marks the proper time of the first apoapsis passage.

To obtain the physical meaning of the remaining two coordinates, it is best to consider geometric relations which follow from the sine and cosine laws for spherical triangles (see Fig. 2.2).

First, there is a relation between P_3 in P_2:

$$P_3 = P_2 \cos\iota \ , \tag{A.21}$$

where ι is the inclination of the orbital plane. This is, essentially, a relation between z-component of the angular momentum (l_z) and the magnitude of the angular momentum (l). So, instead of (l, l_z), we can use (l, ι) (or, instead of (P_2, P_3), use (P_2, ι)).

Because the orbit is planar, it is better to introduce the true anomaly λ (see Fig. 2.2) than to use two angles (θ, ϕ) or proper time τ to describe the orbit. The true anomaly can be calculated from:

$$[\lambda, l] = 1 \tag{A.22}$$

$$\dot{\lambda} = [\lambda, H] = \frac{l}{r^2} \ , \tag{A.23}$$

and/or from the geometric relations between the angles (θ, ϕ) and (ω, Ω):

$$\sin(\lambda + \omega) = \frac{\cos\theta}{\sin\iota} \tag{A.24}$$

$$\cos(\lambda + \omega) = \cos(\phi - \Omega)\sin\theta \tag{A.25}$$

$$\sin(\phi - \Omega) = \sin(\lambda + \omega)\frac{\cos\iota}{\sin\theta} \tag{A.26}$$

$$\tan\frac{\phi - \Omega}{2} = \frac{\sin(\lambda + \omega)\cos\iota}{\sin\theta + \cos(\lambda + \omega)} \ . \tag{A.27}$$

These relations give:

$$\sqrt{P_2^2 - \frac{P_3^2}{\sin^2\theta}} = P_2\frac{\sin\iota\cos(\lambda + \omega)}{\sin\theta} \tag{A.28}$$

$$\cos(\lambda+\omega)d\lambda = -\frac{\sin\theta}{\sin\iota}d\theta \ , \tag{A.29}$$

which simplifies equations (A.19) and (A.20) for Q^2 and Q^3:

$$Q^2 = \int_{r_a}^{r}(...)dr - \int_{\pi/2}^{\theta}\frac{\sin\theta}{\sin\iota\cos(\lambda+\omega)}d\theta = \int_{r_a}^{r}(...)dr + \int_{-\omega}^{\lambda}d\lambda = \int_{r_a}^{r}(...)dr + (\lambda+\omega) \tag{A.30}$$

$$Q^3 = \phi - \arctan\left(\frac{P_3\cot\theta}{\sqrt{P_2^2 - P_3^2/\sin^2\theta}}\right) = \phi - \arctan\left(\frac{\cot\iota\cos\theta}{\cos(\lambda+\omega)}\right) \ . \tag{A.31}$$

The remaining integral in the above equation for Q^2 gives the angle from the apoapsis, but since the true anomaly λ is already measured from the apoapsis, it follows that $Q^2 = \omega$, i.e. the longitude of the apoapsis. If we invert equation (A.31) and take into account the geometric relations, we find

$$\tan(\phi - Q^3) = \frac{\cot\iota\cos\theta}{\cos(\lambda+\omega)} = \frac{\cot\iota\cot\theta}{\cos(\phi-\Omega)} = \tan(\phi-\Omega) \ , \tag{A.32}$$

so, obviously, $Q^3 = \Omega$.

A.2 Radial integrals

The r integrals in equations (A.17) – (A.19) can be calculated after introducing a new variable u

$$u = \frac{2M}{r} \tag{A.33}$$

and two dimensionless parameters a and b

$$a = \frac{2ME}{l} = \frac{2MP_1}{P_2} \qquad b = \frac{8M^2P_0}{P_2^2} \ . \tag{A.34}$$

With these, the variables Q^0, Q^1 and Q^2 are rewritten as:

$$Q^0 = -\tau_a = -\tau + \frac{2Ma}{E}\int_{u_3}^{u}\frac{du}{u^2\sqrt{a^2 - u^2(1-u) + b(1-u)}} \tag{A.35}$$

$$Q^1 = -t_a = -t + 2Ma\int_{u_3}^{u}\frac{du}{u^2(1-u)\sqrt{a^2 - u^2(1-u) + b(1-u)}} \tag{A.36}$$

$$Q^2 = \omega = -\int_{u_3}^{u}\frac{du}{\sqrt{a^2 - u^2(1-u) + b(1-u)}} + \lambda + \omega \ , \tag{A.37}$$

which are the well known equations of orbit and time, with the already known solutions (Čadež et al. 2010; Delva et al. 2011; Kostić 2012; Gomboc 2001):

$$Q^0 = -\tau_a = -\tau + \frac{t}{E} - \frac{2n}{\tilde{l}u_3}\left(\Pi(n_1;\chi|m) + \frac{u_3}{1-u_3}\Pi(n_2;\chi|m)\right) \tag{A.38}$$

$$Q^1 = -t_a = -t + \frac{2na}{u_3^2}\left[\left(1 + u_3 + \frac{n_1^2 - m}{2(m-n_1)(n_1-1)}\right)\Pi(n_1;\chi|m) + \frac{u_3^2}{1-u_3}\Pi(n_2;\chi|m)\right.$$
$$\left. + \frac{n_1/2}{(m-n_1)(n_1-1)}\left(\mathrm{E}(\chi|m) - \left(1 - \frac{m}{n_1}\right)\mathrm{F}(\chi|m) - \frac{n_1 \sin 2\chi\sqrt{1 - m\sin^2\chi}}{2(1 - n_1\sin^2\chi)}\right)\right] \tag{A.39}$$

$$Q^2 = \omega = -n\mathrm{F}(\chi|m) + \lambda + \omega \ , \tag{A.40}$$

where F, E, and Π are the elliptic integrals of the first, the second, and the third kind, respectively, (definitions are from Wolfram (1996)) and χ is such that

$$u(\chi) = u_2 - (u_2 - u_3)\cos^2\chi \ , \tag{A.41}$$

while the parameters u_1, u_2, and u_3 are the roots of the polynomial under the square root in equations (A.35), (A.36) and (A.37):

$$u_1 = \frac{1}{3}\left(1 + 2|\mathcal{D}|\cos\frac{\psi}{3}\right) \tag{A.42a}$$
$$u_2 = \frac{1}{3}\left(1 + 2|\mathcal{D}|\cos\frac{\psi - 2\pi}{3}\right) \tag{A.42b}$$
$$u_3 = \frac{1}{3}\left(1 + 2|\mathcal{D}|\cos\frac{\psi + 2\pi}{3}\right) \ . \tag{A.42c}$$

All the parameters depend only on E and l (i.e. on P_1 and P_2):

$$\alpha = 1 - 9b - \frac{27}{2}a^2 \qquad \beta = -1 - 3b \tag{A.43a}$$
$$D = \alpha^2 + \beta^3 \qquad |\mathcal{D}| = \sqrt{-\beta} \tag{A.43b}$$
$$\psi = 2\arctan\left(\frac{\sqrt{-D}}{\alpha + \sqrt{-\beta^3}}\right) \tag{A.43c}$$
$$m = \frac{u_2 - u_3}{u_1 - u_3} \qquad n = \frac{2}{\sqrt{u_1 - u_3}} \tag{A.43d}$$
$$n_1 = 1 - \frac{u_2}{u_3} \qquad n_2 = \frac{u_2 - u_3}{1 - u_3} \ . \tag{A.43e}$$

For completness, using the inverse of (A.40)

$$\chi(\lambda) = \mathrm{am}\left(\frac{\lambda}{n}\ |m\right) \ , \tag{A.44}$$

we also provide a direct relation between u and λ

$$u(\lambda) = u_2 - (u_2 - u_3)\mathrm{cn}^2\left(\frac{\lambda}{n}|m\right) \tag{A.45}$$

However, it turns out, that the form of (A.42a) – (A.43c) is not the most suitable for GNSS, because due to "weak relativity" precision loss will occur. For this reason, it is

necessary to use the following set of parameters (Čadež et al. 2010):

$$q = \frac{3\sqrt{12\eta^2 + (-81\eta^4 - 324\eta^3 - 378\eta^2 - 108\eta + 3)\,\tilde{l}^{-2} + 24\eta - 12\tilde{l}^{-4}}}{2\tilde{l}\left(1 - 3\tilde{l}^{-2}\right)^{3/2}} \tag{A.46a}$$

$$\psi_a = -\arcsin(q) \tag{A.46b}$$

$$p = \sqrt{1 - 3/\tilde{l}^2} \tag{A.46c}$$

$$u_1 = p + \frac{1/\tilde{l}^2}{1+p} - \frac{4p}{3}\sin^2\frac{\psi_a}{6} \tag{A.46d}$$

$$u_2 = \frac{1}{3}\left(\frac{3/\tilde{l}^2}{1+p} - p\sqrt{3}\sin\frac{\psi_a}{3} + 2p\sin^2\frac{\psi_a}{6}\right) \tag{A.46e}$$

$$u_3 = \frac{1}{3}\left(\frac{3/\tilde{l}^2}{1+p} + p\sqrt{3}\sin\frac{\psi_a}{3} + 2p\sin^2\frac{\psi_a}{6}\right)\ , \tag{A.46f}$$

where $\eta = E - 1$ and $\tilde{l} = l/2M$.

The major semi-axis a and the eccentricity ε of the orbit are trivially calculated from the periapsis $r_p = 2M/u_2$ and the apoapsis $r_a = 2M/u_3$:

$$a = M\left(\frac{1}{u_2} + \frac{1}{u_3}\right) \tag{A.47}$$

$$\varepsilon = \frac{u_2 - u_3}{u_2 + u_3}\ . \tag{A.48}$$

A.3 Derivatives of canonical variables

First, we define a number of auxilliary functions and their derivatives (we use definitions from App. A.2 and App. A.3.1):

$$J = \int_{r_a}^{r} \frac{P_2}{r^2\sqrt{P_1^2 - X(P_2^2/r^2 - 2P_0)}}dr \tag{A.49}$$

$$\begin{aligned}\frac{\partial J}{\partial P_2} = -\frac{n^3}{4P_2 n_A^2}\Big[&(1-u_3)N_{scd} - n_A\big(-2 + 3u_3 + n_A^2 u_3 + n_A(3u_3 - 1)\big)N_{cd} + \\ &+\frac{n_A^2}{m}\big(n_A u_3 + m(-1 + (3+n_A)u_3)\big)N_d - \frac{u_3 n_A^3}{m}\frac{\lambda}{n}\Big] - \frac{\lambda}{P_2}\end{aligned} \tag{A.50}$$

$$\frac{\partial J}{\partial P_1} = \frac{P_1 n^3}{P_2^2 n_A^2 u_3^2}N_{scd} \tag{A.51}$$

$$\frac{\partial J}{\partial P_0} = \frac{n^3}{P_2^2(u_2 - u_3)^2}\left[(1-u_3)N_{scd} - n_A u_3 N_{cd}\right] \tag{A.52}$$

$$I = \int_{r_a}^{r} \frac{P_1}{X\sqrt{P_1^2 - X(P_2^2/r^2 - 2P_0)}}dr \tag{A.53}$$

$$\frac{\partial I}{\partial P_2} = -\frac{\partial J}{\partial P_1} \tag{A.54}$$

$$\frac{\partial I}{\partial P_1} = \frac{4P_1^2 n^3}{P_2^3 n_A^2 u_3^2}\left[\frac{1}{u_3^2}N_{QQscd} + \frac{1}{u_3}N_{Qscd} + \frac{1}{1-u_3}N_{Q'scd}\right] - \\ - \frac{4n}{P_2}\left[\frac{1}{u_3^2}N_{QQ} + \frac{1}{u_3}N_{Q} + \frac{1}{1-u_3}N_{Q'}\right] \tag{A.55}$$

$$\frac{\partial I}{\partial P_0} = \frac{4P_1^2 n^3}{P_2^3 u_3^2 (u_2-u_3)^2}N_{QQscd} \tag{A.56}$$

$$K = \int_{\pi/2}^{\theta} \frac{P_2}{\sqrt{P_2^2 - P_3^2/\sin^2\theta}} d\theta \tag{A.57}$$

$$\frac{\partial K}{\partial P_3} = -\frac{\cot\iota \tan(\lambda+\omega)}{P_2 \sin\iota} \tag{A.58}$$

$$\frac{\partial K}{\partial P_2} = \frac{1}{P_2}\cot^2\iota \tan(\lambda+\omega) \tag{A.59}$$

$$L = \int_{\pi/2}^{\theta} \frac{P_3}{\sin^2\theta\sqrt{P_2^2 - P_3^2/\sin^2\theta}} d\theta \tag{A.60}$$

$$\frac{\partial L}{\partial P_3} = -\frac{\tan(\lambda+\omega)}{P_2 \sin^2\iota} \tag{A.61}$$

$$\frac{\partial L}{\partial P_2} = -\frac{\partial K}{\partial P_3} \tag{A.62}$$

$$\widetilde{M} = \sqrt{P_2^2 - P_3^2/\sin^2\theta} \tag{A.63}$$

$$\frac{\partial \widetilde{M}}{\partial \theta} = \frac{P_3 \cot\theta \cot\iota}{\sin\theta\cos(\lambda+\omega)} \tag{A.64}$$

$$\frac{\partial \widetilde{M}}{\partial P_3} = -\frac{\cot\iota}{\sin\theta\cos(\lambda+\omega)} \tag{A.65}$$

$$\frac{\partial \widetilde{M}}{\partial P_2} = \frac{\sin\theta}{\sin\iota\cos(\lambda+\omega)} \tag{A.66}$$

$$\widetilde{R} = \frac{du}{d\lambda} = \frac{2(u_2-u_3)}{n}\mathrm{sn}(\frac{\lambda}{n}|m)\mathrm{cn}(\frac{\lambda}{n}|m)\mathrm{dn}(\frac{\lambda}{n}|m) \tag{A.67}$$

$$N = \frac{1}{X}\left(\frac{P_1^2}{X} - \frac{P_2^2}{r^2} + 2P_0\right) \tag{A.68}$$

$$\sqrt{N} = \frac{P_2}{4X}\widetilde{R} \tag{A.69}$$

$$\frac{\partial\sqrt{N}}{\partial r} = \frac{2}{P_2 r^2 \widetilde{R}}\left(-N + \frac{P_2^2}{r^2} - \frac{P_1^2}{X^2}\right) \tag{A.70}$$

$$\frac{\partial\sqrt{N}}{\partial P_2} = -\frac{2}{r^2\widetilde{R}} \tag{A.71}$$

$$\frac{\partial\sqrt{N}}{\partial P_1} = \frac{2P_1}{P_2 X \widetilde{R}} \tag{A.72}$$

$$\frac{\partial\sqrt{N}}{\partial P_0} = \frac{2}{P_2 \widetilde{R}} \tag{A.73}$$

$$G = \int_{r_a}^{r} \frac{1}{\sqrt{P_1^2 - X(P_2^2/r^2 - 2P_0)}} dr \tag{A.74}$$

$$\frac{\partial G}{\partial P_2} = -\frac{\partial J}{\partial P_0} \tag{A.75}$$

$$\frac{\partial G}{\partial P_1} = \frac{\partial I}{\partial P_0} \tag{A.76}$$

$$\frac{\partial G}{\partial P_0} = \frac{4n^3}{n_A^2 u_3^3 P_2^3} \left[\frac{1}{u_3} N_{QQscd} - N_{Qscd} \right] \tag{A.77}$$

which we use to rewrite the equations (2.115) – (2.122) in the following form:

$$F_1 = Q^1 + t + I(P_0, P_1, P_2, r) = 0 \tag{A.78}$$

$$F_2 = Q^2 - J(P_0, P_1, P_2, r) + K(P_2, P_3, \theta) = 0 \tag{A.79}$$

$$F_3 = Q^3 - \phi - L(P_2, P_3, \theta) = 0 \tag{A.80}$$

$$F_4 = p_t + P_1 = 0 \tag{A.81}$$

$$F_5 = p_\theta + \widetilde{M}(P_2, P_3, \theta) = 0 \tag{A.82}$$

$$F_6 = p_\phi - P_3 = 0 \tag{A.83}$$

$$F_7 = p_r + \sqrt{N(P_0, P_1, P_2, r)} = 0 \tag{A.84}$$

$$F_8 = \widetilde{Q}^0 + G(P_0, P_1, P_2, r) = 0 \ , \tag{A.85}$$

where $\widetilde{Q}^0 = Q^0 + \tau$, however, for simplicity, hereafter we omit the tilde sign and write simply Q^0 (note, that the following derivatives are unaffected by this change).

Now we have a system of 8 equations, which defines implicit relations between (q^μ, p_μ) and (Q^μ, P_μ). Using the rules for derivatives of implicit functions, the following expressions for derivatives $\frac{\partial p_\mu}{\partial Q^\mu}, \frac{\partial q^\mu}{\partial Q^\mu}, \frac{\partial p_\mu}{\partial P_\mu}, \frac{\partial q^\mu}{\partial P_\mu}$ are obtained:

$$\frac{\partial t}{\partial Q^1} = -1 \qquad \frac{\partial r}{\partial Q^1} = \frac{\partial \theta}{\partial Q^1} = \frac{\partial \phi}{\partial Q^1} = \frac{\partial p_t}{\partial Q^1} = \frac{\partial p_r}{\partial Q^1} = \frac{\partial p_\theta}{\partial Q^1} = \frac{\partial p_\phi}{\partial Q^1} = 0 \tag{A.86}$$

$$\frac{\partial t}{\partial Q^2} = \frac{\partial r}{\partial Q^2} = 0 \qquad \frac{\partial \theta}{\partial Q^2} = -\frac{1}{F_{2,\theta}} \qquad \frac{\partial \phi}{\partial Q^2} = -\frac{F_{3,\theta}}{F_{2,\theta}} = F_{3,\theta} \frac{\partial \theta}{\partial Q^2} \tag{A.87}$$

$$\frac{\partial p_t}{\partial Q^2} = \frac{\partial p_r}{\partial Q^2} = 0 \qquad \frac{\partial p_\theta}{\partial Q^2} = \frac{F_{5,\theta}}{F_{2,\theta}} = -F_{5,\theta} \frac{\partial \theta}{\partial Q^2} \qquad \frac{\partial p_\phi}{\partial Q^2} = 0 \tag{A.88}$$

$$\frac{\partial t}{\partial Q^3} = \frac{\partial r}{\partial Q^3} = \frac{\partial \theta}{\partial Q^3} = \frac{\partial p_t}{\partial Q^3} = \frac{\partial p_r}{\partial Q^3} = \frac{\partial p_\theta}{\partial Q^3} = \frac{\partial p_\phi}{\partial Q^3} = 0 \qquad \frac{\partial \phi}{\partial Q^3} = 1 \tag{A.89}$$

$$\frac{\partial t}{\partial P_1} = -F_{1,P_1} + \frac{F_{1,r}}{F_{8,r}} F_{8,P_1} = -F_{1,P_1} + F_{1,r} \frac{\partial r}{\partial P_1} \tag{A.90}$$

$$\frac{\partial r}{\partial P_1} = -\frac{F_{8,P_1}}{F_{8,r}} = F_{8,P_1}\frac{\partial r}{\partial Q^0} \tag{A.91}$$

$$\frac{\partial \theta}{\partial P_1} = \left(\frac{F_{2,r}F_{8,P_1}}{F_{8,r}} - F_{2,P1}\right)\frac{1}{F_{2,\theta}} = -\left(F_{2,r}\frac{\partial r}{\partial P_1} + F_{2,P1}\right)\frac{1}{F_{2,\theta}} \tag{A.92}$$

$$\frac{\partial \phi}{\partial P_1} = F_{3,\theta}\frac{\partial \theta}{\partial P_1} \qquad \frac{\partial p_t}{\partial P_1} = -1 \tag{A.93}$$

$$\frac{\partial p_r}{\partial P_1} = -F_{7,P_1} + \frac{F_{7,r}F_{8,P_1}}{F_8, r} = -F_{7,P_1} - F_{7,r}\frac{\partial r}{\partial P_1} \tag{A.94}$$

$$\frac{\partial p_\theta}{\partial P_1} = \frac{F_{5,\theta}}{F_{2,\theta}F_{8,r}}(-F_{2,r}F_{8,P_1} + F_{2,P1}F_{8,r}) = -F_{5,\theta}\frac{\partial \theta}{\partial P_1} \qquad \frac{\partial p_\phi}{\partial P_1} = 0 \tag{A.95}$$

$$\frac{\partial t}{\partial P_2} = -F_{1,P_2} + \frac{F_{1,r}F_{8,P_2}}{F_{8,r}} = -F_{1,P_2} - F_{1,r}\frac{\partial r}{\partial P_2} \tag{A.96}$$

$$\frac{\partial r}{\partial P_2} = -\frac{F_{8,P_2}}{F_{8,r}} = F_{8,P_2}\frac{\partial r}{\partial Q^0} \tag{A.97}$$

$$\frac{\partial \theta}{\partial P_2} = \frac{1}{F_{2,\theta}}\left(\frac{F_{2,r}F_{8,P_2}}{F_{8,r}} - F_{2,P_2}\right) = -\frac{1}{F_{2,\theta}}\left(F_{2,r}\frac{\partial r}{\partial P_2} + F_{2,P_2}\right) \tag{A.98}$$

$$\frac{\partial \phi}{\partial P_2} = F_{3,P_2} + F_{3,\theta}\frac{\partial \theta}{\partial P_2} \qquad \frac{\partial p_t}{\partial P_2} = 0 \tag{A.99}$$

$$\frac{\partial p_r}{\partial P_2} = -F_{7,P_2} + \frac{F_{7,r}F_{8,P_2}}{F_{8,r}} = -F_{7,P_2} - F_{7,r}\frac{\partial r}{\partial P_2} \tag{A.100}$$

$$\frac{\partial p_\theta}{\partial P_2} = -\frac{F_{5,P_2}}{F_{2,\theta}}\left(F_{2,r}\frac{F_{8,P_2}}{F_{8,r}} - F_{2,P_2}\right) - F_{5,P_2} = -F5, \theta\frac{\partial \theta}{\partial P_2} - F_{5,P_2} \tag{A.101}$$

$$\frac{\partial p_\phi}{\partial P_2} = 0 \qquad \frac{\partial t}{\partial P_3} = \frac{\partial r}{\partial P_3} = 0 \qquad \frac{\partial \theta}{\partial P_3} = -\frac{F_{2,P_3}}{F_{2,\theta}} \tag{A.102}$$

$$\frac{\partial \phi}{\partial P_3} = F_{3,P_3} - \frac{F_{2,P_3}F_{3,\theta}}{F_{2,\theta}} = F_{3,P_3} + F_{3,\theta}\frac{\partial \theta}{\partial P_3} \qquad \frac{\partial p_t}{\partial P_3} = \frac{\partial p_r}{\partial P_3} = 0 \tag{A.103}$$

$$\frac{\partial p_\theta}{\partial P_3} = -F_{5,P_3} + \frac{F_{2,P_3}F_{5,\theta}}{F_{2,\theta}} = -F_{5,P_3} - F_{5,\theta}\frac{\partial \theta}{\partial P_3} \qquad \frac{\partial p_\phi}{\partial P_3} = 1 \tag{A.104}$$

$$\frac{\partial t}{\partial Q^0} = \frac{F_{1,r}}{F_{8,r}} = -F_{1,r}\frac{\partial r}{\partial Q^0} \qquad \frac{\partial r}{\partial Q^0} = -\frac{1}{F_{8,r}} \qquad \frac{\partial \theta}{\partial Q^0} = \frac{F_{2,r}}{F_{2,\theta}F_{8,r}} \tag{A.105}$$

$$\frac{\partial \phi}{\partial Q^0} = \frac{F_{2,r}F_{3,\theta}}{F_{2,\theta}F_{8,r}} = \frac{\partial \theta}{\partial Q^0}F_{3,\theta} \qquad \frac{\partial p_t}{\partial Q^0} = 0 \qquad \frac{\partial p_r}{\partial Q^0} = \frac{F_{7,r}}{F_{8,r}} = -F_{7,r}\frac{\partial r}{\partial Q^0} \tag{A.106}$$

$$\frac{\partial p_\theta}{\partial Q^0} = -\frac{F_{2,r}F_{5,\theta}}{F_{2,\theta}F_{8,r}} = -F_{5,\theta}\frac{\partial \theta}{\partial Q^0} \qquad \frac{\partial p_\phi}{\partial Q^0} = 0 \tag{A.107}$$

$$\frac{\partial t}{\partial P_0} = -F_{1,P_0} + \frac{F_{1,r}F_{8,P_0}}{F_{8,r}} = -F_{1,P_0} - F_{1,r}\frac{\partial r}{\partial P_0} \qquad \frac{\partial r}{\partial P_0} = -\frac{F_{8,P_0}}{F_{8,r}} \tag{A.108}$$

$$\frac{\partial \theta}{\partial P_0} = \frac{F_{2,r}F_{8,P_0}}{F_{2,\theta}F_{8,r}} - \frac{F_{2,P_0}}{F_{2,\theta}} = -\frac{1}{F_{2,\theta}}\left(F_{2,r}\frac{\partial r}{\partial P_0} + F_{2,P_0}\right) \qquad \frac{\partial \phi}{\partial P_0} = F_{3,\theta}\frac{\partial \theta}{\partial P_0} \tag{A.109}$$

$$\frac{\partial p_t}{\partial P_0} = 0 \qquad \frac{\partial p_r}{\partial P_0} = -F_{7,P_0} + \frac{F_{7,r}F_{8,P_0}}{F_{8,r}} = -F_{7,P_0} - F_{7,r}\frac{\partial r}{\partial P_0} \tag{A.110}$$

$$\frac{\partial p_\theta}{\partial P_0} = -F_{5,\theta}\frac{\partial \theta}{\partial P_0} \qquad \frac{\partial p_\phi}{\partial P_0} = 0 \tag{A.111}$$

where $F_{i,Q^\mu} = \partial F_i/\partial Q^\mu$ and $F_{i,P_\mu} = \partial F_i/\partial P_\mu$. The functions F_{i,Q^μ} and F_{i,P_μ} in (A.86) – (A.111) are replaced with derivatives in (A.49) – (A.77) to obtain the final expressions for the derivatives (here we list only the derivatives with values $\neq \{-1, 0, 1\}$):

$$\frac{\partial \theta}{\partial Q^2} = -\frac{\sin\iota\cos(\lambda+\omega)}{\sin\theta} \qquad \frac{\partial \phi}{\partial Q^2} = \frac{\cos\iota}{\sin^2\theta} \qquad \frac{\partial p_\theta}{\partial Q^2} = \frac{P_2\cos\theta\cos^2\iota}{\sin^3\theta} \tag{A.112}$$

$$\frac{\partial t}{\partial P_1} = -\frac{\partial I}{\partial P_1} + \frac{4P_1^2 n^3}{P_2^3 u_3^2 (u_2-u_3)^2 X} N_{QQscd} \tag{A.113}$$

$$\frac{\partial r}{\partial P_1} = -\frac{4P_1^2 n^2}{P_2^2 u_3^2 (u_2-u_3)} \mathrm{sn}(\frac{\lambda}{n}|m)\mathrm{cn}(\frac{\lambda}{n}|m)\mathrm{dn}(\frac{\lambda}{n}|m) N_{QQscd} \tag{A.114}$$

$$\frac{\partial \theta}{\partial P_1} = \frac{\sin\iota\cos(\lambda+\omega)}{\sin\theta}\frac{P_1 n^3}{P_2^2(u_2-u_3)^2}[N_{scd} - Q^2 N_{QQscd}] \tag{A.115}$$

$$\frac{\partial \phi}{\partial P_1} = -\frac{\cos\iota}{\sin^2\theta}\frac{P_1 n^3}{P_2^2(u_2-u_3)^2}[N_{scd} - Q^2 N_{QQscd}] \tag{A.116}$$

$$\frac{\partial p_r}{\partial P_1} = -\frac{2P_1}{P_2 X \widetilde{R}} + \frac{P_1 n^3}{P_2^3(u_2-u_3)^2}\left(-N + \frac{P_2^2}{r} - \frac{P_1^2}{X^2}\right) Q^2 N_{QQscd} \tag{A.117}$$

$$\frac{\partial p_\theta}{\partial P_1} = -\frac{\cos^2\iota\cos\theta}{\sin^3\theta}\frac{P_1 n^3}{P_2(u_2-u_3)^2}[N_{scd} - Q^2 N_{QQscd}] \tag{A.118}$$

$$\frac{\partial t}{\partial P_2} = \frac{P_1 n^3}{P_2^2(u_2-u_3)^2}\left[\left(1 - \frac{1-u_3}{X}\right) N_{scd} + \frac{n_A u_3}{X} N_{cd}\right] \tag{A.119}$$

$$\frac{\partial r}{\partial P_2} = \frac{n^2}{P_2(u_2-u_3)}\mathrm{sn}(\frac{\lambda}{n}|m)\mathrm{cn}(\frac{\lambda}{n}|m)\mathrm{dn}(\frac{\lambda}{n}|m)[(1-u_3)N_{scd} - n_A u_3 N_{cd}] \tag{A.120}$$

$$\begin{aligned}\frac{\partial \theta}{\partial P_2} = \frac{\sin\iota\cos(\lambda+\omega)}{\sin\theta}\Bigg(&\frac{n^3}{4P_2 n_A^2} Q^2[(1-u_3)N_{scd} - n_A u_3 N_{cd}] + \\ &+ \frac{\partial J}{\partial P_2} - \frac{1}{P_2}\cot^2\iota\tan(\lambda+\omega)\Bigg)\end{aligned} \tag{A.121}$$

$$\frac{\partial \phi}{\partial P_2} = -\frac{\cot\iota\tan(\lambda+\omega)}{P_2\sin\iota} - \frac{\cot\iota}{\sin\theta\cos(\lambda+\omega)}\frac{\partial\theta}{\partial P_2} \tag{A.122}$$

$$\frac{\partial p_r}{\partial P_2} = \frac{2}{r^2\widetilde{R}} - \frac{n^3 Q^2}{4P_2^2 n_A^2}\left(-N + \frac{P_2^2}{r} - \frac{P_1^2}{X^2}\right)[(1-u_3)N_{scd} - n_A u_3 N_{cd}] \tag{A.123}$$

$$\frac{\partial p_\theta}{\partial P_2} = -\frac{\sin\theta}{\sin\iota\cos(\lambda+\omega)}\left(1 + \frac{P_2\cos^2\iota\cot\theta}{\sin^2\theta}\frac{\partial\theta}{\partial P_2}\right) \tag{A.124}$$

$$\frac{\partial \theta}{\partial P_3} = \frac{\cot\iota\sin(\lambda+\omega)}{P_2\sin\theta} \qquad \frac{\partial \phi}{\partial P_3} = \frac{\cos(\lambda+\omega)\sin(\lambda+\omega)}{P_2\sin^2\theta} \tag{A.125}$$

$$\frac{\partial p_\theta}{\partial P_3} = \frac{\cot\iota\cos(\lambda+\omega)}{\sin^3\theta} \qquad \frac{\partial t}{\partial Q^0} = \frac{P_1}{X} \qquad \frac{\partial r}{\partial Q^0} = -\frac{P_2\widetilde{R}}{2} \tag{A.126}$$

$$\frac{\partial \theta}{\partial Q^0} = -\frac{P_2}{r^2}\frac{\sin\iota\cos(\lambda+\omega)}{\sin\theta} \qquad \frac{\partial \phi}{\partial Q^0} = \frac{P_2}{r^2}\frac{\cos\iota}{\sin^2\theta} \tag{A.127}$$

$$\frac{\partial p_r}{\partial Q^0} = \frac{1}{r^2}\left(-N + \frac{P_2^2}{r} - \frac{P_1^2}{X^2}\right) \qquad \frac{\partial p_\theta}{\partial Q^0} = \frac{P_2^2}{r^2}\frac{\cos^2\iota\cos\theta}{\sin^3\theta} \tag{A.128}$$

$$\frac{\partial t}{\partial P_0} = \frac{4P_1 n^3}{P_2^3 u_3^2 (u_2-u_3)^2}\left[\frac{u}{1-u}N_{QQscd} - \frac{u_3}{X}N_{Qscd}\right] \tag{A.129}$$

$$\frac{\partial r}{\partial P_0} = -\frac{4n^2}{u_3(u_2-u_3)P_2^2}\mathrm{sn}(\frac{\lambda}{n}|m)\mathrm{cn}(\frac{\lambda}{n}|m)\mathrm{dn}(\frac{\lambda}{n}|m)\left[\frac{1}{u_3}N_{QQscd} - N_{Qscd}\right] \tag{A.130}$$

$$\frac{\partial \theta}{\partial P_0} = -\frac{\sin\iota\cos(\lambda+\omega)}{\sin\theta}\left(\frac{P_2}{r^2}\frac{\partial G}{\partial P_0} - \frac{\partial J}{\partial P_0}\right) \tag{A.131}$$

$$\frac{\partial \phi}{\partial P_0} = \frac{\cos\iota}{\sin^2\theta}\left(\frac{P_2}{r^2}\frac{\partial G}{\partial P_0} - \frac{\partial J}{\partial P_0}\right) \tag{A.132}$$

$$\frac{\partial p_r}{\partial P_0} = -\frac{2}{P_2\widetilde{R}} + \frac{1}{r^2}\left(-N + \frac{P_2^2}{r} - \frac{P_1^2}{X^2}\right)\frac{\partial G}{\partial P_0} \tag{A.133}$$

$$\frac{\partial p_\theta}{\partial P_0} = \frac{P_2\cos\theta\cos^2\iota}{\sin^3\theta}\left(\frac{P_2}{r^2}\frac{\partial G}{\partial P_0} - \frac{\partial J}{\partial P_0}\right) \tag{A.134}$$

A.3.1 Special Functions

We use the following parameters: m from (A.43d), $m_1 = 1-m$, $\chi = \mathrm{am}(x|m)$, $n_A = -n_1$, $n'_A = -n_2$, where n_1 and n_2 are defined in (A.43e). To facilitate the comparison with Allison (1989), we use their notation.

$$N_s = \int \frac{dx}{\mathrm{sn}^2(x|m)} = x - \frac{\mathrm{cn}^2(x|m)\mathrm{dn}^2(x|m)}{\mathrm{sn}^2(x|m)} - \mathrm{E}(\chi|m) \tag{A.135}$$

$$N_c = \int \frac{dx}{\mathrm{cn}^2(x|m)} = \frac{1}{m_1}\left(\frac{\mathrm{sn}(x|m)\mathrm{dn}(x|m)}{\mathrm{cn}(x|m)} + m_1 x - \mathrm{E}(\chi|m)\right) \tag{A.136}$$

$$N_d = \int \frac{dx}{\mathrm{dn}^2(x|m)} = \frac{1}{m_1}\left(\frac{-m\mathrm{sn}(x|m)\mathrm{cn}(x|m)}{\mathrm{dn}(x|m)} + \mathrm{E}(\chi|m)\right) \tag{A.137}$$

$$N_{cd} = \int \frac{dx}{\mathrm{cn}^2(x|m)\mathrm{dn}^2(x|m)} = \frac{1}{m_1}\left(N_c - mN_d\right) \tag{A.138}$$

$$N_{scd} = \int \frac{dx}{\mathrm{sn}^2(x|m)\mathrm{cn}^2(x|m)\mathrm{dn}^2(x|m)} = N_s + \frac{1}{m_1}\left(N_c - m^2 N_d\right) \tag{A.139}$$

$$Q = 1 + n_A\mathrm{sn}^2(x|m) \tag{A.140}$$

$$Q' = 1 + n'_A\mathrm{sn}^2(x|m) \tag{A.141}$$

$$N_Q = \int \frac{dx}{Q} = \Pi(-n_A|\chi|m) \tag{A.142}$$

$$N_{Q'} = \int \frac{dx}{Q'} = \Pi(-n'_A|\chi|m) \tag{A.143}$$

$$N_{Qs} = \int \frac{dx}{Q\mathrm{sn}^2(x|m)} = N_s - n_A N_Q \tag{A.144}$$

$$N_{Qc} = \int \frac{dx}{Q\mathrm{cn}^2(x|m)} = \frac{1}{1+n_A}(N_c + n_A N_Q) \tag{A.145}$$

$$N_{Qd} = \int \frac{dx}{Q\mathrm{dn}^2(x|m)} = \frac{1}{m+n_A}(mN_d + n_A N_Q) \tag{A.146}$$

$$N_{Q's} = \int \frac{dx}{Q'\mathrm{sn}^2(x|m)} = N_s - n'_A N_{Q'} \tag{A.147}$$

$$N_{Q'c} = \int \frac{dx}{Q'\mathrm{cn}^2(x|m)} = \frac{1}{1+n'_A}(N_c + n'_A N_{Q'}) \tag{A.148}$$

$$N_{Q'd} = \int \frac{dx}{Q'\mathrm{dn}^2(x|m)} = \frac{1}{m+n'_A}(mN_d + n'_A N_{Q'}) \tag{A.149}$$

$$N_{Qscd} = \int \frac{dx}{Q\mathrm{sn}^2(x|m)\mathrm{cn}^2(x|m)\mathrm{dn}^2(x|m)} = N_{Qs} + \frac{1}{m_1}(N_{Qc} - m^2 N_{Qd}) \tag{A.150}$$

$$N_{Q'scd} = \int \frac{dx}{Q'\mathrm{sn}^2(x|m)\mathrm{cn}^2(x|m)\mathrm{dn}^2(x|m)} = N_{Q's} + \frac{1}{m_1}(N_{Q'c} - m^2 N_{Q'd}) \tag{A.151}$$

$$\begin{aligned} N_{QQ} = \int \frac{dx}{Q^2} = \frac{1}{2(1+n_a)(m+n_A)} \Big[& \frac{n_A^2 \mathrm{sn}(x|m)\mathrm{cn}(x|m)\mathrm{dn}(x|m)}{Q} + \\ & + n_A \mathrm{E}(\chi|m) - (m+n_A)x + (n_A^2 + 2n_A(1+m) + 3m)N_Q \Big] \end{aligned} \tag{A.152}$$

$$N_{QQs} = \int \frac{dx}{Q^2\mathrm{sn}^2(x|m)} = N_s - n_A(N_Q + N_{QQ}) \tag{A.153}$$

$$N_{QQc} = \int \frac{dx}{Q^2\mathrm{cn}^2(x|m)} = \frac{1}{(n_A+1)^2}\left(n_A(n_A+1)N_{QQ} + n_A N_Q + N_c\right) \tag{A.154}$$

$$N_{QQd} = \int \frac{dx}{Q^2\mathrm{dn}^2(x|m)} = \frac{1}{(n_A+m)^2}\left(n_A(n_A+m)N_{QQ} + n_A m N_Q + m^2 N_d\right) \tag{A.155}$$

$$\begin{aligned} N_{QQscd} &= \int \frac{dx}{Q^2\mathrm{sn}^2(x|m)\mathrm{cn}^2(x|m)\mathrm{dn}^2(x|m)} = N_{QQs} + \frac{1}{m_1}\left(N_{QQc} - m^2 N_{QQd}\right) \\ &= -\frac{1}{(1+n_A)^2}\left(n_A^2(1+n_A)N_{QQd} + (2+n_A)n_A^2 N_{Qd} + n_A(2+n_A)N_{cd}\right) + N_{scd} \end{aligned} \tag{A.156}$$

Some additional useful integrals:

$$\int \frac{\mathrm{sn}^2(x|m)dx}{\mathrm{cn}^2(x|m)\mathrm{dn}^2(x|m)} = N_{cd} - N_d \tag{A.157}$$

$$\int \frac{\mathrm{sn}^4(x|m)dx}{\mathrm{cn}^2(x|m)\mathrm{dn}^2(x|m)} = N_{cd} - N_d - \frac{1}{m}N_d + \frac{1}{m}x \tag{A.158}$$

$$\int \frac{Q^2 dx}{\mathrm{sn}^2(x|m)\mathrm{cn}^2(x|m)\mathrm{dn}^2(x|m)} = N_{scd} + (2n_A + n_A^2)N_{cd} - n_A^2 N_d \tag{A.159}$$

$$\begin{aligned} \int \frac{Q^3 dx}{\mathrm{sn}^2(x|m)\mathrm{cn}^2(x|m)\mathrm{dn}^2(x|m)} = & \int \frac{Q^2 dx}{\mathrm{sn}^2(x|m)\mathrm{cn}^2(x|m)\mathrm{dn}^2(x|m)} + \\ & n_A(1+n_A)^2 N_{cd} - n_A^2(2 + n_A + \frac{n_A}{m})N_d + \frac{n_A^3}{m}x \end{aligned} \tag{A.160}$$

$$\int \frac{Q^2 dx}{\mathrm{cn}^2(x|m)\mathrm{dn}^2(x|m)} = (1+n_A)^2 N_{cd} - n_A(2+n_A+\frac{n_A}{m})N_d + \frac{n_A^2}{m}x \quad \text{(A.161)}$$

$$\int_{\pi/2}^{\theta} \left(P_2^2 - \frac{P_3^2}{\sin^2\theta}\right)^{-1/2} d\theta = -\frac{\lambda+\omega}{P_2} \quad \text{(A.162)}$$

$$\int_{\pi/2}^{\theta} \left(P_2^2 - \frac{P_3^2}{\sin^2\theta}\right)^{-3/2} d\theta = -\frac{\cot^2\iota\tan(\lambda+\omega)}{P_2^3} - \frac{\lambda+\omega}{P_2^3} \quad \text{(A.163)}$$

$$\int_{\pi/2}^{\theta} \left(P_2^2 - \frac{P_3^2}{\sin^2\theta}\right)^{-3/2} \frac{d\theta}{\sin^2\theta} = -\frac{\tan(\lambda+\omega)}{P_2^3\sin^2\iota} \quad \text{(A.164)}$$

Appendix B

Multipole momenta

B.0.2 Planets, the Moon, the Sun

We consider the Newtonian gravitational potential of celestial bodies $\Phi^{\ominus}$ in a point of space around the Earth $\mathbf{r}$ and far away from celestial bodies in the Earth-centered inertial (ECI) system, such as International Celestial Reference System (ICRS)/J2000.0 Ma et al. (1997); Souchay (2006); Petit and Luzum (2010), written as

$$\Phi^{\ominus}(t, \mathbf{r}) = \sum_i \frac{GM_i}{\|\mathbf{r}_i - \mathbf{r}\|} , \tag{B.1}$$

where M_i are the masses of celestial bodies and $\mathbf{r}_i$ are vectors pointing to the celestial body. The latter are functions of time and are supplied by JPL's Horizons System NASA JPL's Solar System Dynamics group (2013) in ICRS/J2000.0.

We associate to vectors $\mathbf{r}_i$ and $\mathbf{r}$ spherical coordinates $(r_i, \theta_i, \varphi_i)$ and (r, θ, φ), respectively. The spherical coordinates $(r, \theta, \varphi) \in \mathbb{R}_+ \times [0, \pi] \times [0, 2\pi]$ are related to Cartesian coordinates (x, y, z) as

$$(x, y, z) = r(\sin\theta\cos\varphi, \sin\theta\sin\varphi, \cos\theta) . \tag{B.2}$$

Because $r_i \gg r$, we can write the reciprocal distance in $\Phi^{\ominus}$ (B.1) as a series of Legendre polynomials (Abramowitz and Stegun 1964):

$$\begin{aligned} \frac{1}{\|\mathbf{r}_i - \mathbf{r}\|} &= \frac{1}{r_i} \frac{1}{\sqrt{1 - 2\mathbf{r}\cdot\mathbf{r}_i/r_i + (r/r_i)^2}} \\ &= \frac{1}{r_i} \sum_{n=0}^{\infty} \left(\frac{r}{r_i}\right)^n P_n(\cos\gamma_i) \end{aligned} \tag{B.3}$$

where $\cos\gamma_i$ is a scalar product of unit vectors $\mathbf{r}_i/\|\mathbf{r}_i\|$ and $\mathbf{r}/\|\mathbf{r}\|$:

$$\cos\gamma_i = \cos\theta_i\cos\theta + \sin\theta_i\sin\theta\cos(\varphi_i - \varphi) . \tag{B.4}$$

According to the addition theorem of Legendre polynomials (Arfken 1985), we can further expand Legendre polynomials in (B.3) as

$$P_n(\cos\gamma_i) = \frac{4\pi}{2n+1}\sum_{m=-n}^{n} Y_n^{m*}(\theta_i,\varphi_i)Y_n^m(\theta,\varphi)\,, \tag{B.5}$$

with $()^*$ denoting the complex conjugate and Y_n^m representing the spherical harmonics (Arfken 1985). By substituting $P_n(\cos\gamma_i)$ in (B.3) with (B.5), we can expand the potential $\Phi^{\ominus}$ (B.1) in terms of spherical harmonics

$$\Phi^{\ominus}(t,\mathbf{r}) = \sum_{n=0}^{\infty}\sum_{m=-n}^{n} r^n M_{nm}^{\ominus}(t)Y_n^m(\theta,\varphi)\,, \tag{B.6}$$

where we identify the interior multipole moments associated to the celestial bodies given by

$$M_{nm}^{\ominus}(t) = \frac{4\pi G}{2n+1}\sum_i \frac{M_i}{r_i^{n+1}(t)}Y_n^{m*}(\theta_i(t),\varphi_i(t))\,, \tag{B.7}$$

which are time dependent if position of celestial bodies relative to our reference system is changing with time. Note that $M_{nm}^{\ominus}$ are complex with the symmetry

$$M_{nm}^{\ominus\,*} = (-1)^m M_{n,-m}^{\ominus}\,, \tag{B.8}$$

which makes the potential $\Phi^{\ominus}$ a real valued function.

B.0.3 Earth tides

The Earth's Newtonian gravitational potential $\Phi^{\oplus}$, called geopotential, is time varying, because the deformed Earth is rotating and the gravitational influence of other, external celestial bodies deforms the Earth. The external bodies change Earth's shape, and these changes are called *the solid Earth tides*, while the shape of the fluid on the surface of the Earth is called *the ocean tides*. Here we take into account only the most important external bodies, i.e. the Moon and the Sun.

We start by discussing the Newtonian gravitational potential Φ in the Earth centered Earth fixed (ECEF) system, such as the International Terrestrial Reference Systems (ITRS) Petit and Luzum (2010), and then transform it into the Earth-centered inertial (ECI) system, such as International Celestial Reference System (ICRS)/J2000.0 Ma et al. (1997); Souchay (2006); Petit and Luzum (2010).

In the spherical coordinates defined in subsection B.0.2 and based on ITRS, the geopotential can be written in terms of the spherical harmonics Y_n^m as

$$\Phi^{\oplus}(t,\mathbf{r}) = \sum_{n=0}^{\infty}\sum_{m=-n}^{n} \frac{M_{nm}(t)}{r^{n+1}}Y_n^m(\theta,\varphi)\,, \tag{B.9}$$

where $M_{nm}(t) \in \mathbb{C}$ are called the complex multipole moments depending on time t and possessing the symmetry $M_{n,-m} = (-1)^m M_{n,m}^*$. In the chosen coordinate system, which is attached to Earth's mass centre, there is no dipole contribution: $M_{1m} = 0$.

In geodesy and related fields, see e.g. Torge (2001), the geopotential is expressed using the time dependent normalized geopotential coefficients $\overline{C}_{nm}(t)$ and $\overline{S}_{nm}(t)$ and normalized Legendre polynomial P_{nm} as

$$\Phi^{\oplus}(t,\mathbf{r}) = \frac{GM_{\oplus}}{r}\left\{1 + \sum_{n=2}^{\infty}\left(\frac{r_{\oplus}}{r}\right)^{n} \cdot \sum_{m=0}^{n}\left[\overline{C}_{nm}(t)\cos(m\varphi) + \overline{S}_{nm}(t)\sin(m\varphi)\right]\overline{P}_{nm}(\cos\theta)\right\}, \tag{B.10}$$

where $M_{\oplus}$ and $r_{\oplus}$ are the mass and the mean radius of Earth, respectively. The normalized Legendre polynomial are defined as

$$\overline{P}_{nm} = (-1)^{m} N_{nm} P_{n}^{m}\ , \tag{B.11}$$

where the normalization factor is

$$N_{nm} = \sqrt{\frac{(2-\delta_{m,0})(2n+1)(n-m)!}{(n+m)!}}\ , \tag{B.12}$$

and P_n^m are standard Legendre polynomials (Abramowitz and Stegun 1964).

Note that the sum over n in (B.10) runs only from the quadrupole term due to choice of coordinate system, and by definition, $S_{n0} = 0$ for all n.

The normalized geopotential coefficients are connected to the complex multipoles in (B.9) for positive orders $m > 0$ via formula

$$M_{nm} = (-1)^{m}\sqrt{\frac{4\pi}{2-\delta_{m,0}}} GM_{\oplus} r_{\oplus}^{n} T_{nm}\ , \tag{B.13}$$

where we introduce a complex normalized geopotential coefficient

$$T_{nm} = \overline{C}_{nm} - \mathrm{i}\,\overline{S}_{nm}\ , \tag{B.14}$$

which is used in tide calculations as it allows us to work with both real geopotential coefficients in the same expression.

The complex normalized geopotential coefficients T_{nm} can be decomposed into a sum of constant (time average) coefficients T_{nm}^{0} and its perturbation, i.e., time dependent coefficients $T_{nm}^{\mathrm{e}}(t)$ and $T_{nm}^{\mathrm{o}}(t)$ corresponding to Earth and ocean tides, respectively:

$$T_{nm}(t) = T_{nm}^{0} + T_{nm}^{\mathrm{e}}(t) + T_{nm}^{\mathrm{o}}(t)\ . \tag{B.15}$$

The constant contributions T_{nm}^{0} are up to degree 360 available from Earth Gravitational Model 1996 (EGM96) (Lemoine and Center 1998). In the following subsections, we separately discuss each of the perturbations to T_{nm}.

Solid Earth tides

The solid Earth tides represent deformations of the Earth due to gravitational forces of other celestial bodies. Following the International Earth rotation and reference systems service (IERS) Conventions (Petit and Luzum 2010, Ch. 6) and Montenbruck and Gill (2005, Sec. 3.7.2), we write the complex geopotential coefficients of solid Earth as a sum of contributions due to presence of the Moon ☾ ($j = 1$) and the Sun ☉ ($j = 2$):

$$T^{\mathrm{e}}_{nm}(t) = \frac{k_{nm}}{2n+1} \sum_{j=1}^{2} \frac{M_j}{M_\oplus} \left(\frac{r_\oplus}{r_j}\right)^{n+1} \overline{P}_{nm}(\sin\theta_j) e^{-\mathrm{i}m\varphi_j} \,, \tag{B.16}$$

where M_j, r_j, θ_j and φ_j are the mass, the distance from the Earth center, the latitude and the east longitude from Greenwich, respectively, of the jth body in ITRS. The position $(r_j, \theta_j, \varphi_j)$ as a function of time is provided by Astronomical Almanac (U.S. Nautical Almanac Office 2012) together with The Explanatory Supplement (Seidelmann et al. 1992).

The k_{nm} are the nominal Love numbers describing Earth's response to (n, m)-multipoles of the external potential and depend on the considered Earth model. Here we assume that the Earth is elastic and use the numbers reported in Table B.1.

Table B.1: Nominal values of the Love numbers for the solid tides of elastic Earth model (Petit and Luzum 2010).

(n,m)	(2,0)	(2,1)	(2,2)	(3,0)	(3,1)	(3,2)	(3,3)
k_{nm}	0.29525	0.29470	0.29801	0.093	0.093	0.093	0.094

With such description, we capture only the main body deformations, whereby the motion of the poles is left out of discussion. These can be included as perturbations of the moments, but their dynamical model is fundamentally different. The position of poles is affected by Chandler wobble of period 435 days, see e.g. Stacey and Davis (2008), annual oscillation forced by seasonal displacement of air and water masses and diurnal and semi-diurnal variations forced by oceanic tides. The model describing perturbations of multipole coefficients is given in Moyer (2005, Sec. 5.2.8.) and concrete data can be found in Petit and Luzum (2010, Sec 6.4.).

Ocean tides

Gravitational forces of celestial bodies cause the displacement of the ocean water on the surface of the Earth. The surface of the ocean follows an equipotential surface of the gravitational potential. The ocean tides are influenced mainly by presence of the Moon and the Sun and only these are taken into account in present ocean tide models. For further reading see e.g. Petit and Luzum (2010, Sec 6.5.).

The ocean tide can be broken down into its independent constituents representing perpetual dynamics of ocean surface of incommensurable frequency. A. T. Doodson in

Doodson (1921) introduced an efficient practical labeling system of labeling constituents based on non-negative numbers m_i. Each tide constituent, which is practically relevant, can be labeled by a Doodson number as

$$m_1 m_2 m_3, m_4 m_5 m_6 \ , \tag{B.17}$$

which is constructed as a concatenation of m_i with comma "," serving as a separator. There exists an alternative labeling of tide constituents introduced by G. H. Darwin (1845-1912) and labels are called the Darwin symbols, which are useful for textual referencing of tides. Few of the most influential tide constituents used in our analysis are listed in Table B.2. K_1 is Lunisolar diurnal constituent, which with O_1, expresses the effect of the Moon's declination. They account for diurnal inequality and, at extremes, diurnal tides. For a given constituent f labeled by the Doodson number m_i we introduce

Table B.2: The few first most significant tidal constituents in decreasing order of significance.

Description	Darwin symbol	Doodson number
Principal lunar semidiurnal	M_2	255,555
Principal solar semidiurnal	S_2	273,555
Larger lunar elliptic semidiurnal	N_2	245,655
Lunar diurnal	K_1	165,555
Lunar diurnal	O_1	145,555

Doodson coefficients $n_i \in \mathbb{Z}$,

$$m_1 = n_1 \ , \qquad m_i = n_i + 5 \quad \text{for} \quad i = 2, \ldots, 6 \ . \tag{B.18}$$

We are interested in the perturbations of the geopotenial due to ocean tides. According to Montenbruck and Gill (2005, Sec. 3.7.2) and the IERS Conventions (Petit and Luzum 2010), the geopotential coefficients due to ocean tides can be represented as a sum over constituents f

$$T^{\mathrm{o}}_{nm}(t) = \sum_f \sum_{s\in\{+,-\}} [\mathcal{C}^s_{f,nm} - \mathrm{i}s\, \mathcal{S}^s_{f,nm}] e^{s\,\mathrm{i}\theta_f(t)} \ , \tag{B.19}$$

where $\theta_f(t)$ is the Doodson argument θ_f defined as a linear combination of six Doodson fundamental arguments β_i given by

$$\theta_f(t) = \sum_{i=1}^{6} n_i \beta_i(t) \ , \tag{B.20}$$

and $\mathcal{C}^s_{f,nm}$ and $\mathcal{S}^s_{f,nm}$ are geopotential harmonic amplitudes corresponding to constituent f and multipoles indices (n, m). For details on the tidal dynamics see McCarthy and Seidelmann (2009). The amplitudes $\mathcal{C}^s_{f,nm}$ and $\mathcal{S}^s_{f,nm}$ based on Finite element solutions of global tides for year 2004 (FES2004) (Lyard et al. 2006) are provided by R. Biancale (Biancale 2012).

Transforming multipoles from ITRS to ICRS

Here we outline the transformation of multipoles while transforming coordinates of geopotential from ITRS into ICRS. The transformation of coordinates from ICRS into ITRS is given as a time dependent rotation

$$\mathbf{r}_{\mathrm{ITRS}} = \mathbf{R}(t)\mathbf{r}_{\mathrm{ICRS}}\,, \tag{B.21}$$

where $\mathbf{r}_{\mathrm{ITRS}}$ and $\mathbf{r}_{\mathrm{ICRS}}$ are vectors of Cartesian coordinates in ITRS and in ICRS, respectively, and time t variable. For details see Montenbruck and Gill (2005, Sec. 5.2) with references to the IERS Conventions Petit and Luzum (2010, Ch. 5). The rotation matrix $\mathbf{R}(t)$ is defined as a product of rotation matrices $\mathbf{P}(t)$, $\mathbf{N}(t)$, $\mathbf{\Theta}(t)$ and $\mathbf{\Pi}(t)$ corresponding to coordinate transformation due to precession, nutation, Earth rotation around its own axis, and polar motions, respectively:

$$\mathbf{R}(t) = \mathbf{\Pi}(t)\mathbf{\Theta}(t)\mathbf{N}(t)\mathbf{P}(t)\,. \tag{B.22}$$

Each of the rotation matrices $\mathbf{P}(t)$ (Montenbruck and Gill 2005, Eq. 5.46), $\mathbf{N}(t)$ (Montenbruck and Gill 2005, Eq. 5.62), $\mathbf{\Theta}(t)$ (Montenbruck and Gill 2005, Eq. 5.67), and $\mathbf{\Pi}(t)$ (Montenbruck and Gill 2005, Eq. 5.75) can be expressed as products of elementary rotations $\mathbf{R}_{\mathrm{x}}$, $\mathbf{R}_{\mathrm{y}}$ and $\mathbf{R}_{\mathrm{z}}$ around x, y and z axis, respectively:

$$\begin{aligned}
\mathbf{P}(t) &= \mathbf{R}_{\mathrm{z}}(-z)\mathbf{R}_{\mathrm{y}}(\theta)\mathbf{R}_{\mathrm{z}}(-\zeta)\,,\\
\mathbf{N}(t) &= \mathbf{R}_{\mathrm{x}}(-\epsilon-\Delta\epsilon)\mathbf{R}_{\mathrm{z}}(-\Delta\psi)\mathbf{R}_{\mathrm{x}}(\epsilon)\,,\\
\mathbf{\Theta}(t) &= \mathbf{R}_{\mathrm{z}}(\mathrm{GAST})\,,\\
\mathbf{\Pi}(t) &= \mathbf{R}_{\mathrm{y}}(-x_p)\mathbf{R}_{\mathrm{x}}(-y_p)
\end{aligned} \tag{B.23}$$

where angles of rotation z, θ, ζ, ϵ, $\Delta\epsilon$, $\Delta\psi$, GAST, x_{p} and y_{p} depend in time only. The elementary rotations using notation $c = \cos\phi$ and $s = \sin\phi$ are defined as

$$\mathbf{R}_{\mathrm{x}}(\phi) = \begin{pmatrix} 1 & 0 & 0\\ 0 & c & s\\ 0 & -s & c \end{pmatrix}, \tag{B.24}$$

$$\mathbf{R}_{\mathrm{y}}(\phi) = \begin{pmatrix} c & 0 & -s\\ 0 & 1 & 0\\ s & 0 & c \end{pmatrix}, \tag{B.25}$$

$$\mathbf{R}_{\mathrm{z}}(\phi) = \begin{pmatrix} c & s & 0\\ -s & c & 0\\ 0 & 0 & 1 \end{pmatrix}. \tag{B.26}$$

The angles of rotation are given as power series in the time argument – Julian date since J2000 using terrestrial time (TT) for precession and nutation and using universal time (UT1) for Earth's rotation and polar motion. For details see Montenbruck and Gill (2005, p. 167, 175, 181). It is clear from the definition of the rotation matrix $R(t)$ (B.22) that it can be written as a product of $p(=9)$ elementary rotations

$$\mathbf{R}(t) = \mathbf{R}_{x_1}(t_1)\ldots\mathbf{R}_{x_p}(t_r)\,, \tag{B.27}$$

where x_i denotes the axis ith rotation and t_i is the corresponding angle of rotation depending on time t.

Lets introduce a direction vector $\hat{\mathbf{r}} := \mathbf{r}/\|\mathbf{r}\|$ in Cartesian coordinate system written in spherical coordinates $(r, \theta, \varphi) \in \mathbb{R}_+ \times [0, \pi] \times [0, 2\pi]$ as

$$\hat{\mathbf{r}} = (\sin\theta\cos\varphi, \sin\theta\sin\varphi, \cos\theta) \,, \tag{B.28}$$

and define a spherical harmonics in that direction $Y_n^m(\hat{\mathbf{r}}) := Y_n^m(\theta, \varphi)$.

Finally, the geopotential in ICRS coordinates Φ^{ICRS} can be compactly expressed with the geopotential in ITRS coordinates as

$$\begin{aligned} \Phi^{\oplus,\mathrm{ICRS}}(t, \mathbf{r}) &= \Phi^{\oplus}(t, \mathbf{R}(t)\mathbf{r}) \,, \\ &= \sum_{nm} M_{nm}^{\oplus}(t) r^{-n-1} Y_n^m(\mathbf{R}(t)\hat{\mathbf{r}}) \,. \end{aligned} \tag{B.29}$$

We can expand the spherical harmonics with rotating argument $Y_n^m(\mathbf{R}(t)\hat{\mathbf{r}})$ into spherical harmonics

$$Y_n^m(\mathbf{R}(t)\hat{\mathbf{r}}) = \sum_{m'=-n}^{n} U_{m',m}^n(t) Y_n^{m'}(\hat{\mathbf{r}}) \,, \tag{B.30}$$

by taking into account the orthogonality of spherical harmonics

$$\int_\Omega \mathrm{d}\Omega(\hat{\mathbf{r}})\, Y_{n'}^{m'*}(\hat{\mathbf{r}}) Y_n^m(\hat{\mathbf{r}}) = \delta_{n,n'}\delta_{m,m'} \tag{B.31}$$

and introducing a time dependent transition matrix for spherical harmonics given by

$$U_{m',m}^n(t) = \int_\Omega \mathrm{d}\Omega(\hat{\mathbf{r}})\, Y_n^{m'*}(\hat{\mathbf{r}}) Y_n^m(\mathbf{R}(t)\hat{\mathbf{r}}) \,, \tag{B.32}$$

with a differential of the solid angle $\mathrm{d}\Omega(\hat{\mathbf{r}}) = \sin\theta \mathrm{d}\theta\mathrm{d}\varphi$ on domain $\Omega = \{(\theta, \varphi) \in [0, \pi] \times [0, 2\pi]\}$. Matrix

$$\mathbf{U}^n(t) = [U_{m',m}^n(t)]_{m',m=-n}^n \tag{B.33}$$

is unitary. The spherical harmonics with an argument rotating around specific axis can be expanded into spherical harmonics as

$$Y_m^n(\mathbf{R}_i(t)\hat{\mathbf{r}}) = \sum_{m'=-n}^{n} Y_{m'}^n(\hat{\mathbf{r}}) [\mathbf{U}_i^n(t)]_{m',m} \,, \tag{B.34}$$

by introducing the rotation matrices $\mathbf{U}_i^n(t)$ in the basis of spherical harmonics defined via the Wigner D-matrix $D_{m',m}^n$ (Varshalovich et al. 1988):

$$\begin{aligned} [\mathbf{U}_{\mathrm{x}}^n(t)]_{m',m} &= D_{m',m}^n\left(\frac{\pi}{2}, t, -\frac{\pi}{2}\right) \,, \\ [\mathbf{U}_{\mathrm{y}}^n(t)]_{m',m} &= D_{m',m}^n(0, t, 0) \,, \\ [\mathbf{U}_{\mathrm{z}}^n(t)]_{m',m} &= D_{m',m}^n(0, 0, t) \,, \end{aligned} \tag{B.35}$$

where $[\cdot]_{a,b}$ denotes the matrix element of indices (a, b). By using the expression for $Y^n_m(\mathbf{R}_i(t)\hat{\mathbf{r}})$ (B.34) for each elementary rotation $\mathbf{R}_i(t)$ in the product forming $\mathbf{R}(t)$ (B.27) we can write

$$Y^n_m(\mathbf{R}(t)\hat{\mathbf{r}}) = \sum_{m'=-n}^{n} Y^n_{m'}(\hat{\mathbf{r}})[\mathbf{U}^n_{x_p}(t_p)\dots\mathbf{U}^n_{x_1}(t_1)]_{m',m} \,. \tag{B.36}$$

By plugging this expression in equation (B.32) we obtain the transition matrix expressed as product rotation matrices in basis of spherical harmonics:

$$\mathbf{U}^n(t) = \mathbf{U}^n_{x_p}(t_p)\dots\mathbf{U}^n_{x_1}(t_1) \,. \tag{B.37}$$

By using the expansion (B.30) in formula (B.29) and exchanging the order summation, we obtain potential in geopotential in ICRS:

$$\Phi^{\oplus,\mathrm{ICRS}}(t,\mathbf{r}) = \sum_{nm} M^{\oplus,\mathrm{ICRS}}_{n,m'}(t) r^{-n-1} Y^m_n(\hat{\mathbf{r}}) \,, \tag{B.38}$$

which is expressed using the multipole moments in ICRS $M^{\oplus,\mathrm{ICRS}}_{n,m'}$ given by

$$M^{\oplus,\mathrm{ICRS}}_{n,m'}(t) = \sum_{m=-n}^{n} U^n_{m',m}(t) M_{n,m}(t) \,. \tag{B.39}$$

Appendix C

Contents of ESA SVN

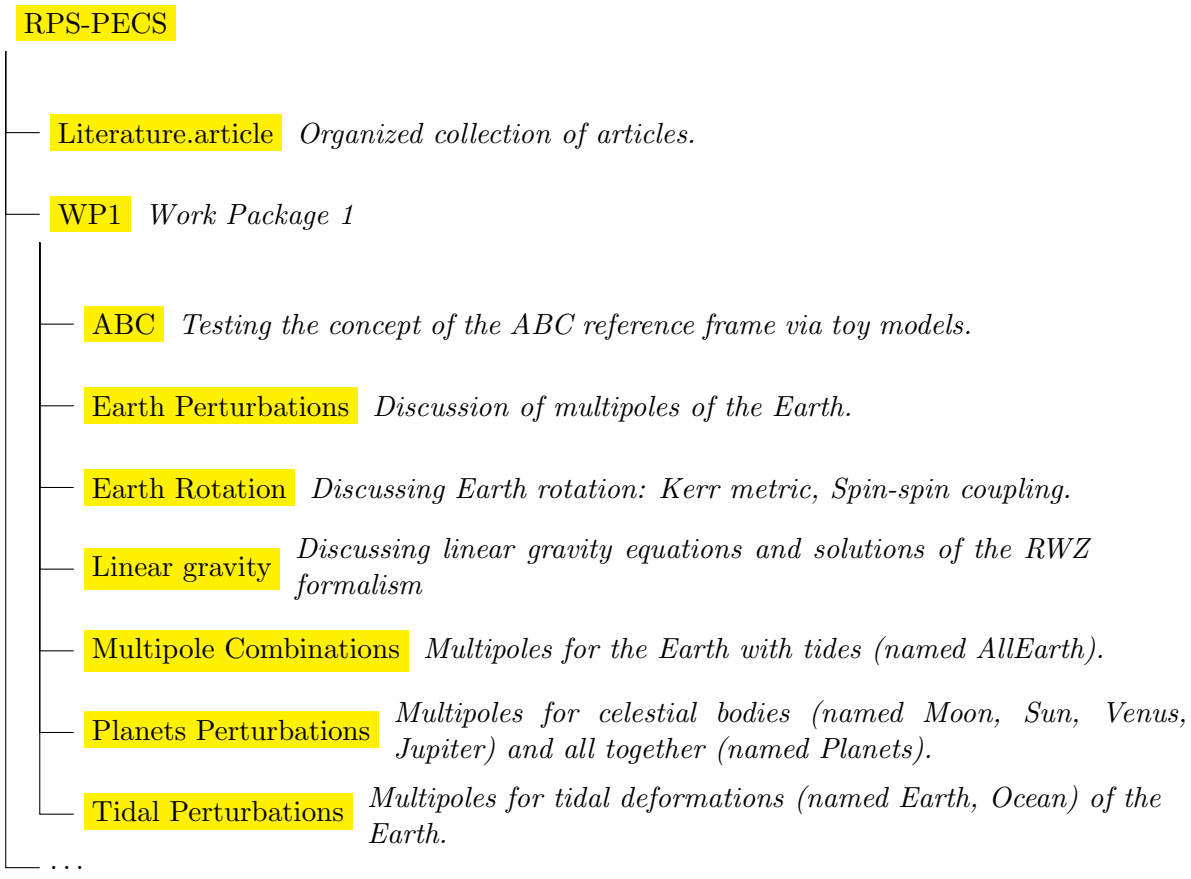

Figure C.1: Directory structure of ESA's SVN.

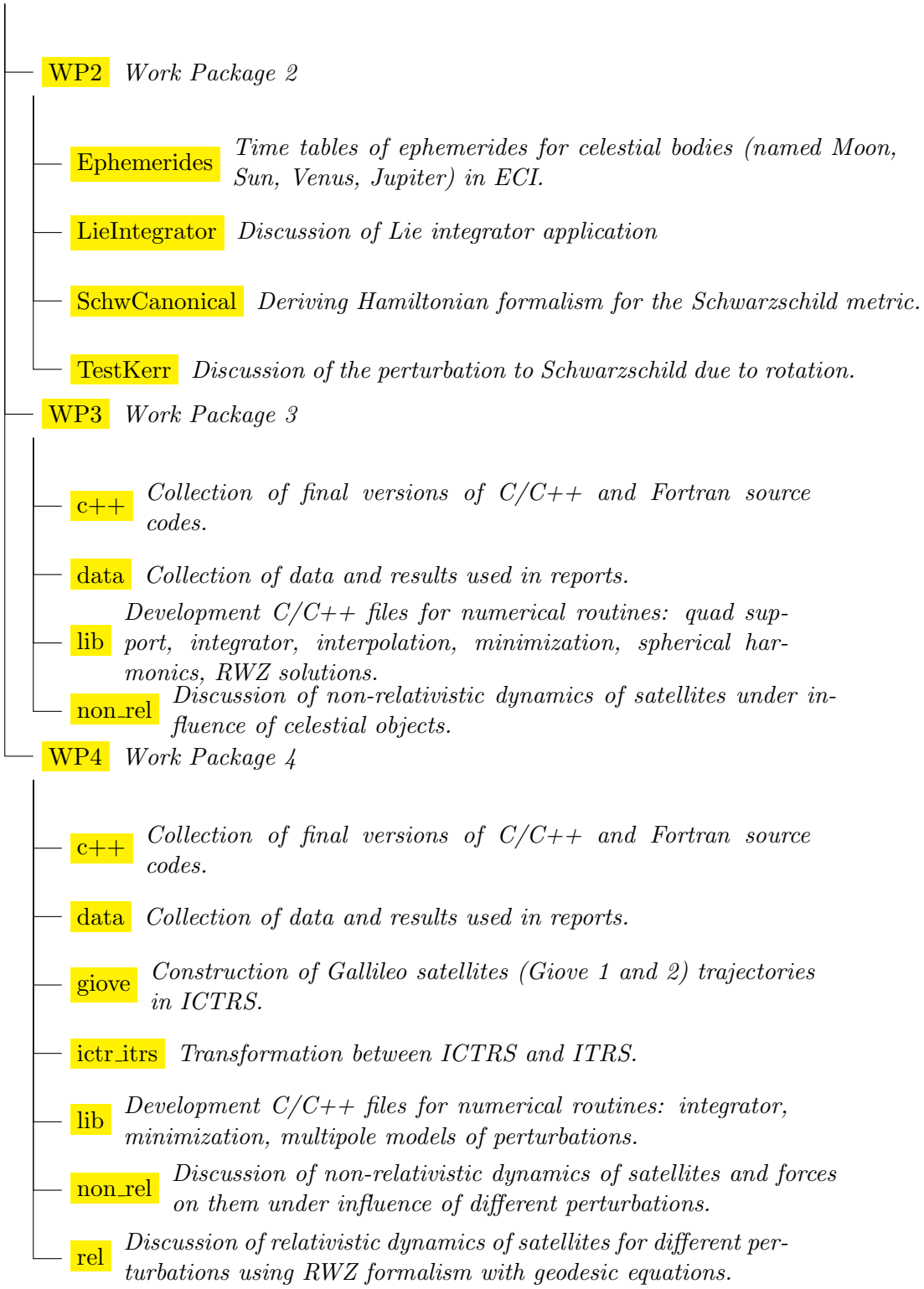

Figure C.2: Continuing...